

**EFFECTS OF THE USE OF ULTRASONIC WAVES ON BIODIESEL
PRODUCTION IN ALKALINE TRANSESTERIFICATION OF BLEACHED
TALLOW AND VEGETABLE OILS: CAVITATION MODEL**

By

Fabio Alape Benítez

A thesis submitted in partial fulfillment of the requirements for the degree of

DOCTOR OF PHILOSOPHY


in

CHEMICAL ENGINEERING


UNIVERSITY OF PUERTO RICO - MAYAGÜEZ CAMPUS

2004

Approved by:


Edna Negrón, Ph. D.
Member, Graduate Committee


4/26/2004
Date


David Suleiman, Ph. D.
Member, Graduate Committee


26-Apr.-2004
Date


Arturo Portnoy, Ph. D.
Member, Graduate Committee


26/Apr/2004
Date


José Colucci Ríos, Ph. D.
President, Graduate Committee


April 23, 2004
Date


Ernesto Riquelme, Ph. D.
Representative of Graduate Studies

April 26, 2004
Date


Nelson Cardona, Ph. D.
Chairperson, Department of Chemical Engineering

April 26, 2004
Date


José A. Mari-Mutt, Ph. D.
Director of Graduate Studies

April 26, 2004
Date

ABSTRACT

Experiments of biodiesel production via methanolysis were performed at methanol/triglyceride molar ratios of 3, 4.5, and 6 and temperatures of 25 °C, 40 °C and 60 °C; the reaction was monitored by HPLC, X-Ray, and GC-MS until equilibrium. A mathematical model called CAVITATION MODEL was developed to deal with mass transfer aspects of the alkaline transesterification reaction of vegetable oils; a comparison between the cavitation model and diffusion through spherical pores was made. Gas-vapor bubble dynamics for the methanol-soybean oil and methanol-tallow system were examined at 40 °C and 42 °C, respectively. The Rayleigh-Plesset equations were used to describe the isothermal growth and adiabatic collapse of the bubble formed when a field of ultrasound at 20 KHz is applied. Temperatures of 2265 K and 426 K were estimated for a bubble in soybean oil-methanol and tallow-methanol systems, respectively. These “Hot Spots” could be responsible for the increment of the temperature occurred and the acoustic streaming observed during the alkaline transesterification reaction. Also, a diffusion analysis with the pore model was made to predict the concentration profile of the triglycerides within the liquid drops of alcohol created after the collapse of the gas-vapor bubbles; spherical shapes were studied. A computational model was made in MathCad to evaluate the effectiveness at different Thiele modulus values in order to estimate mass transfer coefficients for the most critical conditions of pure diffusion and these coefficients were compared with those found by the cavitation model estimation. Pictures of the reactant system soybean oil-methanol-potassium hydroxide, with the red dyed methanol using phenolphthalein, showed that the alkalinity of the system represented by potassium hydroxide remains in the interface alcohol-oil and then is displaced into the glycerol or down layer. The present study serves as a basis for the analysis of heterogeneous reactions with immiscible liquids using ultrasonic agitation.

RESUMEN

En este estudio se realizaron experimentos de producción de biodiesel via metanólisis considerando relaciones molares de metanol/triglicérido de 3, 4.5, y 6; y temperaturas de 25 °C, 40 °C y 60 °C. La reacción fue observada hasta equilibrio por cromatografía líquida, cromatografía gaseosa y fluorescencia de rayos X. Para analizar aspectos de transferencia de masa usando ultrasonido como medio de agitación se desarrolló un modelo matemático llamado “CAVITATION MODEL”, el cual se comparó con el modelo de difusión de poros esféricos. La dinámica de estos sistemas de burbujas gas-vapor, conteniendo metanol-aceite de soya y metanol-cebo sometidos a frecuencias ultrasónicas de 20 KHz y potencias aplicadas alrededor de 30 W, se examinó mediante la solución de las ecuaciones de Rayleigh-Plesset usando un programa desarrollado en MathCad. El primer sistema mencionado se evaluó a 40 °C y el segundo a 42 °C de temperatura global, encontrándose temperaturas locales de colapso de burbuja de 2265 K y 426 K para el sistema aceite de soya-metanol y el sistema cebo-metanol, respectivamente. Se cree que estas condiciones de colapso son en gran parte las responsables del rápido incremento de temperatura observado durante la reacción catalizada tanto por hidróxido de potasio como por la agitación acústica presente. Usando un programa desarrollado en MathCad se pudo además estimar el coeficiente de transferencia de masa para el triglicérido en metanol. El criterio que se usó para discernir sobre el paso controlante de la reacción incorporó el nuevo modelo de cavitación y el modelo de poros esféricos, creando así una base para realizar este tipo de análisis en reacciones donde los reactivos son líquidos inmiscibles y se usa agitación ultrasónica.

DEDICATORY

To my wife Esperanza,
my son Juan Francisco,
my family,
and my friends.

ACKNOWLEDGMENTS

First of all, I want to thank God for giving me the opportunity to earn my doctoral degree (Ph. D.) in chemical engineering.

To Doctor Jose Colucci for his help, support and guidance that was given me both personally and academically.

To the chemical engineering department, and the laboratory NREL-DOE, for the continuous economic support given to me during my doctoral studies.

To Professors of my graduate committee: Arturo Portnoy, Edna Negron, Ernesto Riquelme, and David Suleiman, because their participation in this work was very important to me.

To Doctor Jaime Benitez, an special human being and professor of the chemical engineering department, whose recommendations and technical support were very important for the project.

To my Colombian and Puerto Rican families, and my friends for their unconditional help and support.

To Doctor Nairmen Mina and his family for their friendship.

To all graduate and subgraduate students of research and partners for their participation in this study.

TABLE OF CONTENTS

LIST OF FIGURES	viii
LIST OF TABLES	xii
INTRODUCTION	1
LITERATURE REVIEW	6
Vegetable oils	6
Transesterification	8
Esterification	11
Other uses of Alkyl esters	15
Ultrasound	16
Diffusion and Mass Transfer	20
OBJECTIVES	28
THEORY	29
Cavitation	29
Quasistatic Regime: Blake Threshold	29
Non-Quasistatic Regime: Bubble dynamics	33
Stable cavitation	33
Transient cavitation	35
Intensity of Power	36
Calorimetric measurement	39
Real electric Power to the transducer	40
Acoustic streaming	40
Mixing	43
The mechanism of dispersion of fluids	44
Dispersion in mixing vessels	46
Mean Velocity of the Net Fluid Displacement	51
Mean Drop Diameter	52
Mixing and chemical reaction: Heterogeneous systems in Tank reactors	53
Mass Transfer with Chemical Reactions in porous catalysts:	55
Mass Transfer with Chemical Reactions Shrinking Model:	59
Estimation of Diffusion and reaction limited regimes	63
PROCEDURE	65
State of the Art	65

Materials and Reagents.....	65
Laboratory Equipment Start Up	66
Experiment design	71
Sampling and Chemical Analysis.....	72
RESULTS.....	75
Optimal conditions	75
Photographic analysis.....	77
Cavitation Model.....	80
Transient Cavitation	82
Isothermal case.....	84
Adiabatic case.....	85
Diffusion Model and mass transfer coefficient, k_{MT}	96
Pore model for mass transfer and reaction rate limiting the chemical reaction. ..	102
CONCLUSIONS AND RECOMMENDATIONS.....	107
BIBLIOGRAPHY	109
APPENDIX 1 : Bubble Dynamic Simulations for the system soybean oil-methanol at 15 W	113
APPENDIX 2 : Bubble Dynamic Simulations for the system soybean oil-methanol at 9.84 W	123
APPENDIX 3: Bubble Dynamic Simulations for the system tallow-methanol at 15 W	133
APPENDIX 4: Bubble Dynamic Simulations for the system tallow-methanol at 12.54 W	143
APPENDIX 5: Mass transfer diffusion into a sphere.....	153

LIST OF FIGURES

Figure 1. Molecular structure of tristearin, a triglyceride of the stearic acid (C18:0).....	6
Figure 2. Transesterification of tryglycerides with alcohol to produce glycerol and alkyl esters (Biodiesel).	9
Figure 3. Transesterification of tryglycerides with alcohol to produce glycerol and alkyl esters (Biodiesel).	11
Figure 4. Concentration of compounds vs. time in the transesterification of palm oil at 50 °C, molar ratio of oil/methanol was 6, catalyst was 1% KOH (taken from JAOCS, Vol 77, No. 12 (2000) p. 1264	12
Figure 5. Production of stearic acid and glycerol from tristearin by using an excess of water.	13
Figure 6. Soap formation from oleic acid and alkali in the saponification reaction.....	14
Figure 7. Acid esterification of free fatty acids with methanol to produce methyl esters, Biodiesel, and water.	14
Figure 8. Saponification of methyl esters producing soap and methanol.....	15
Figure 9. Experimental Set-up (taken from Vichare et al., 2001).	27
Figure 10. Bubble: forming and collapsing (Taken from Mason, 1999).....	30
Figure 11. Pressure in the liquid, P_L , versus bubble radius, R , according to Blake Threshold (Taken from Harkin et al. (1999)).	32
Figure 12. Maximum relative radius R_{max}/R_0 as a function of R_0 . $f = 14.3$ KHZ; $P_A = 4$ bars (taken from Young, 1989).	36
Figure 13. Acoustic streaming produced with a probe system of ultrasound (Taken from Mason, 1999).	41
Figure 14. Mass transfer with chemical reaction in a spherical catalyst	57

Figure 15. Shrinking model diffusion for the removal of carbon from a spherical catalyst.....	60
Figure 16. Tri-glycerides calibration curve. Method of quantification by areas.....	68
Figure 17. Di-glycerides calibration curve. Method of quantification by areas.....	69
Figure 18. Methyl esters calibration curve. Method of quantification by areas.....	69
Figure 19. Experimental setup for transesterification of Biodiesel, Taken from Borrero (2002).....	73
Figure 20. Studentized residuals obtained for the apparent equilibrium yield in the statistical screening.....	76
Figure 21. Reactant system before ultrasonic agitation, pure soybean oil and methanol-KOH at 40 °C.....	78
Figure 22. Reaction time of 3 minutes, pure soybean oil and methanol-KOH at 40 °C	79
Figure 23. System operated a higher power intensities of 52 W for soybean oil and methanol at 40 °C.....	79
Figure 24. End of reaction, reactants and products without ultrasonic agitation.....	80
Figure 25. Experimental determination of dT/dt for the system methanol-soybean oil.	86
Figure 26. Experimental determination of dT/dt for the system methanol-tallow.	88
Figure 27. Isothermal bubble of methanol growing in soybean oil, results of simulation at 9.84 W of power absorbed by the system and 40 °C using mathcad.....	89
Figure 28. Adiabatic bubble of methanol growing in soybean oil and then collapsing, results of simulation at 9.84 W of power absorbed by the system and 40 °C using mathcad.....	90
Figure 29. Dynamic of the bubble of methanol in soybean oil during its lifetime, results of simulation at 9.84 W of power absorbed by the system and 40 °C using mathcad.....	90

Figure 30. Isothermal bubble of methanol growing in soybean oil, results of simulation at 15 W of power absorbed by the system and 40 °C using mathcad.....	91
Figure 31. Adiabatic bubble of methanol growing in soybean oil and then collapsing, results of simulation at 15 W of power absorbed by the system and 40 °C using mathcad.....	91
Figure 32. Dynamic of the bubble of methanol in soybean oil during its lifetime, results of simulation at 15 W of power absorbed by the system and 40 °C using mathcad.....	92
Figure 33. Isothermal bubble of methanol growing in tallow, results of simulation at 12.54 W of power absorbed by the system and 42 °C using mathcad.....	92
Figure 34. Adiabatic bubble of methanol growing in tallow and then collapsing, results of simulation at 12.54 W of power absorbed by the system and 42 °C using mathcad.....	93
Figure 35. Dynamic of the bubble of methanol in tallow during its lifetime, results of simulation at 12.54 W of power absorbed by the system and 42 °C using mathcad.....	93
Figure 36. Isothermal bubble of methanol growing in tallow, results of simulation at 15 W of power absorbed by the system and 42 °C using mathcad.....	94
Figure 37. Adiabatic bubble of methanol growing in tallow and then collapsing, results of simulation at 15 W of power absorbed by the system and 42 °C using mathcad.....	94
Figure 38. Dynamic of the bubble of methanol in tallow during its lifetime, results of simulation at 15 W of power absorbed by the system and 42 °C using mathcad.....	95
Figure 39. Procedure to develop a mathematical model in order to predict the mass transfer coefficients in the alkaline transesterification of soybean oil with methanol.	100
Figure 40. Graphical determination of constants of the model proposed for ultrasonic transesterification of Soybean Oil at 25 °C, and an alcohol-oil molar ratio of 6:1.	102

Figure 41. Effectiveness versus Thiele modulus for a second order reaction in an spherical drop.	103
Figure 42. Sensitivity of the Thiele modulus to variations of drop size and diffusivities.	104

LIST OF TABLES

Table 1. Structural formula, melting, and boiling points of fatty acids and methyl esters (Taken from Graboski and McCormick, 1998).....	7
Table 2. Chemical composition of common oils and greases (Taken from Kincs, 1985).....	8
Table 3. Mixes of standards to construct calibration curves to quantify Tri, di-glycerides and methyl esters.....	68
Table 4. Data obtained experimentally to perform the statistical screening of temperature and alcohol/oil molar ratio.	75
Table 5. Stoichiometric table for the transesterification of oils with alcohol when an alcohol-oil molar ratio of 6:1 is used, z_i is the extent of the reaction i based on the initial moles of alcohol.	77
Table 6. Results obtained in simulations of power absorbed by the system methanol-soybean oil at 40 °C under ultrasound irradiation of 20,000 Hz using a molar ratio alcohol-oil of 6:1.	89
Table 7. Results obtained in simulations of power absorbed by the system methanol-tallow at 42 °C under ultrasound irradiation of 20,000 Hz using a molar ratio alcohol-oil of 6:1.	95
Table 8. Data used to calculate k_1 from experiments with soybean oil at 25 °C, an alcohol-oil molar ratio of 6:1.....	101
Table 9. Analysis of rate controlling by Weisz-Prater criterion for alkaline transesterification of soybean oil catalyzed by potassium hydroxide.	105
Table 10. Mass transfer and type of agitation estimated at different size of drops.....	106

INTRODUCTION

The Otto-cycle engine is the familiar gasoline engine used in automobiles and airplanes. The efficiencies of state of the art Otto-cycle engines range between 20 and 25 percent. In other words, only this percentage of the heat energy of the fuel is transformed into mechanical energy. The efficiency of the diesel engine, which is in general governed by the same factors that control the efficiency of Otto-cycle engines, is inherently greater than that of any Otto-cycle engine, and is today slightly more than 40 percent. Diesels are, in general, slow-speed engines with crankshaft speeds of 100 to 750 revolutions per minute (rpm) as compared to 2500 to 5000 rpm for typical Otto-cycle engines. Some types of diesel engines, however, have speeds up to 2000 rpm. Because diesel engines use compression ratios of 14:1 or more, they are generally more heavily built than Otto-cycle engines, but this disadvantage is counterbalanced by their greater efficiency and the fact that they can be operated on less expensive fuel oils .

The idea of using vegetal oil as an engine fuel dates back to 1895, when the French-born German engineer Rudolf Christian Karl Diesel (1858-1913), developed the first engine to run on peanut oil, as he demonstrated at the World Exhibition in Paris in 1900. However, using raw vegetable oils for diesel engines during prolonged times can cause numerous engine-related problems. The increased viscosity and low volatility of vegetable oils lead to severe engine deposits, injector coking and piston ring sticking (Kanakci, 2001).

Walton, in 1938, reported on pioneer work with vegetable oils and suggested an early concept for biodiesel. Three oils were examined in a diesel engine, which utilized 0.416 lb/bph-hour of fuel, similar to a modern engine in efficiency. Steady-state testing showed that soybean oil, palm oil and cottonseed oil all gave fuel economies of 90-91% compared to petroleum diesel at wide open throttle and various speeds. Whole oils were

reported to form carbon deposits and exhibited pour point problems; palm oil corroded copper and brass significantly. Because of the difficulties experienced, Walton suggested splitting off the triglycerides and using the resulting fatty acids as fuel (Graboski and McCormick, 1998).

Biodiesel, an alternative diesel fuel, is made from renewable biological sources such as vegetable oils and animal fats. Chemically, it is defined as the alkyl esters of long chain fatty acids derived from renewable lipid sources (triglycerides). It is environmentally friendly, being biodegradable, and produces significantly less carbon monoxide, sulfur dioxide, hydrocarbons, particulates and air toxic emissions than diesel. Fatty acid alkyl esters (FAAE) can be used as biodiesel fuel or can be used as an additive or extender to diesel fuel.

In the United States, investigations on vegetable oils started as far back as 1978 and focused on soybean oil methyl ester as biodiesel fuel. In South Africa, biodiesel fuel initiatives were reported in 1981. In Germany and Austria, the rapeseed methyl ester was tested in diesel engines for the first time in 1982. In 1985 a small pilot plant was built in Austria and the production of rapeseed methyl ester was started using a new technology at ambient pressure and temperature. Commercial production of biodiesel was started in Europe in 1990.

In 1997, the production of biodiesel fuel was 550,000 tonnes in Europe, 10,000 tonnes in Malaysia and 9,000 tonnes in North America. In 2000 the annual production of biodiesel fuel in Europe was 1,210,000 tonnes. The production increased 2.2 times in three years (Kann et al., 2002).

The most common method used to produce Biodiesel is the alkaline transesterification process. In it, two immiscible phases, triglycerides and methanol, react in the presence of potassium hydroxide during one or two hours in a batch reactor,

producing glycerol and methyl esters which can be separated using gravitational settling. Then, the upper layer rich in fatty acid methyl esters, FAME's, is refined using two successive liquid extractions with water. The final product is known as Biodiesel. The lower phase is mainly glycerol. Methanol is recovered and the catalyst converted into potassium phosphate, a fertilizer, by adding phosphoric acid.

It seems that the reaction can only occur in the interfacial region between the liquids and thus is a very slow process. A vigorous mixing is required to increase the area of contact between the two immiscible phases, and this produces an emulsion. Mason reported hydrolysis of immiscible liquids, oils in aqueous NaOH, using ultrasound (Mason, 1999).

Ultrasound is the process of propagation of the compression (rarefaction) waves with frequencies above the range of human hearing, i.e. above 15-16 KHz. (Shutilov, 1988). Typical commercial ultrasonic instruments known as "probe systems" have a piezoelectric transducer powered by a generator that couples energy into a chemical reaction by means of a horn or velocity transformer (SONICSYSTEMS, 1986).

The probe system used in this study operates at a frequency of 20 KHz. It has a digital wattmeter to measure the power applied to the transducer to maintain the amplitude for any given output control setting. As the load or pressure on the horn face increases, the power supply develops more power. The heart of the converter is a lead zirconate titanate electrostrictive element which, when subjected to an alternating voltage, expands and contracts. The converter vibrates in a longitudinal direction and transmits this motion to the horn tip immersed in the solution, which causes cavitation (Branson, 1998).

Cavitation implies the opening of holes in liquids. Depending on the circumstances, these holes can be filled either by gases already dissolved in the liquid, in

which case the phenomenon is sometimes called *gaseous cavitation* or *pseudocavitation*, or, in the absence of such dissolved gases, by the vapor of the liquid itself (*vapor cavitation* or *true cavitation*). It is quite clear that the conditions for the appearances of these two kinds of cavitation can be quite different and that two processes must be examined separately (Beyer and Letcher, 1969).

It's known that the application of ultrasound in chemical processing enhances both the mass transfer and chemical reactions; this science is called Sonochemistry. It offers the potential for shorter reaction cycles, cheaper reagents, and less extreme physical conditions, leading to less expensive and perhaps chemical producing smaller plants. Existing literature on sonochemical reacting systems is chemistry-intensive, and applications of this novel means of reaction in environmental remediation and pollution prevention seem almost unlimited. For example, environmental sonochemistry is a rapidly growing area that deals with the destruction of organics in aqueous solutions. However, some theoretical and engineering aspects are not yet fully understood (Adewuyi, 2001).

The cavitation phenomenon is also accompanied by the emission of visible radiation, which is given the name sonoluminescence. Some researchers take advantage of this phenomenon doing estimations of the bubbles collapse conditions from the intensity of the light emitted by the system, this area is being explored too.

Another important phenomenon called “acoustic streaming”, has been identified when ultrasound is applied to liquid systems. It consists mainly of a hydrodynamic vertical flow near the sound source and its intensity depends on the ability of the medium to absorb the acoustic energy (usually the energy absorbed by the medium generates an increase in temperature). This ability can be modified by the presence of electrolytic salts.

Other undesired effects of the sonochemical processes are: erosion of emitter and reactor surface, creation of noise and acceleration of by-product formation (Löning et al., 2002).

For the Ultrasound agitation case, ultrasound application generates cavitation bubbles, which generate shockwaves when they collapse by implosion, forcing the oil and the methanol to join.

In the present study a mathematical model was developed in order to obtain a fundamental understanding of the oil/alcohol transesterification reaction under ultrasound mixing conditions.

LITERATURE REVIEW

Vegetable oils

All natural fats and oils are esters of fatty acids and glycerol. These are known as glycerides or triglycerides (TG). With few exceptions, the carboxylic acids (fatty acids) from which the fats and oils are derived are all straight-chain compounds ranging in size from 3 to 18 carbons. Figure 1 shows the molecular structure of stearic acid (C18:0). This triglyceride (TG) has a molecular weight of 892 g/g-mol and it is found in corn and canola oils (refined rapeseed oil is known as canola oil and it is very common in Canada).

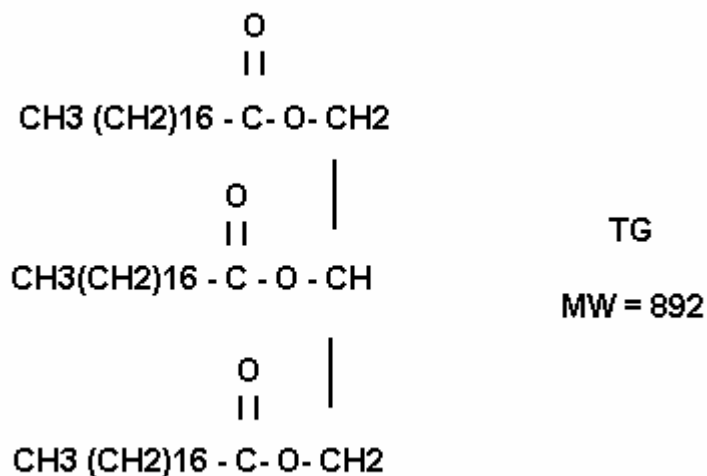


Figure 1. Molecular structure of tristearin, a triglyceride of the stearic acid (C18:0)

The chemical composition of fat and oil esters is dependent upon the length and degree of unsaturation of the fatty acid alkyl chains. Table 1 shows the chemical structure of the fatty acid chains found in the most common biodiesel source materials (Graboski and McCormick, 1998).

Table 1. Structural formula, melting, and boiling points of fatty acids and methyl esters (Taken from Graboski and McCormick, 1998).

Acid Chain	C	Structure	Fatty Acids		Methyl esters	
			Melt. Point (°C)	Boil. Point (°C)	Melt. Point (°C)	Boil. Point (°C)
Caprylic	8	$\text{CH}_3(\text{CH}_2)_6\text{COOH}$	16.5	239	-40	193
Capric	10	$\text{CH}_3(\text{CH}_2)_8\text{COOH}$	31.3	269	-18	224
Lauric	12	$\text{CH}_3(\text{CH}_2)_{10}\text{COOH}$	43.6	304	5.2	262
Myristic	14	$\text{CH}_3(\text{CH}_2)_{12}\text{COOH}$	58.0	332	19	295
Palmitic	16	$\text{CH}_3(\text{CH}_2)_{14}\text{COOH}$	62.9	349	30	338
Palmitoleic	16	$\text{CH}_3(\text{CH}_2)_5\text{CH}=\text{CH}(\text{CH}_2)_7\text{COOH}$	33	-	0	-
Stearic	18	$\text{CH}_3(\text{CH}_2)_{16}\text{COOH}$	69.9	371	39.1	352
Oleic	18	$\text{CH}_3(\text{CH}_2)_7\text{CH}=\text{CH}(\text{CH}_2)_7\text{COOH}$	16.3	-	-	349
Linoleic	18	$\text{CH}_3(\text{CH}_2)_4\text{CH}=\text{CHCH}_2\text{CH}=\text{CH}(\text{CH}_2)_7\text{COOH}$	-5	-	-35	366
Linolenic	18	$\text{CH}_3\text{CH}_2\text{CH}=\text{CHCH}_2\text{CH}=\text{CHCH}_2\text{CH}=\text{CH}(\text{CH}_2)_7\text{COOH}$	-11	-	-	-
Arachidic	20	$\text{CH}_3(\text{CH}_2)_{18}\text{COOH}$	75.2	-	50	-
Eicosenoic	20	$\text{CH}_3(\text{CH}_2)_7\text{CH}=\text{CH}(\text{CH}_2)_9\text{COOH}$	23	-	-15	-
Behenic	22	$\text{CH}_3(\text{CH}_2)_{20}\text{COOH}$	80	-	54	-
Erucic	22	$\text{CH}_3(\text{CH}_2)_7\text{CH}=\text{CH}(\text{CH}_2)_{11}\text{COOH}$	34	-	-	-

Except for C_3 and C_5 compounds, only acids with an even number of carbons occur naturally in plants and terrestrial animals. Acids may be saturated (contain only single bonds) or unsaturated (contain one or more double bonds). The saturated acids exhibit higher melting points than the unsaturated acids. Stearic acid, for example, is solid at 70 °C, while oleic acid melts at 16 °C. The only difference is a single double bond in the structure of the oleic acid.

It is important to note that, according to the lipid groups classification made by Thiele in 1970, saturated fatty acids and derivatives are classified as apolars. However, unsaturated fatty acids and derivatives are classified as polarizables. Triglycerides as polars and free fatty acids as charged.

Table 2 presents the typical fatty acid composition of potential biodiesel source materials.

Table 2. Chemical composition of common oils and greases (Taken from Kincs, 1985).

Fatty acid	OIL				FAT	
	Soybean	Cottonseed	Palm	Coconut	Lard	Tallow
Lauric	0.1	0.1	0.1	46.5	0.1	0.1
Myristic	0.1	0.7	1	19.2	1.4	2.8
Palmitic	10.2	20.1	42.8	9.8	23.6	23.3
Stearic	3.7	2.6	4.5	3.0	14.2	19.4
Oleic	22.8	19.2	40.5	6.9	44.2	42.4
Linoleic	53.7	55.1	10.1	2.2	10.7	2.9
Linolenic	8.6	0.6	0.2	0	0.4	0.9

In addition to triglycerides, fats contain a number of minor components such as phosphatides, sterols, steryl esters, fat-soluble vitamins A and D, and tocopherols (which act as antioxidants and have vitamin E activity). All natural oils contain significant proportions of at least four fatty acids. This yield 40 different combinations on the three positions of the glycerol molecule, or 40 triglycerides with different chemical and physical properties (Deuel, 1951).

Transesterification

Biodiesel may be manufactured in batch or continuous systems by transesterification, also called alcoholysis or interesterification. In transesterification, one ester is converted to another. The reaction is catalyzed by either acid or base and involves a reaction with an alcohol. As typically practiced, a basic catalyst, such as sodium or potassium hydroxide, is used to convert the glycerol based triesters (or triacyl glycerides) which make up fats and oils to methanol based monoesters (or methylesters) yielding free glycerol as a byproduct.

A catalyst is usually used to improve the reaction rate and yield. Because the reaction is reversible, excess alcohol is used to shift the equilibrium to the products side. Alcohols are primary and secondary monohydric aliphatic alcohols having 1-8 carbon atoms. Among the alcohols that can be used in the transesterification process are methanol, ethanol, propanol, butanol, and amyl alcohol. Methanol and ethanol are used most frequently, especially methanol because of its low price and its physical and chemical advantages – polar and shortest chain alcohol (Fangrui and Hanna, 1999).

Branched-chain alcohols, such as isopropyl and 2-butyl have been used in transesterifications of oils and fats in order to reduce the crystallization temperature of biodiesel (Lee, et. al., 1995).

Alkaline transesterification is strongly influenced by free fatty acids (FFA), and water content in the raw material. FFA and water content should be kept below 0.5% and 0.06%, respectively to minimize side reactions.

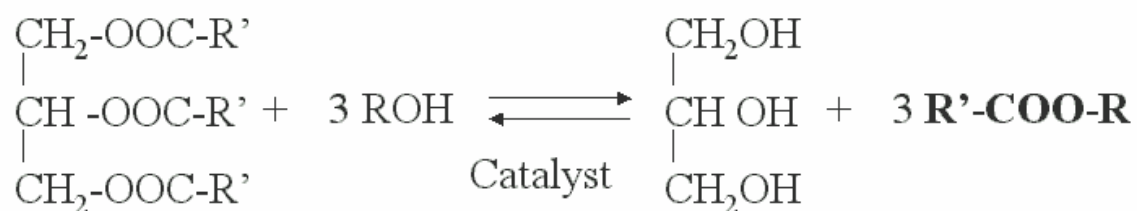


Figure 2. Transesterification of tryglycerides with alcohol to produce glycerol and alkyl esters (Biodiesel).

At slightly above room temperature this reaction proceeds to conversion of 90-97%, in an excess of methanol, within approximately 1 hr. The remaining 3-10% is

glycerol, mono/di/triglycerides, and free fatty acids. Much of the free fatty acid is converted to soap (sodium or potassium salt of the fatty acid) and water.

Up to 0.5 wt% catalyst is required to promote the transesterification. In most processing flow sheets the catalyst is not recovered and recycled. Thus, fresh catalyst must be continuously added. Washing to remove the spent catalyst is often accomplished with water yielding a significant amount of wastewater from the process. The byproduct glycerol is nearly insoluble in biodiesel and in the feed stock oil and thus forms a separate liquid phase. The biodiesel may require distillation to remove traces of glycerides. The glycerol may be purified by vacuum distillation.

Biodiesel can be made from waste oils as well. Methods for producing esters from waste cooking oils containing significant quantities of free fatty acids require additional catalyst, compared to conventional transesterification, to neutralize the free fatty acids by converting them to soap prior to transesterification. These soaps separate from the biodiesel during the final washing (Graboski and McCormick, 1998).

The alkali-catalyzed reaction mechanism consists of three steps. The first step is an attack on the carbonyl carbon atom of the triglyceride molecule by the anion, the methoxide ion, to form a tetrahedral intermediate. In the second step this intermediate reacts with the methanol to regenerate the anion. In the last step, rearrangement of the tetrahedral intermediate results in the formation of a fatty acid ester and a diglyceride. When NaOH, KOH, K_2CO_3 or other similar catalysts were mixed with alcohol, the actual catalyst alkoxide group is formed. A small amount of water generated in the reaction may cause soap formation during transesterification (Fangrui and Hanna, 1999).

The accepted stepwise reactions for the basic transesterification of soybean oil and Palm oil were presented by Freedman and Darnoko, respectively (Freedman, et.al., 1986; Darnoko and Cheryan, 2000):



Figure 3. Transesterification of tryglycerides with alcohol to produce glycerol and alkyl esters (Biodiesel).

Darnoko and Cheryan (2000) using a batch reactor in the palm oil transesterification found the kinetic constant of each reaction and showed graphically one pseudo-second order behavior for the initial stages of the reaction, followed by first-order or zero-order kinetics for the overall reaction. Kinetics of palm oil transesterification with methanol using KOH as catalyst in a batch reactor was studied at 50, 55, 60 and 65 °C using a methanol/oil molar ratio of 6:1 during 90 minutes. To follow the progress of the reaction by the determination of triglyceride, diglyceride, monoglyceride, total methyl esters and glycerol, a gel-permeation chromatography instrument was used. Typical concentrations versus reaction time are shown in Figure 4.

Esterification

Oils can be converted into free fatty acids by excess of water. This occurs because a triglyceride can react with water to produce free fatty acids and glycerol,

according to the reverse reaction of Fisher esterification. An example of this is presented in Figure 5.

Oils with high contents of FFA, can also be converted into biodiesel via acid esterification using sulfuric acid as catalyst. In these cases the transesterification doesn't proceed because the excess of alkali required to neutralize FFA is enough to modify the function of the alkali from catalyst to reactant driving the reaction into soap formation as shown in Figure 6. An example of the acid esterification of oleic acid with methanol is presented in Figure 7. The saponification of methyl esters producing soap and methanol is shown in the Figure 8.

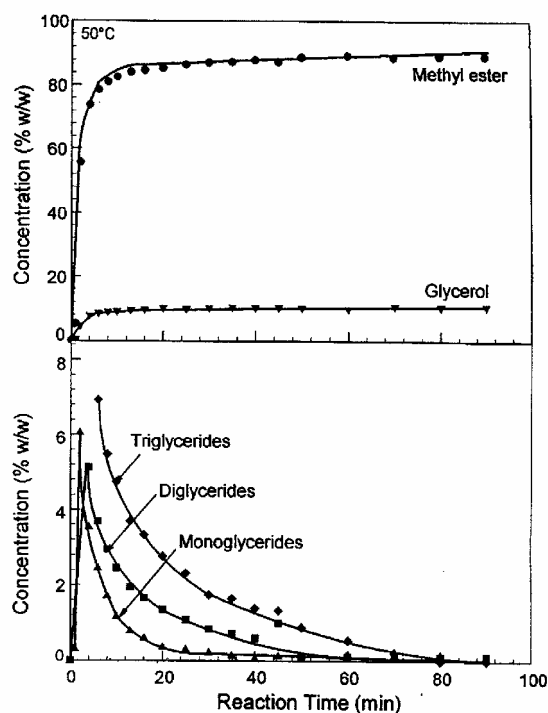


Figure 4. Concentration of compounds vs. time in the transesterification of palm oil at 50 °C, molar ratio of oil/methanol was 6, catalyst was 1% KOH (taken from JAOCS, Vol 77, No. 12 (2000) p. 1264

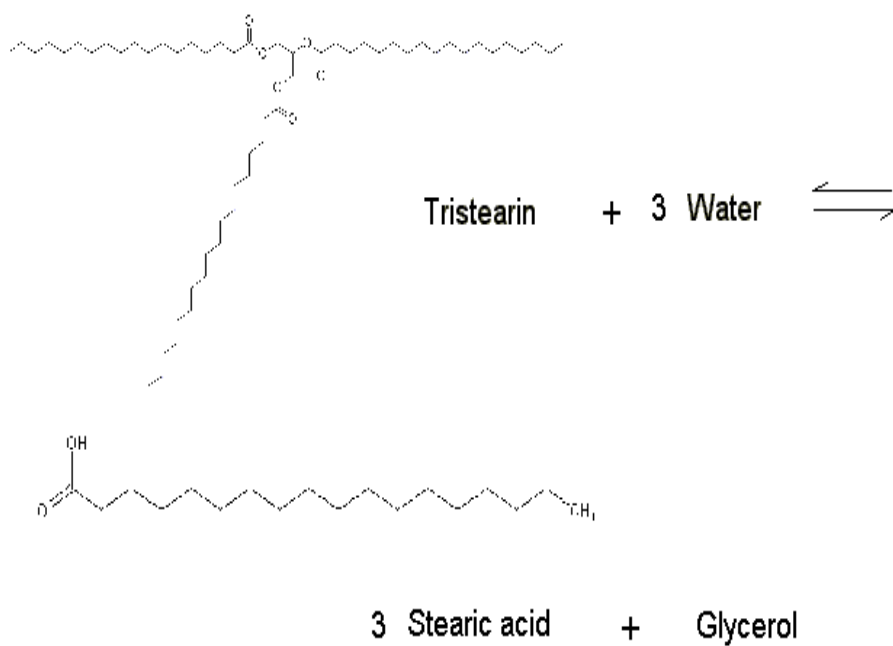


Figure 5. Production of stearic acid and glycerol from tristearin by using an excess of water.

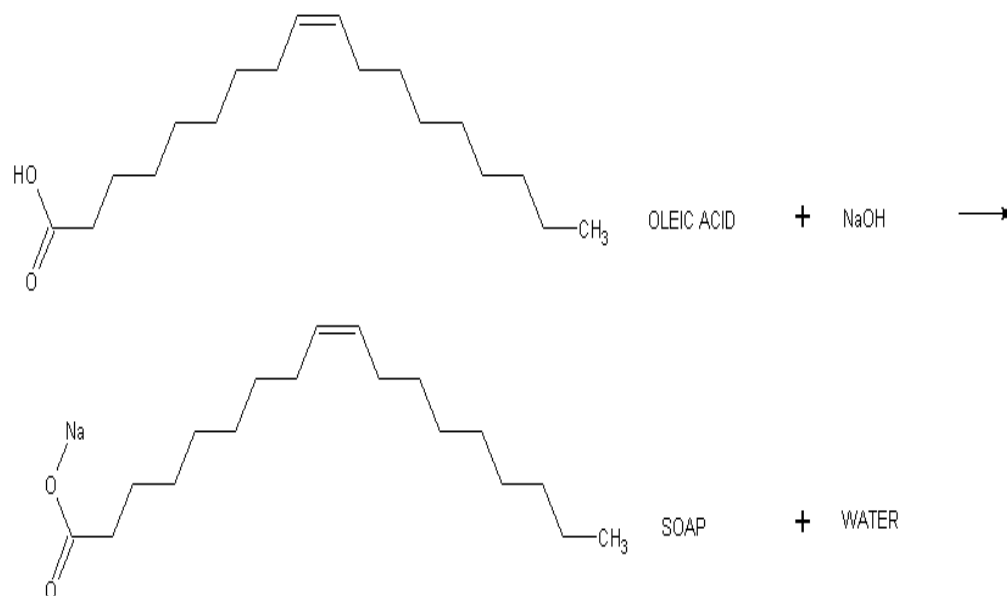


Figure 6. Soap formation from oleic acid and alkali in the saponification reaction.

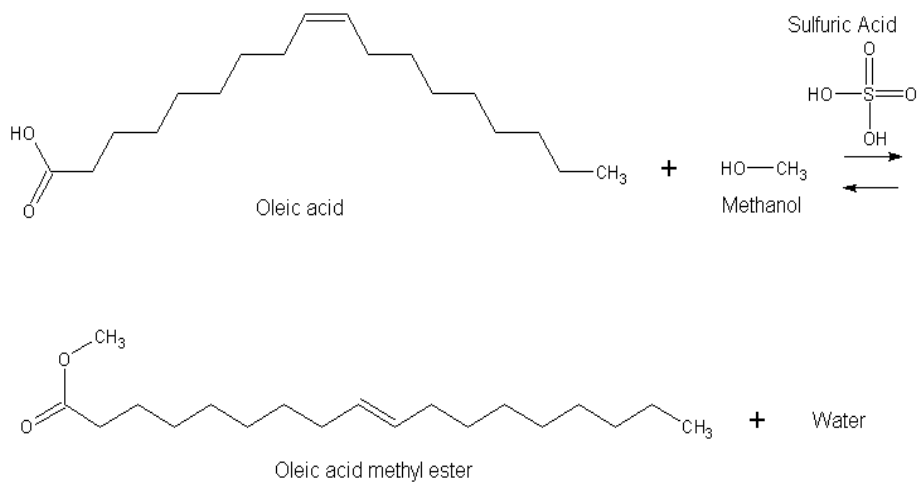


Figure 7. Acid esterification of free fatty acids with methanol to produce methyl esters, Biodiesel, and water.

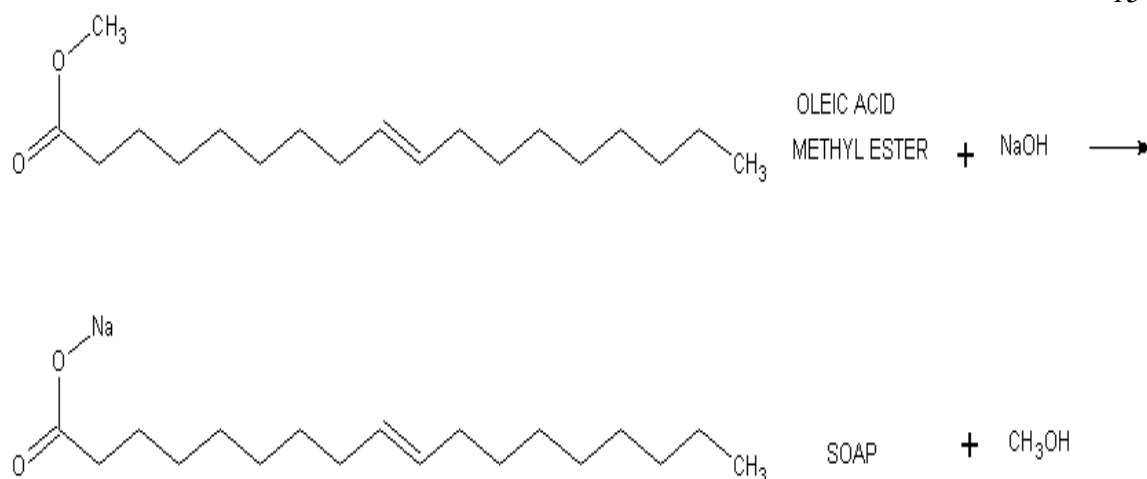


Figure 8. Saponification of methyl esters producing soap and methanol

Kusdiana and Saka (2001) reported the conversion, without using any catalyst, of rapeseed oil with FFA into methyl esters, biodiesel, by using supercritical methanol at 350 °C. Esterification of free fatty acids occurs simultaneously with the transesterification reaction of triglycerides.

Other uses of Alkyl esters

During the last two decades the demand of power generation has outgrown the supply due to rapid industrialization throughout the world. To meet this demand continuous efforts are being made not only to generate more but also to conserve the energy generated by improving the system design. Introduction of power capacitors at various strategic points of the distribution network makes the system more reliable apart from conserving energy.

Central Power Research Institute (Bangalore, India), has successfully developed methyl ester of rapeseed oil (MRSO) which satisfies all the capacitor fluid requirements, from vegetable source – rapeseed oil. They manufactured ten LT power capacitors (10 kVAR 440V) using MRSO, eight of these capacitors have been installed in some industries around Bangalore with the help of Karnataka Electricity Board and have been working satisfactorily for two years (Keshavamurthy and Sridhar, 1998).

Ultrasound

Ultrasound tends to be divided into three categories: power ultrasound (20-100 kHz), high-frequency ultrasound (100 kHz-1MHz) and diagnostic ultrasound (1-10MHz). The earliest applications of ultrasound were at the higher frequencies, and primarily involved imaging of one sort of another. In 1931, for instance, the first patent was obtained for using ultrasonic waves to detect flaws in solids- the forerunner of today's nondestructive testing of metals and structures. And throughout World War II, the U.S. Navy and its allies had the benefit of sonar (sound navigation ranging) in their searches for enemy submarines (Noble, 2002).

It is clear that the growing interest in ultrasound technology is being fueled by developments in transducer technology. An early application of 2-KW transducer , for instance, was used in oil wells to reduce the viscosity of crude oil before it was pumped to the surface. Sonicators are being used in the paint and pigment industry to disperse dyes and inks, and in the ceramics industries to degas slips and create denser castings. Applications in the biotech sector include the lysing of cells to extract proteins, while the chemical industry uses the equipment to form emulsions, catalyze reactions and reduce particle size (Noble, 2002).

As mentioned above ultrasound has a lot of potential for systems with inherent mixing deficiencies. An experimental determination of the residence time distribution, RTD, on high frequency ultrasonic reactors using a NaCl solution as tracer and an inlet pulse as stimulus technique, showed that it is possible to get a perfect mixing without mechanical stirring as soon as ultrasonic irradiation operates. Fresh water was continuously fed by one peristaltic pump into a PVC ultrasonic cylindrical reactor (diameter 10 cm height 10 cm) of 500 KHz and the perturbation caused by the rapid injection of $5 \times 10^{-7} \text{ m}^3$ of a NaCl solution (0.20 Kg m^{-3}) on the input flow was analyzed by a conductivity electrode located at the outlet pipe (Gondrexon et al., 1998).

Different experiments carried out in the ultrasonic reactor at 0, 40, 70 and 100 W of ultrasonic power; 1.66×10^{-7} , 3.33×10^{-7} , 5×10^{-7} , 6.66×10^{-7} and $1 \times 10^{-6} \text{ m}^3 \text{ s}^{-1}$ of input liquid flow rate; and/or 1×10^{-4} , 2×10^{-4} , and $3 \times 10^{-4} \text{ m}^3$ of volume of reactor, determined that under these experimental conditions when ultrasonic irradiation is applied the experimental sonochemical reactor seems to behave like an ideal flow system.

According to Gondrexon et al., (1998) this CSTR behavior is obtained by the combined effect of acoustic streaming and the propagation of the acoustic waves in the liquid. It is important to note that the nature and efficiency of these effects are firstly related to the frequency of the wave and to the ultrasonic energy. However the reflection and transmissions of waves are an additional factor as the presence or not of standing waves, and the shape and dimensions of the reactor have to be taken into account since they determine the ultrasonic energy distribution in the volume.

Ultrasound has been used to enhance solid-liquid chemical process rates. Tekin et al., (2001) observed that the effect of ultrasound over the dissolution rate of phosphate rock in nitric acid is on the pre-exponential factor A of the Arrhenius equation:

$$k = Ae^{-E_a/RT} \quad (1)$$

Where:

$$A = \alpha(1 + \gamma W)^\beta$$

W = Ultrasound power, Watts

k = First-order reaction rate constant based on unit surface, cm/min

E_a = Energy of Activation, KJ/mol-K

R = Gases constant, KJ/mol

α, β, γ constants which depend on the reaction.

To investigate the effect of ultrasound power input on the reaction kinetics, they conducted experiments in both the presence (ultrasound power of 10.96, 16.43, 21.91 and 27.39 W) and absence of ultrasound, always keeping a constant magnetic stirring of 800 rpm to avoid particles to settled down the reactor. The setting of the power input was controlled varying the amplitude of the ultrasound generator (a linear dependence between amplitude setting and power input was found by calorimetric method).

The conversion-time data were analyzed for different acid concentrations, particle sizes and temperatures applying the kinetically controlled first-order rate “shrinking core” model. This fits the rate better than the diffusion-controlled model.

The estimated activation energy of the reaction with ultrasound was 15.97 kJ/mol. It was estimated from the Arrhenius equation; a very similar value of 16 kJ/mol was found in the non-ultrasound experiments. Thus, ultrasound doesn't influence the activation energy of this reaction.

The dependence of the pre-exponential factor A of the Arrhenius equation with the ultrasound power for this reaction is well described by the model proposed above when $\alpha=144$, $\beta=2.54$ and $\gamma=1.659$.

It is important to note that in many processes a decrease of the ultrasonic effects with increasing temperature can be observed. In chemical conversions this fact often requires an optimization procedure: high ultrasonic efficiencies are achieved only at low temperatures, when the reaction kinetics are very slow. As the poor ultrasonic effects at high temperatures lead to very low efficiencies, the influence of the temperature should also be found in recording the power quantities in an ultrasonic system (Löning, 2002).

Ultrasound emulsification was carried out successfully on the system water/kerosene/polyethoxylated (20 EO) sorbitan monostearate. A study performed by Abismail et al. (1999) with these systems determined that the power ultrasound gives smaller average drop sizes, expressed as Sauter diameters, than those produced by mechanical agitation.

A Sauter diameter can be calculated from the raw data of a laser granulometer as:

$$d_{32} = \frac{\sum n_i d_i^3}{\sum n_i d_i^2} \quad (2)$$

Emulsions of 80 ml were prepared at room temperature, dissolving different amounts of surfactant polyethoxylated(20 EO)sorbitan monostearate in distilled water, adding kerosene as oil and supplying energy over a controlled period of time.

These investigators found that after 30 seconds the d_{32} is three times smaller with ultrasound than with mechanical agitation (0.37 μ m vs 1.14 μ m) for an oil volume fraction of 0.25 and a surfactant concentration of 10 g/L, however less energy was applied with the ultrasound horn (Misonix sonicator XL 2020, 20 KHz, 130 W) than with the mechanical agitator (Ultra-Turrax, 10000 rpm, 170 W).

From the point of view of lower dissipated energy, experiments with water evidenced a better performance of ultrasound, 53 W, than mechanical agitation, 120 W.

Diffusion and Mass Transfer

Diffusion is the movement, under the influence of a physical stimulus, of an individual component through a mixture. The most common cause of diffusion is a concentration gradient of the diffusing component. A concentration gradient tends to move the component in such a direction as to equalize concentrations and destroy the gradient. However, diffusion can also be caused by a pressure gradient, by a temperature gradient, or by the application of an external force field, as in a centrifuge (McCabe et al., 1985).

Molecular diffusion is a slow process, which is concerned with the movement of individual molecules through a substance by virtue of their thermal energy. The diffusivity or diffusion coefficient of a component A in solution in B, in m^2/s , is defined as the ratio of its flux J_A , in $\text{mol}/(\text{m}^2 \cdot \text{s})$, to its concentration gradient, in $\text{mol}/(\text{m}^3 \cdot \text{m})$.

$$J_A = -D_{AB} \frac{\partial C_A}{\partial z} \quad (3)$$

Which is Fick's first law written for the z direction. The negative sign emphasizes that diffusion occurs in the direction of a drop in concentration (Treybal, 1980).

In the turbulent region, relatively large portions of the fluid, called eddies, move rapidly from one position to the other with an appreciable component of their velocity in the direction perpendicular to the surface past which the fluid is flowing. These

eddies bring with them dissolved material, and the eddy motion thus contributes considerably to the mass-transfer process (Treybal, 1980).

Since the understanding of turbulent flow is incomplete, the equations for turbulent diffusion are written in a manner similar to that for molecular diffusion:

$$J_A = -(D_{AB} + \varepsilon_M) \frac{\partial C_A}{\partial z} \quad (4)$$

where D_{AB} is the molecular diffusivity in m^2/s and ε_M is the mass eddy diffusivity in m^2/s . The value of ε_M is a variable and is near zero at the interface or surface and increases as the distance from the wall increases (Geankoplis, 1983).

If an average value $\bar{\varepsilon}_M$ is used and integrating between points 1 and 2,

$$J_{A1} = \frac{D_{AB} + \bar{\varepsilon}_M}{z_2 - z_1} (C_{A1} - C_{A2}) \quad (5)$$

The flux of A from the surface A_1 relative to the whole bulk phase is based on the surface area A_1 since the cross-sectional area may vary. The value of $z_2 - z_1$, the distance of the path, is often not known. Hence equation above is simplified introducing a convective mass transfer coefficient k'_c , in length/time, to be determined experimentally (Geankoplis, 1983):

$$J_{A1} = k'_c (C_{A1} - C_{A2}) \quad (6)$$

Brendel et al., (2002) found a good estimation of mass transfer and reaction rates in a two-phase CSTR reactor using a new approach which consists of a free-model estimation of unknown fluxes from corrupted concentration measurements in both phases, followed by the application of an appropriate kinetic model.

They focused on the flux estimation of a liquid-vapor non-equilibrium system with mass transfer between phases and a chemical reaction taking place in the liquid phase. It is assumed that in the vapor-phase, the source/sink is induced only by the flux migrating from or to the liquid phase, while in the liquid phase mass transfer and chemical reaction are superimposed. The unknown source terms $w_i(t)^v$ and $w_i(t)^l$ can be interpreted as unknown inputs in the dynamical model and this combined with the mass balance of concentration C_i for component i in the liquid phase leads to the following equations:

$$\frac{\partial C_i}{\partial t} = \frac{1}{V_r} (C_i^{input} \dot{V}_{total}^{input} - C_i \dot{V}_{total}^{out} + w_i^l) \quad (7)$$

$$r_i = w_i^v + w_i^l \quad (8)$$

$$j_i = w_i^v \quad (9)$$

where:

C_i : Concentration of component i in the liquid phase determined by chemical analysis.

V_r : Volume of the reactor.

\dot{V} : Volumetric flow rate, [Volume/time]

r_i : Reaction rate.

j_i : Mass transfer rate.

Then, the estimation of mass transfer and reaction rates from concentrations data for each phase is possible by formulation and solution of an optimal control problem.

For one multicomponent phase in a CSTR, each $w_i(t)$ is found introducing a new variable y_i :

$$y_i(t) = c_i(t)V_r - c_i(t_o)V_r - \int_{t_0}^t c_i^{in}(\tau)\dot{V}_{total}^{in} - c_i(\tau)\dot{V}_{total}^{out} d\tau \quad (10)$$

$$\frac{\partial y_i(t)}{\partial t} = w_i(t) \quad (11)$$

Finally the mass transfer and kinetic rates are determined by algebraic transformations from the $w_i(t)$'s. The authors emphasize in the use of regularizing methods for discrete and noisy measurements due to the derivative cannot be calculated directly.

Mixing

When two immiscible liquids meet at the mixing impeller, shear stresses occur in the outlet stream which produce drops of one phase within the other. Equilibrium is established between break up and coalescence as the mixture circulates in the tank. The result is to produce a range of drop sizes (Millich and Carraher, 1977).

Average drop and size distribution will depend upon the mixing variables and the flow pattern as well as the physical properties of the two liquids. Many types of immiscible liquid systems are encountered in organic synthesis. The more common systems are water and hydrocarbons, polymerizations, and acidic or alkaline solutions to be combined in organic liquids.

The terms emulsion and dispersion are often used interchangeably. However, a dispersion is a general term implying distribution, whereas an emulsion is a special case of dispersion with a stable nonsettling and non coalescing distribution of colloidal-sized drops of one liquid in another. A familiar example of an emulsion is homogenized milk and oil in water emulsion.

Production of the small drop size required for an emulsion generally calls for much higher impeller speeds and power input than for a dispersion. However chemical reagents are frequently added to give surface effects, to lower the interfacial tension, and to allow production of smaller drops. Very little stirring is required to produce large interfacial areas in such cases.

A dispersion is a dynamic mixture that exists because energy is continuously supplied to the mixture itself. Since the droplet size will be larger than that prevailing in an emulsion, considerable less power is required for the desired result.

The dispersed phase may be either of the two fluids, regardless of their volume. Generally, if a radial-flow impeller is located just below the interface of the two fluids at the start of the mixing process, the lighter or upper phase will be drawn into the lower phase and dispersed in it. This dispersion exists only as long as the mixer is in operation at the proper speed. A speed change can often result in a phase inversion.

There is an economic limit to the minimum drop obtainable with a particular drop mixing setup. Correlations between drop size and power input indicate that a small drop size or a larger interfacial area can be achieved only at the expense of relatively high power consumption.

With approximately uniform mixing turbulence throughout the tank, the suspended droplets will be subdivided until they reach an equilibrium drop size as a result of two opposing mechanisms: drop coalescence and drop break up. The intensity of turbulence will not be uniform throughout a tank. In those areas where less turbulence occurs, colliding droplets will coalesce to form larger droplets. When a larger droplet is transported to an area of higher turbulence, it will be broken up.

A properly designed fluid reaction vessel for an immiscible liquid system will establish a dynamic equilibrium to control droplet size and interfacial area to the greatest practical degree.

Since many reactions depend on effective mass transfer across liquid-liquid interfaces, it is important to obtain the maximum practical interfacial area. The selection of the impeller and speed will vitally affect the drop size and dispersion and, accordingly, the interfacial area. However, if the drop size is too small the dispersion will be difficult to separate. Various immiscible liquid systems exhibit different responses to flow and to fluid shear stresses or turbulence. Obviously this means that it is important to determine which is more critical (flow or turbulence) and the acceptable ratio of flow to turbulence (or head).

The ultimate stability of an emulsion is determined by the interfacial tension, drop size, and chemical ingredients and is favored by low interfacial tension. Emulsification is ordinarily obtained in special equipment that is designed to produce

high liquid shear stresses. Homogenizers, which produce shear stresses and high turbulence, are used for rapid emulsion formation. For example, in a saponification reaction when an alkali solution is to be added to an oil, the addition should be made as near the eye of the impeller as possible. This will assure the most rapid generation of small drops and distribute them quickly in the impeller flow. Rapid distribution and uniformity of area will promote rapid reaction and result in the most efficient use of the chemicals.

If a mixer produces a dispersion where some drops are smaller than the stable drop size, these drops coalesce to a higher average size. If the mixer is producing stable drop sizes, the emulsion will remain in this stable condition.

Impeller location is vital in any dispersion action in immiscible liquid mixing. Depending upon the fluid properties of the two phases, it may be possible that only one phase can be dispersed in the other, or it may be possible to disperse either phase. If only one phase can be dispersed in the other, then the impeller can be located in either phase. If it is possible to disperse either phase, then starting a batch operation with the impeller in the desired continuous phase will make that phase the continuous one. If, in a batch operation, dual impellers are used at lower mixer speeds and power levels, and one is used in each phase, two separate dispersions would be obtained. At high horsepower levels, however, the most stable dispersed phase would eventually become the predominant one.

In the case of acoustic cavitation, absorption of the ultrasonic wave during its propagation in the cavitating liquid is responsible for an energy gradient that induces a macroscopic liquid flow called acoustic streaming. Acoustic streaming causes the mixing effects experienced in the liquid, and therefore, it is important in the design of sonochemical reactors. Vichare et al., (2001) did a mixing time analysis in a

sonochemical reactor. They established a relationship between the mean horn surface velocities (frequency \times amplitude) and the mean velocities estimated from the mixing time measurements. A correlation has been developed for the prediction of the mixing time, the time required for 95% mixing to be complete, using a method similar to that used for liquid jet mixing. The experiments were conducted using an ultrasonic horn of 22.7 kHz with different cross-sectional area of the horn tip.

Two beakers of 1 and 2 liters filled with water served as batch reactors and the mixing time measurements were done with the help of a digital conductivity meter and a chart recorder to record the variation of conductivity with time when a pulse of 1% NaCl solution was added to the water in the vessel as indicated in the following figure.

According to the results obtained by these investigators, the wave patterns formed in this system are complex and can be considered as the mixture of spherical and planar waves. The range of the average liquid circulation determined in this study was 9.8-50 cm/s near to values of 5-50 cm/s found by particle image velocimetry (PIV) technique used in other studies. Both can be compared with the theoretical displacement velocity of 4.48 cm/s.

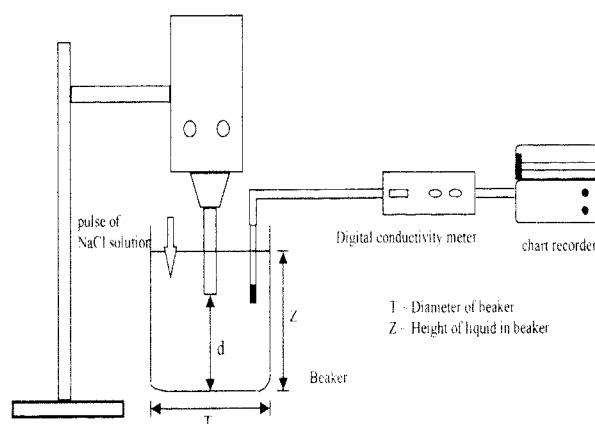


Figure 9. Experimental Set-up (taken from Vichare et al., 2001).

OBJECTIVES

To develop a mathematical model to simulate Oil/Alcohol transesterification reaction under ultrasound mixing conditions accounting for effects of type of alcohol, type of feedstock, temperature, and intensity of sonication on the reaction rate during Biodiesel formation.

THEORY

In this chapter the theory of the most relevant topics related to this research are discussed including cavitation, mixing and mass transfer models.

Cavitation

Cavitation Phenomena have been widely studied by utilizing both linear and nonlinear theory. However nonlinear theory is required in order to deal with the behaviour of bubble containing gas or vapor in hydrodynamical applications, and in acoustical applications where the pressure amplitude is relatively high.

Quasistatic Regime: Blake Threshold

The standard Blake cavitation threshold allows to identify the critical radius, which separates stable and unstable bubbles that are in equilibrium. The Blake Threshold pressure is the standard measure of static acoustic cavitation. Bubbles forced at pressures exceeding the Blake Threshold grow quasistatically without bound (See Figure 10).

“Quasistatic” means that the liquid pressure changes slowly and uniformly with inertial and viscous effects remaining negligible during expansion or contraction of the bubble. At equilibrium, the pressure, P_B , inside a spherical bubble of radius R is related to the pressure, P_L , of the outside liquid through the normal stress balance across the surface:

$$P_L = P_B - (2\sigma/R) \quad (12)$$

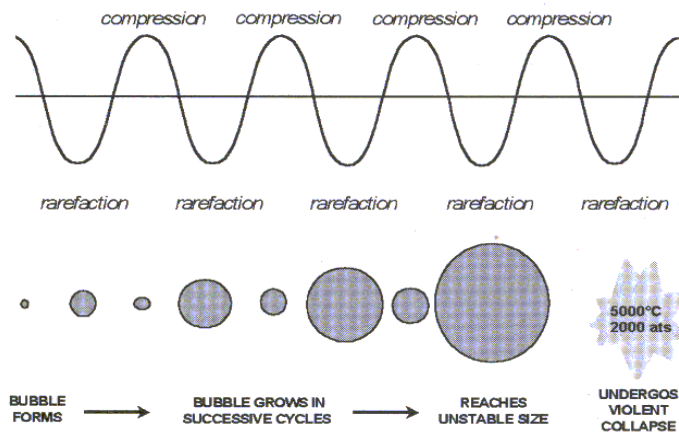


Figure 10. Bubble: forming and collapsing (Taken from Mason, 1999).

where σ is the surface tension of the liquid. For vapor cavitation, $P_B \equiv P_v$, the vapor pressure of the liquid. This means that, in this case, the cavitation bubble can be stable only if the pressure liquid is lower than the vapor pressure by $2 \frac{\sigma}{R}$.

In the other case, when both vapor and gas cavitation are present inside the bubble, $P_B \equiv P_v + P_g$.

For isothermal conditions, assuming ideality, the pressure of gas is given by the equation of the state:

$$P_g \equiv (P_0^\infty - P_v + \frac{2\sigma}{R_0}) \left(\frac{R_0}{R}\right)^{3(\gamma=1)} \quad (13)$$

where:

P_0^∞ : Static pressure of the liquid at equilibrium.

R_0 : Radius of Bubble at equilibrium.

γ : Polytropic index of the gas, for isothermal conditions it takes the value of one.

Defining a constant term \tilde{G} ; $\tilde{G} = (P_0^\infty - P_v + \frac{2\sigma}{R_0})R_0^3$; the equation (12)

becomes:

$$P_L = P_v + \frac{\tilde{G}}{R^3} - \frac{2\sigma}{R} \quad (14)$$

Equation (14) above is represented by Figure 11, which shows a minimum value at a critical radius labeled R_{crit} . For values of P_L which are above the critical value P_{Lcrit} , but below the vapor pressure P_v , Equation (14) yields two possible solutions for the radius R . Bubbles whose radius are less than the Blake radius, R_{crit} , are stable to small disturbances, whereas bubbles with R greater than R_{crit} , are unstable to small disturbances.

Differentiating P_L , respect to R , in order to find the minimum, the following expressions are established:

$$R_{crit} = \left(\frac{3\tilde{G}}{2\sigma} \right)^{1/2} ; P_{Lcrit} = P_v - \left(\frac{32\sigma^3}{27\tilde{G}} \right)^{1/2} ;$$

and

$$R_{crit} = \frac{4\sigma}{3(P_v - P_{Lcrit})} \quad (15)$$

In the quasistatic regime, it can be assumed that surface tension dominates, then P_v is ignored. So that, $P_0^\infty \ll \frac{2\sigma}{R_0}$ and $\tilde{G} \approx 2\sigma R_0^2$.

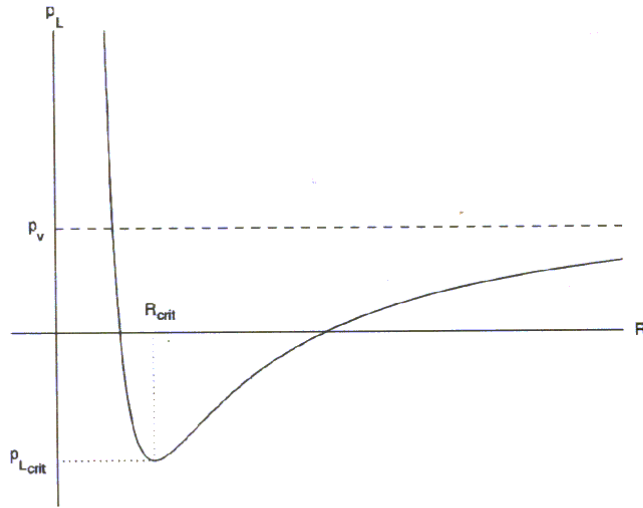


Figure 11. Pressure in the liquid, P_L , versus bubble radius, R , according to Blake Threshold (Taken from Harkin et al. (1999)).

Defining a new variable, P_{Blake} , as

$$P_{Blake} = P_0^\infty - P_{Lcrit} \quad (16)$$

Combining equations the following is obtained:

$$P_{Blake} = P_0^\infty + 0.77 \frac{\sigma}{R_0} \quad (17)$$

In summary, in the quasistatic regime where the Blake threshold is valid (remember that it must be valid to neglect inertial and viscous effects), P_{Blake} is the amplitude of the low frequency acoustic pressure beyond which acoustic forcing at higher pressure is sure to cause cavitation. This criterion is especially important for gas bubbles in liquids when surface tension is the dominant effect, and it could be applied to cases in which the frequency of the applied sound field is very much less than the natural frequency of oscillation of the bubble.

Non-Quasistatic Regime: Bubble dynamics

In contrast when the acoustic pressure fields are not quasistatic, bubbles generally evolve in highly non-linear fashions. Two distinct types of bubble motion are possible: in the first are stable cavities or bubbles that oscillate for many periods of the sound field, whereas in the second are transient cavities that exist for less than one cycle.

An important characteristic to note in the acoustic cavitation is that the change in the radius of the bubble could not be proportional to the sound pressure, and the high compressibility of the gas bubbles means that much potential energy is obtained from the sound waves when the bubbles expand and that kinetic energy is concentrated in very small volumes when the bubbles collapse, producing very high local pressures and temperatures.

Stable cavitation

This cavitation could be related to small changes in volume, and then linear theory applies and yields much useful information. The case of an empty spherical

bubble expanding and collapsing, is expressed for an incompressible fluid by the following dynamic equation (Young, 1989):

$$\frac{P_{Lwall} - P_{\infty}}{\rho} = R \frac{d^2 R}{dt^2} + \frac{3}{2} \left(\frac{dR}{dt} \right)^2 \quad (18)$$

where:

$P_{Lwall} = P(t)$ = pressure in the liquid at the bubble wall; R is the radius of the bubble, P_{∞} = pressure in the liquid at infinity, ρ = density of the incompressible liquid and t = time.

For a spherical bubble filled with gas, expanding and collapsing, this gas absorbs the energy of the liquid eventually collapsing inwards. This phenomenon is expressed for an incompressible fluid by the following dynamic equation (Young, 1989):

$$R \frac{d^2 R}{dt^2} + \frac{3}{2} \left(\frac{dR}{dt} \right)^2 = \frac{1}{\rho} \left[\left(P_0 + \frac{2\sigma}{R_0} \right) \left(\frac{R_0}{R} \right)^{3\gamma} - \frac{2\sigma}{R} - P_{\infty} \right] \quad (19)$$

If viscous effects of the liquid are considered, taking μ as the shear viscosity of the liquid, the equation above will become:

$$R \frac{d^2 R}{dt^2} + \frac{3}{2} \left(\frac{dR}{dt} \right)^2 = \frac{1}{\rho} \left[\left(P_0 + \frac{2\sigma}{R_0} \right) \left(\frac{R_0}{R} \right)^{3\gamma} - \frac{2\sigma}{R} - \frac{4\mu}{R} \left(\frac{dR}{dt} \right) - P_{\infty} \right] \quad (20)$$

Equations (18), (19) and (20) are special cases of dynamic of bubbles, they are often called the Rayleigh-Plesset equation.

To find solutions to Rayleigh-Plesset equation when a sound field exists in the liquid, the pressure of liquid, P , in the vicinity of the bubble is represented by:

$$P = P_0 + P_A \cos \omega t \quad (21)$$

Where P_0 is the steady pressure in the absence of the sound field (usually approximately equal to atmospheric pressure), ω is the angular frequency and P_A is the amplitude of the driving pressure.

Transient cavitation

In this cavitation, the expansion of the bubble is very fast to a radius much greater than the maximum radius reached during stable cavitation. Then it collapses violently, often disintegrating into a mass of smaller bubbles. The bubble wall reaches at least the speed of sound in the liquid.

In Figure 12, the maximum relative radius is plotted as a function of the initial radius R_0 for $f = 14.3$ kHz and an acoustic pressure amplitude of 4 bar. For R_0 about 5×10^{-3} cm, a cavity expands to about $10 R_0$, As R decreases, the maximum relative radius rapidly increases until it equals 1000 for R_0 about 2×10^{-5} cm. After reaching a maximum, the curves drops abruptly until $R_{\max}/R_0 = 1$.

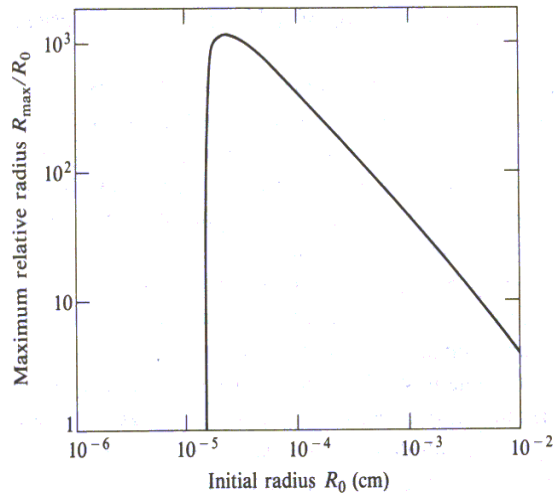


Figure 12. Maximum relative radius R_{\max}/R_0 as a function of R_0 . $f = 14.3$ KHz; $P_A = 4$ bars (taken from Young, 1989).

A stable cavity can be transformed into a transient cavity if the acoustic pressure amplitude is slightly increased; the necessary condition for this transformation is that the relative maximum radius on expansion should be greater than a minimum value given by:

$$\left(\frac{R_{\max}}{R_0} \right) = \left(\frac{7.48 P_g}{P_0} \right)^{1/3} \quad (22)$$

Intensity of Power (Mason, 1999), (Carlin et al., 1972), (Shutilov, 1988)

The intensity of sonication is directly proportional to the square of the amplitude of vibration of the ultrasonic source.

In the case of planar waves, I in W/m^2 , is given by:

$$I = \frac{\rho_l c (a^2 (2\pi f)^2)}{2} \quad (23)$$

where:

ρ_l = Density of liquid, Kg/m^3

c = Velocity of the sound in the liquid, m/s

a = Amplitude of oscillation of the horn, m

f = Frequency of ultrasound, Hz

In equation (23), it's necessary to consider the velocity of the sound if the liquid system contains small gas bubbles; these systems are known as bubbly liquids.

The following equation found by van Wijngaarden, and presented by Young, is used to determine the Velocity of the sound for bubbly liquids if the bubble have oscillations at steady state and surface tension is neglected (Young, 1989):

$$c^2 = \frac{P_\infty}{\rho_l \delta (1 - \delta)} \quad (24)$$

where:

$P_\infty = P_0^\infty$: Static pressure of the liquid, Pa

δ = Void fraction, volume occupied by the bubbles in a unit volume of the mixture.

In general, an increase in intensity will provide an increase in the sonochemical effects, but there are limits to the ultrasonic energy input to the system:

- A minimum intensity for sonication is required to reach the cavitation threshold. This minimum depends upon the frequency.
- When a large amount of ultrasonic power enters a system, a great number of cavitation bubbles are generated in the solution. Many of these will coalesce forming larger, more longer-lived bubbles. These will certainly act as a barrier to the transfer of acoustic energy through the liquid.
- At high vibrational amplitudes the source of ultrasound will not be able to maintain contact with the liquid throughout the complete cycle. Technically this is known as decoupling, and results in a great loss in efficiency of transfer of power from the source to the medium. Decoupling is more pronounced when large numbers of cavitation bubbles build up at or near the emitting surface of the transducer.
- The transducer material used in the sonicator will eventually break down as the increasing dimensional changes in the transducer become large enough to fracture the material.

Several examples exist of situations where above a certain energy input the sonochemical effect is reduced, but a particularly good example is the effect of increasing power on the yield of iodine from the sonication of aqueous KI. The initial response of iodine yield appears to be proportional to power, but this effect is reduced beyond 40W and drops dramatically above 100W where decoupling occurs.

Calorimetric measurement

Calorimetry can be used to measure the Intensity of power entering to a sonochemical reaction. It consists of the determination of the initial rate of heating produced when a system is irradiated by power ultrasound.

For the system the temperature is recorded against time, at intervals of a few seconds, using a thermocouple placed in the reaction itself. From the temperature, T, versus time, t, the temperature rise at time zero, $(dT/dt)_0$, is determined as:

$$Power = \left(\frac{dT}{dt} \right)_0 C_p m \quad (25)$$

where:

C_p = Heat capacity of the solvent, $J\ Kg^{-1}\ K^{-1}$

m = mass of solvent used, Kg

Power = Acoustic power entering to the system, Watts

If this power is dissipated into the system from a probe tip with an area measured in cm^2 , A, then the Intensity of Power, I in W/cm^2 , is given by:

$$I = \frac{\left(\frac{dT}{dt} \right)_0 C_p m}{A} \quad (26)$$

Real electric Power to the transducer

This method uses a wattmeter in order to measure the electrical power to the transducer both when the system is running in air and when it is immersed in the reaction mixture. The transmitted electrical power is the difference between these values. From this the acoustic power entering the reaction can be calculated if the acoustical efficiency is known.

Acoustic streaming (Mason, 1999), (Vichare et al., 2001)

The reactor geometry is an important factor that affects the application of sound in a liquid medium. Sound field produces a time-independent circulation called acoustic streaming. If this streaming is of microscopic scale it is called microstreaming, which depends on ultrasonic frequency, acoustic intensity, viscosity of liquid and reactor geometry. Figure 13 shows a circulation within a probe system containing a liquid medium.

The mean velocity of the net fluid displacement from the vibrating horn face, v_h in m/s, from the planar wave analysis can be computed as:

$$v_h = af \quad (27)$$

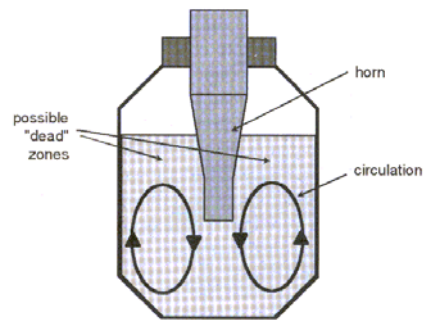


Figure 13. Acoustic streaming produced with a probe system of ultrasound (Taken from Mason, 1999).

where:

$a =$ Amplitude of oscillation of the horn, m

$f =$ Frequency of ultrasound, Hz

It should be noted, however, that the mean velocity of the horn tip is indeed zero as the horn is vibrating in a sinusoidal way. Still, the horn constantly imparts momentum to the different fluid packet every time due to the pressure field created by the vibrating horn surface. The assumptions of equating the sound field to fluid displacement assumes that no energy is lost in random turbulence, and that all the energy is associated with the bulk fluid motion. This is adequate, as the fraction of energy dissipated in the cavitation events is a small fraction of the total energy associated with the sound field and, therefore, the majority of the energy is dissipated in the fluid motion.

The average liquid circulation velocity, v_c in m/s, defined as the maximum distance traveled by a liquid package to complete mixing, is calculated using the equation below:

$$v_c = \frac{5(L)}{\theta_{mix}} \quad (28)$$

where:

L = Loop Length, calculated as the diameter of the beaker plus 2 times the height of the liquid in the beaker, m

θ_{mix} = Mixing time, s

In addition, an assumption that minimum five circulations are required for complete mixing to take place was done.

The value of θ_{mix} can be determined by experimentation or by an empirical correlation, an example of the latter is the formula found by Vichare et al. (2001):

$$\theta_{mix} = 7 \times 10^6 d^{-0.235} \left[\frac{Z^{\frac{3}{2}} T^3 (T + 2Z)^{-2} d_h^{-4}}{v_h^2 g^{\frac{1}{2}} \mu^{-2} \rho_l^2} \right] \quad (29)$$

where:

θ_{mix} = mixing time, s

d = Jet length, m

Z = height of liquid in the beaker, m

- $T =$ diameter of beaker, m
 $d_h =$ diameter of the horn, m
 $v_h =$ velocity of the horn, m/s
 $g =$ acceleration due to gravity, m/s²
 $\mu =$ viscosity of liquid, Ns/m²
 $\rho_l =$ density of liquid, Kg/m³

Mixing (Uhl and Gray, 1967)

The mixing or the dispersion of one phase in another phase with which the first is immiscible is important in many chemical engineering operations such as heat and mass transfer with and without reactions. Dispersion not only brings about a large increase in the interfacial area available for material or heat transfer but also places the fluids in a state of motion which increases the specific rates of both of the above transfer processes.

Dispersions of one fluid into another are produced by injecting one phase into the other as a jet or sheet when surface tension forces cause the latter to collapse into a dispersion of drops or bubbles. Some principles of efficient contacting in continuous dispersed-phase flow may be seen by consideration of the relationship

$$a_i = \frac{6H}{D_p} \quad (30)$$

where:

$a_i =$ Interfacial area per unit volume of mixed phases, m²/m³

$H =$ Fractional volumetric hold-up of dispersed phase.

$D_p =$ Equivalent, mean spherical diameter of one drop or bubble of the dispersed phase, m

The interfacial area may be increased by increasing the hold-up or by reducing the bubble or drop diameter. For a fine-grained dispersion the bubbles or drops obey Stoke's law, $v_t \propto D_p^2$, where v_t is the velocity of rise or fall of the sphere. Moreover $H \propto 1/v_t$, for a fixed dispersed-phase flow rate, so that $a \propto 1/D_p^3$. These arguments, which favor the use of fine-grained dispersions, have to be scrutinized in the light of energy necessary to produce them.

The mechanism of dispersion of fluids

The interdispersion of immiscible fluids is brought about by fluid dynamical forces which have to overcome the static force of surface tension. Such surface forces resist dispersion by attempting to retain bubble or drop sphericity and prevent gross distortion leading to break-up. The dynamic forces which bring about dispersion may be due to buoyancy or induced fluid flow creating viscous or inertial forces which, if they do not act equally over the surface of a drop or bubble, may cause it to deform and eventually break-up. A consequence of these dynamic forces acting unequally over the surface of the drop or bubble is internal circulation of the fluid within the drop or bubble which induces viscous stresses therein. These internal stresses also oppose distortion and break-up.

The three stresses mentioned above are:

Shear stress $\propto \tau$;

Surface Tension $\propto \sigma/D_p$;

$$\text{Viscous stress in dispersed phase} \propto \mu_d/D_p \sqrt{\frac{\tau}{\rho_d}}$$

where the first force, which may lead to dispersion, is resisted by the other two and:

$\tau =$ External shear stress acting on a drop or bubble

$\sigma =$ Fluid interfacial surface tension

$\mu =$ Fluid viscosity

$\rho_d =$ Fluid density

In many cases of practical interest, the viscous stress of the dispersed phase may be ignored, so that for these cases, a dispersed phase particle size equilibrium is reached. This occurs when the ratio of shear to surface tension stresses has a particular value which may be characteristic of the dispersion equipment and perhaps also of the physical properties of the dispersion. Thus the dimensionless Weber number is defined as:

$$N_{we} = \frac{\tau D_p}{\sigma} \quad (31)$$

If the Weber number is evaluated for dispersions in dynamic equilibrium in a particular piece of dispersion equipment where the shear stress is known, the maximum drop or bubble size will thereby be related to the interfacial tension. Thus, D_p will be the maximum diameter of the drop or bubble which can survive at dynamic equilibrium in a flow or turbulent field of shear stress.

A simple application of the above principles is found in the break-up of liquid drops falling through other immiscible liquids or gases. Here the stress due to buoyancy is $\frac{1}{6}(D_p \Delta \rho g)$, and the Weber number is therefore $(D_p^2 \Delta \rho g)/(6\sigma)$.

Experimentally it has been found that a critical value of $N_{We} = 2.4$ defines the break-up of the drop.

Dispersion in mixing vessels

In mixing vessels, mechanical agitation is employed to create shear stress by means of turbulence and it is necessary to evaluate the shear stress due to this turbulence.

Turbulent flow produces primary eddies which have a wavelength or scale of similar magnitude to the dimensions of the main flow stream. These large primary eddies are unstable and disintegrate into smaller eddies until all their energy is dissipated by viscous flow. When the Reynolds number of the main flow is high, most of the kinetic energy is contained in the large eddies, but nearly all of the dissipation occurs in the smallest eddies. If the scale of the main flow is large compared with that of the energy dissipating eddies, a wide spectrum of intermediate eddies exist which contain and dissipate little of the total energy.

Kolmogoroff (1941) concludes that all eddies which are much smaller than the primary eddies are statistically independent of them and that the properties of these small eddies are determined by the local energy dissipation rate per unit mass of fluid. Thus, if a small volume of fluid is considered whose dimensions are small compared with the scale of the main flow, the fluctuating components of the velocity are equal,

and this so-called local isotropic turbulence exists even though the turbulent motion of the larger eddies may be far from isotropic. For local isotropic turbulence the smallest eddies are responsible for most of the energy dissipation and their scale is given by Kolmogoroff (1941) as:

$$l = \frac{\mu_c^{3/4}}{\rho_c^{1/2}} \left(\frac{P}{V} \right)^{-1/4} \quad (32)$$

The mean square fluctuating velocity over a distance d in a turbulent fluid field where $L \gg d \gg l$ (L being the scale of the primary eddies and l that of the smallest eddies) is given by Batchelor (1951) as:

$$\overline{u^2} \propto \left(\frac{P}{V} \right)^{2/3} \left(\frac{d}{\rho_c} \right)^{2/3} \quad (33)$$

The theory of local isotropy may be used to get information on the turbulent intensity in the small volume around the particle. Thus, $\sqrt{\overline{u_{D_p}^2}}$ is a statistical parameter describing the flow of fluid around a particle of diameter, D_p , and may be used in place of the velocity of the particle in the Reynolds and Weber numbers of the particle. It may be concluded that the shear stress due to turbulence is given by:

$$\tau = C1 \rho_c \left(\frac{P D_p}{V \rho_c} \right)^{2/3} \quad (34)$$

where:

C_1 = Constant, a value of 2 was used by Batchelor (1951).

P/V = Power input per volume unit of fluid.

Subscript c indicates properties of the continuous medium.

From the definition of Weber number, taking N_{We} as a constant, characteristic of the mixing equipment, the following expression for D_p is obtained:

$$D_p \propto \frac{\sigma^{0.6}}{\rho_c^{0.2} (P/V)^{0.4}} \quad (35)$$

Shinnar and Church (1960) proposed a semitheoretical argument to predict the effect of coalescence in mixing vessels. Thus the energy of adhesion, E , between two drops of diameter, D_p , is postulated as:

$$E = D_p A \quad (36)$$

Where A , is the force needed to separate two drops to infinity. For dispersion equilibrium, the energy of adhesion is equal to the turbulent energy causing dispersion, so that from the equation (34), which gives the turbulence force per unit area of a drop, the following equation is obtained:

$$\frac{\rho_c^{1/3} \left(\frac{P}{V} \right)^{2/3} D_p^{11/3}}{D_p A} = \text{const.} \quad (37)$$

where,

$$D_p \alpha (A)^{3/8} \left(\frac{P}{V} \right)^{-1/4} \rho_c^{-1/8} \quad (38)$$

Or at constant power number and system properties:

$$D_p \alpha \left(\frac{1}{N} \right)^{3/4} \quad (39)$$

Where:

N = Speed of the impeller in r.p.m.

Calderbank et al. (1965) measured the rate of coalescence in clouds of carbon dioxide bubbles rising through a 10-ft. high column of water according to the following analysis:

If N_b is the number of bubbles in unit volume of dispersion and f is the coalescence frequency factor

$$\frac{-dN_b}{dt} = fN_b \quad (40)$$

where:

$$N_B = \frac{6H}{\pi D_p^3} \quad (41)$$

and

$$t = \frac{h}{v_t} \quad (42)$$

where:

- t = Time.
h = Column height.
 v_t = Average velocity of rise of the bubbles.

Differentiating equation (41):

$$\frac{d(\ln N_B)}{dh} = \frac{d(\ln H)}{dh} - \frac{3d(\ln D_p)}{dh} \quad (43)$$

and incorporating equation (30):

$$\frac{d(\ln N_B)}{dh} = \frac{3d(\ln a)}{dh} - \frac{2d(\ln H)}{dh} \quad (44)$$

Further, from equations (40) and (42) results in:

$$\frac{d(\ln N_B)}{dh} = \frac{-f}{v_t} \quad (45)$$

And combining equations (44) and (45),

$$f = v_t \left[\frac{2d(\ln H)}{dh} - \frac{3d(\ln a)}{dh} \right] \quad (46)$$

Thus from measured changes of H , and a , with height, recorded on semilogarithmic coordinates, the coalescence frequency factor may be evaluated.

The average rising velocity of the bubbles was determined by extrapolation of the hold-up plots to both ends of the column where the inlet and outlet gas flow rates were known.

For conditions under which mass transfer and coalescence take place simultaneously, equation (46) still applies, but in addition, one may write

$$\frac{-dH}{dt} = k_L a \Delta C \quad (47)$$

Where k_L is the liquid-phase mass-transfer coefficient and ΔC is the constant concentration driving force given by $\Delta C = C_i - C$, C_i being the concentration of gas at the gas-liquid interface (the solubility of gas in water in cm^3/cm^3), and C the concentration of gas in the bulk liquid which was measured at the liquid outlet from the column.

From equations (30), (42) and (47),

$$\frac{-d(\ln H)}{dh} = \frac{6k_L \Delta C}{v_i D_p} \quad (48)$$

Equation (48) enables the mass transfer coefficient to be determined from the experimental data to reveal any effect on its value due to coalescence.

Mean Velocity of the Net Fluid Displacement

It is known that high local velocities are obtained by the application of ultrasound in transient cavitation causing an effect of acoustic streaming, but in this case and according to studies presented previously by Vichare et al. (2001), the planar

wave case represented in the equation (27) can be used to explain bulk motion of the fluid if energy lost in random turbulence is neglected (Vichare et. al, 2001).

Combining Equations (23) and (27), and solving for v_h , in m/s:

$$v_h = \sqrt{\frac{I}{2\rho_l c \pi^2}} \quad (49)$$

where:

I = Intensity of power, W/m²

ρ_l = Density of the liquid, kg/m³

c = Speed of sound in the liquid, m/s

Mean Drop Diameter

A drop size distribution is obtained during the emulsion, which can be represented by a mean drop diameter, D_p , as it was shown before in equation (39). There, N is the impeller velocity responsible of the mixing. By analogy, considering that the responsible of the ultrasound mixing is the product of amplitude frequency accounted in the term v_h , we formulate our model for D_p , in m, as:

$$D_p = K_1 \left(\frac{1}{v_h} \right)^{3/4} \quad (50)$$

where:

K_1 = Constant of the reaction system determined experimentally, m^{7/4} · s^{3/4}

v_h = Mean velocity of the net fluid displacement, m/s

Mixing and chemical reaction: Heterogeneous systems in Tank reactors

The interaction of mixing and reaction yield in heterogeneous systems is both poorly formulated and poorly understood. The typical strategy upon a heterogeneous reactor problem is to construct a suitable simplified model to represent the system, collect a body of pilot-plant data, and then hope that the model can be scaled up for plant design.

The interaction of the mixing with reactor performance is used to reduce the mass transfer resistance between the phases. The specific effect of mixing upon reactor performance in tank reactors can be illustrated by a liquid-liquid system in which the reaction occurs only in the dispersed or bubble phase. In this case is very important to note that the rates at which bubbles coalesce has a profound effect upon the reactor operation.

When two dispersed phase liquid drops collide in a stirrer-tank reactor, the drops often coalesce. The union of the two drops is assumed to mix the contents of the drops “perfectly”. It is experimentally verified that the size distribution of drops in a liquid-liquid tank-reactor is quite narrow; simply stated, there is a high probability that a “coalesced” drop will divide into two drops of the original size containing the average concentration of the two original drops. A material balance is made upon the drop concentration distribution:

$$\frac{\partial P}{\partial \tau} = P_0 - P + M \left\{ 4 \int_0^C P(C - \alpha)P(C + \alpha)d\alpha - P \right\} + K \frac{\partial PC^N}{\partial C} \quad (51)$$

where:

A'	=	Reference concentration.
C	=	Dimensionless concentration.
F	=	Volumetric feed rate.
K	=	Dimensionless reaction rate, $(V\phi k_N (A')^{N-1})/(F\phi_f)$
k_D	=	drop mixing rate, the fraction of the dispersed phase which coalesces per unit time.
k_N	=	Nth order irreversible reaction rate constant.
M	=	Dimensionless drop mixing rate, $(k_D V\phi)/(F\phi_f)$.
N	=	Reaction order.
P	=	Dimensionless concentration probability density function, i.e., the probability that the concentration in the dispersed phase will be in the range C to $C+dC$.
P_0	=	Dimensionless inlet concentration probability density function.
V	=	Volume of the tank.
\bullet	=	Dimensionless time, $(t\phi_f F)/(V\phi)$
ϕ, ϕ_f	=	Volume fraction dispersed phase in the tank and inlet.

The mixing of the dispersed phase drops is described by the right-hand term in braces in equation (51). The integral represents the rate at which drops of a specified concentration are formed by coalescence of two drops of the same average concentration. The second term in braces represents the rate at which drops of the specified concentration disappear by mixing with other drops in the tank. The rate at which the coalescence occurs appears in the dimensionless parameter, M . The coalescence rate is a function of stirring rate and dispersed-phase fraction. Other authors have noted that the measured dispersion rate is consistent with:

$$k_D = C_1 \phi^{0.5} N^{2.2} \exp(-C_2 / N^2) \quad (52)$$

where:

N = Stirring rate in r.p.m.

C₁, C₂ = Constants for a particular system and geometry.

Thus, coalescence represents a mixing process in a chemical reactor with which significant changes in the reaction rate or selectivity can be obtained.

Mass Transfer with Chemical Reactions in porous catalysts:

According to hydrodynamic conditions liquid-liquid systems may be regarded either as a solid phase in a fluid-solid system, or as a liquid phase in a gas-liquid system depending on the viscosities. This is the main reason for the small amount of literature found for these systems (Astarita, 1967).

An interesting case of internal diffusion and chemical reaction in spherical catalysts that could be applied in immiscible liquid systems is presented and developed by various authors (Hill, 1977), (Crank, 1979), (Walas, 1991), (Fogler, 1999).

Neglecting external resistance to the mass transfer and assuming that the reactant concentration at the surface is fixed the following equations are derived.

First we perform a steady-state mole balance on species A as it enters, leaves and reacts in a spherical shell of inner radius r and outer radius $r + \Delta r$ of the pellet, see Figure 14:

Input by diffusion = output by diffusion + consumed by reaction

$$\left[4\pi r^2 \left(D_{eff} \frac{\partial C}{\partial r} \right) \right]_{r+\Delta r} = \left[4\pi r^2 \left(D_{eff} \frac{\partial C}{\partial r} \right) \right]_r + K_{kinetic} C^2 (4\pi r^2 \Delta r) \quad (53)$$

Rearranging and dividing by $\bullet r$, when $\bullet r \rightarrow 0$:

$$\frac{1}{r^2} \frac{d}{dr} \left[r^2 \left(D_{eff} \frac{\partial C}{\partial r} \right) \right] = K_{kinetic} C^2 \quad (54)$$

If $D_{eff} = \text{constant}$ and there is not changes in the volume accompanying reaction:

$$\frac{d^2 C}{dr^2} + \frac{2}{r} \frac{dC}{dr} = \frac{K_{kinetic}}{D_{eff}} C^2 \quad (55)$$

with the following Boundary Conditions:

At $r = R$ $C = C_0$ (Conc. of A at the external surface is fixed)

$R=0$ $\frac{dC}{dr} = 0$ (By symmetry)

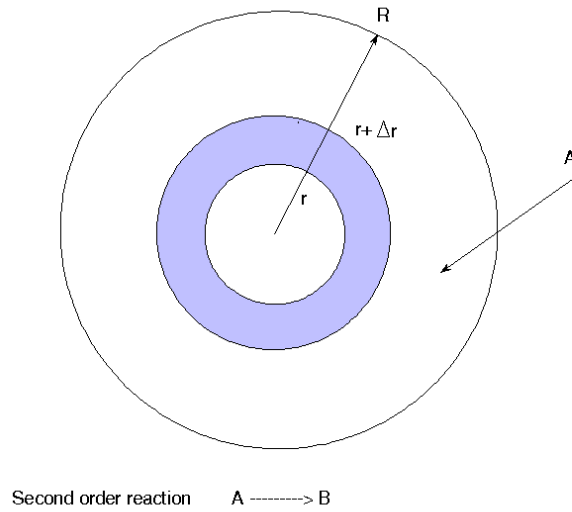


Figure 14. Mass transfer with chemical reaction in a spherical catalyst

Defining a new Thiele modulus, Φ_s , and two dimensionless variables, Y and ρ , to represent the concentration and the radius respectively:

$$\Phi_s = R \sqrt{\frac{K_{kinetic} C_0}{D_{eff}}} \quad (56)$$

$$Y = C/C_0 \quad (57)$$

$$\rho = r/R \quad (58)$$

The initial ordinary differential equation obtained above is transformed into:

$$\frac{d^2 Y}{d\rho^2} + \frac{2}{\rho} \frac{dY}{d\rho} = \Phi_s^2 Y^2 \quad (59)$$

with B.C.:

$$\text{At the surface or } \bullet = 1 \quad Y = 1$$

$$\text{At the center or } \bullet = 0 \quad \frac{dY}{d\rho} = 0$$

To avoid problems of division by zero in the numerical solution of the system, the solution is divided by regions. In the first region, when \bullet is near zero, the L'Hopital's rule is applied:

$$\lim_{x \rightarrow a} \frac{f(x)}{g(x)} = \lim_{x \rightarrow a} \frac{f'(x)}{g'(x)} \quad \text{Then} \quad \frac{\frac{2dY}{d\rho}}{\rho} = \frac{\frac{2d^2Y}{d\rho^2}}{1}$$

Replacing in the ordinary differential equation, ODE, we obtain:

$$3 \frac{d^2Y}{d\rho^2} = \Phi_s^2 Y^2 \quad (60) \quad \text{For } 0 \leq Y \leq 0.1$$

The second region is described by:

$$\frac{d^2Y}{d\rho^2} + \frac{2}{\rho} \frac{dY}{d\rho} = \Phi_s^2 Y^2 \quad (61) \quad \text{For } 0.1 \leq Y \leq 1$$

Numerical integration is started at the center and is then continued for above 10% of the way, first region, and continued the rest of the way, second region, with the complete ODE. An estimate is made of Y_0 at the center; then the solution is completed and examined to see if the requirement $Y=1$ when $\bullet=1$ is met at the surface. The solution obtained in the first region supplies starting values for the solution of the

ODE in the second region. As an intermediate step, the solution of the differential equations supplies the concentration gradient in the sphere, but this result is of less practical interest than the effectiveness.

The effectiveness is given by:

$$\eta = \frac{4\pi R^2 D_{eff} \left(\frac{dC}{dr}\right)_1}{K_{kinetic} (4/3)R^3 C_0^2} = \frac{3\left(\frac{dY}{d\rho}\right)_1}{\Phi_s^2} \quad (62)$$

Mass Transfer with Chemical Reactions Shrinking Model:

The Shrinking core model is used to describe situations in which solid particles are being consumed either by dissolution or reaction and, as result, the amount of the material being consumed is “shrinking”. This model applies to areas ranging from pharmacokinetics (e.g., dissolution of pills in the stomach) to the formation of an ash layer around a burning coal particle, to catalyst regeneration. Illustrations of the principles of this model are found in the texts of Fogler (1999) and Levespiel (1972). The case of removal of carbon from a porous catalyst pellet studied by Fogler (1999) and Levespiel (1972) is described below.

A core of unreacted carbon is contained between $r = 0$ and $r = R_0$. Oxygen diffuses from the outer radius R_0 to the radius R , where it reacts with carbon to form carbon dioxide, which then diffuses out of the porous matrix. The reaction at the solid surface is very rapid, so the rate of the oxygen diffusion to the surface controls the rate of carbon removal from the core. See Figure 15 shown below:

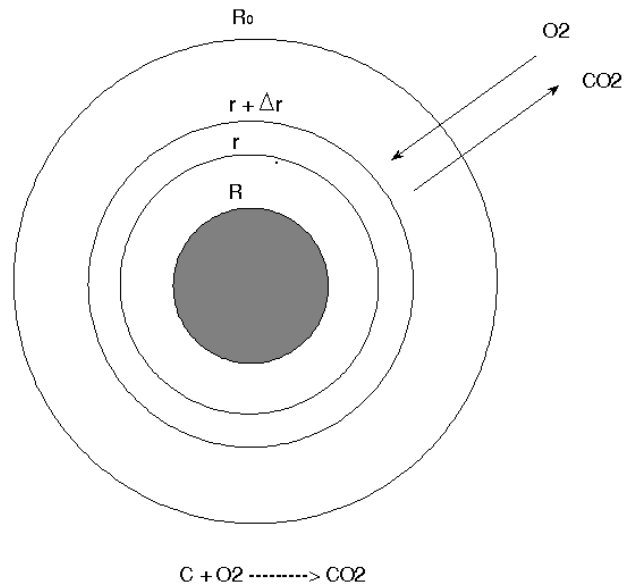


Figure 15. Shrinking model diffusion for the removal of carbon from a spherical catalyst.

Although the core of carbon is shrinking with time (an unsteady-state process), it is assumed that the concentration profiles at any instant in time over the distance $R_0 - R$ are in steady state. This assumption is referred to as the quasi-steady state assumption, QSSA.

In applying a differential oxygen mole balance over the increment Δr located somewhere between R_0 and R , we recognize that O_2 does not react in this region, and reacts only when it reaches the solid carbon interface located in $r = R$. We shall let species A represent O_2 .

$$W_{Ar} 4\pi r^2 \Big|_r - W_{Ar} 4\pi r^2 \Big|_{r+\Delta r} = 0 \quad (63)$$

Where W_{Ar} is the molar flux of oxygen or rate of A diffusion. Now dividing by Dr and taking limit gives:

$$\frac{d(W_{Ar}r^2)}{dr} = 0 \quad (64)$$

For every mol of A that diffuses into the spherical pellet, 1 mol of CO_2 diffuses out, the constitutive equation for Equimolar Counter Diffusion, EMCD, for constant total concentration becomes:

$$W_{Ar} = -D_e \frac{dC_A}{dr} \quad (65)$$

Replacing and dividing by $-D_e$:

$$\frac{d}{dr} \left(\frac{dC_A}{dr} r^2 \right) = 0 \quad (66)$$

with B.C.:

At the outer surface of the particle, $r = R_0$: $C_A = C_{A0}$

At the fresh carbon/gas interface, $r = R(t)$; $C_A = 0$

Integrating twice yields:

$$C_A = -\frac{k_1}{r} + k_2 \quad (67)$$

Using the boundary conditions to eliminate k_1 and k_2 ,

$$\frac{C_A}{C_{A0}} = \frac{1/R - 1/r}{1/R - 1/R_0} \quad (68)$$

Deriving respect to r and multiplying by $(-D_e)$, an expression for the molar flux of oxygen to the gas-carbon interface is found.

$$W_{Ar} = -D_e \frac{dC_A}{dr} = \frac{-D_e C_{A0}}{(1/R - 1/R_0)r^2} \quad (69)$$

Performing an overall balance on elemental carbon and assuming elemental carbon does not enter or leave the particle.

$$r_c'' 4\pi R^2 = \frac{d\left(\frac{4}{3}\pi R^3 \rho_c \phi_c\right)}{dt} \quad (70)$$

Where \bullet_c is the molar density of the carbon and ϕ_c is the volume fraction of carbon in the porous catalyst. Simplifying:

$$\frac{dR}{dt} = \frac{r_c''}{\phi_c \rho_c} \quad (71)$$

The rate of disappearance of carbon is equal to the flux of O_2 to the gas-carbon interface:

$$-r_c'' = -W_{Ar} \Big|_{r=R} = \frac{D_e C_{A0}}{R - R^2 / R_0} \quad (72)$$

The minus sign arises with respect to W_{Ar} because O_2 is diffusing in an inward direction, opposite to the increasing coordinate (r) direction:

$$\frac{-dR}{dt} = \frac{D_e C_{A0}}{\phi_c \rho_c} \left(\frac{1}{R - R^2 / R_0} \right) \quad (73)$$

Integrating with limits $R=R_0$ at $t = 0$, the time necessary for the solid carbon interface to recede inward to a radius R is

$$t_c = \frac{\rho_c R_0^2 \phi_c}{6D_e C_{A0}} \left(1 - 3\left(\frac{R}{R_0}\right)^2 + 2\left(\frac{R}{R_0}\right)^3 \right) \quad (74)$$

The time necessary to consume all the carbon in the catalyst pellet is

$$t_c = \frac{\rho_c R_0^2 \phi_c}{6D_e C_{A0}} \quad (75)$$

Estimation of Diffusion and reaction limited regimes (Fogler, 1999)

In many instances it is of interest to obtain quick estimates to learn which is the rate-limiting step in a heterogeneous reaction. The Weisz-Prater criterion, C_{WP} , uses measured values of the rate of reaction to determine if internal diffusion is limiting the reaction. This criterion is defined as:

$$C_{WP} = \eta \Phi_s^2 \quad (76)$$

If

$$C_{wp} \ll 1$$

There are no diffusion limitations and if

$$C_{wp} \gg 1$$

internal diffusion limits the reaction severely.

PROCEDURE

State of the Art

A literature search of papers, books, databases and internet web-pages related with this project was done continuously during the project. CHEMICAL ABSTRACT, SCIENCEDIRECT, PROQUEST Digital Dissertations and EBSCO commercial Databases, Chemistry WebBook Database of NIST, BRIDGE Database of Department of Energy, and BIODIESEL NATIONAL BOARD web page, have been a good sources of information. Another important search program, called COPERNIC, that uses various search engines was extensively used.

Materials and Reagents

Commercial edible soybean oil and white tallow from Gardner Smith LLC, Houston TX (approximately water and FFA contents of 0.11% and 0.03%) were used. Anhydrous methanol, ethanol, 1-butanol, and 2-propanol (HPLC grade) were supplied by Fisher Scientific. Potassium hydroxide (A.C.S. pellets), glycerol (99.5+%) and tetrahydrofuran, THF, (HPLC grade), by Aldrich Chemical Company, Inc.

Analytical standards of mono-, di-, and triglycerides were purchased from Aldrich Chemical Company, Inc.. The following additional standards recommended by ASTM D6751 and PS 121, a provisional standard of commercial biodiesel, were supplied by Alltech Associates, Inc.: (1) triolein (C18:1, [cis]-9-Octadecenoic acid, triglycerides); (2) tricaprin (C18:1, [cis]-9-Octadecenoic acid, triglycerides); (3) 1,3-diolein (C18:1, [cis]-9-Octadecenoic acid, diglycerides); and (4) monoolein (C18:1, [cis]-9-Octadecenoic acid, monoglycerides). A methyl oleate (C18:1, [cis]-9-Octadecenoic acid, methyl ester) was also acquired.

Laboratory Equipment Start Up

Analytical instruments used in this study have been separately tested with similar materials to those to be analyzed in this project, and each analysis method was validated using their respective standards and guidelines. A description of the equipment employed in this study is presented below:

GC-TC

A GO-MAC gas chromatograph with a silica gel column coupled with a thermal conductivity detector was employed to get rapid identifications of the methanol and glycerol polar phases produced by transesterification.

GC-MS

A Hewlett Packard 6890 Series Gas Chromatograph coupled with a Hewlett Packard 5973 Mass Selective Detector. A J & W Scientific 5% phenylpolydimethylsiloxane (DB-5HT) capillary column, length of 30m, a film thickness of 0.1 μm , upper temperature limit of 400°C, and an internal diameter (ID) of 0.32 mm.

The following parameters and experimental conditions were used:

To determine oils compositions the temperatures of injector and detector were 300°C. Mode injector: Split-less. Oven temperature was held at 50°C for 1 min. After that, the oven temperature was ramped from 50 to 300°C at 20°C/min, and then held at 300°C for 16.5 min., for a total run time of 35 min. Helium was used as carrier gas with a flow rate of 6.6 mL/min and a backpressure of 61.4 kPa. MS detector conditions were

as follow: capillary direct interface 300°C; ion source 230°C; mass/charge 50-550 a.m.u.; scan rate 2.94 scan/sec; electron multiplier 1482V. All liquid samples were diluted at a concentration of 35 grams in 100 mL of THF, and filtrated at 0.2 µm PTFE membrane (Whatman Inc., New Jersey). One microliter samples were injected manually with a syringe (Microliter Syringe 1705 RNR 10 µL; Hamilton Co., Nevada).

HPLC

High Performance Liquid Chromatography (HPLC) was used to evaluate the conversion efficiencies of triglyceride into biodiesel. Analyses were performed using Hewlett Packard series 1100 with a refractive index detector. The size exclusion column was a Princeton SHERE CYANO 60A column from Princeton Chromatography Inc., with a length of 250 mm and ID of 4.6 mm. The mobile phase used was THF (HPLC grade). The column temperature was 25°C and the mobile phase flow rate was held at 0.35 mL/min. A recorder model Water 740 registered the detector signal and performed the integration of the peaks. The run time was 20 min. Approximately, 40 µL sample was injected manually in an injector loop of 20 µL.

Standards of glycerides and biodiesel described in the Materials and Reagents section were used for identification of the peaks of tri-glycerides, di-glycerides and a mix of methyl esters and monoglycerides. After that, a calibration curve with different proportions of tri and di-glycerides as well as methyl esters were made, taking into account the concentration range useful for the experimentation.

Table 3, and Figures 16, 17 and 18, presented by Borrero, show the different mixes of standards used and the calibration curves obtained (Borrero, 2002).

Note the good agreement between the expected compositions by calculation and the curve fit.

Table 3. Mixes of standards to construct calibration curves to quantify Tri, di-glycerides and methyl esters.

Standard No.	Triglyceride [g/ml]	Diglyceride [g/ml]	Methyl ester [g/ml]
1	0.00012	0.00000	0.03858
2	0.00014	0.00007	0.03570
3	0.00008	0.00000	0.03576
4	0.00000	0.00010	0.03578
5	0.00166	0.00044	0.03323
6	0.00566	0.00196	0.02849
7	0.01025	0.00358	0.02243
8	0.01626	0.00547	0.01669
9	0.02133	0.00729	0.00751
10	0.00104	0.00022	0.03652
11	0.00038	0.00029	0.03482
12	0.00024	0.00000	0.03579
13	0.00000	0.00000	0.04058

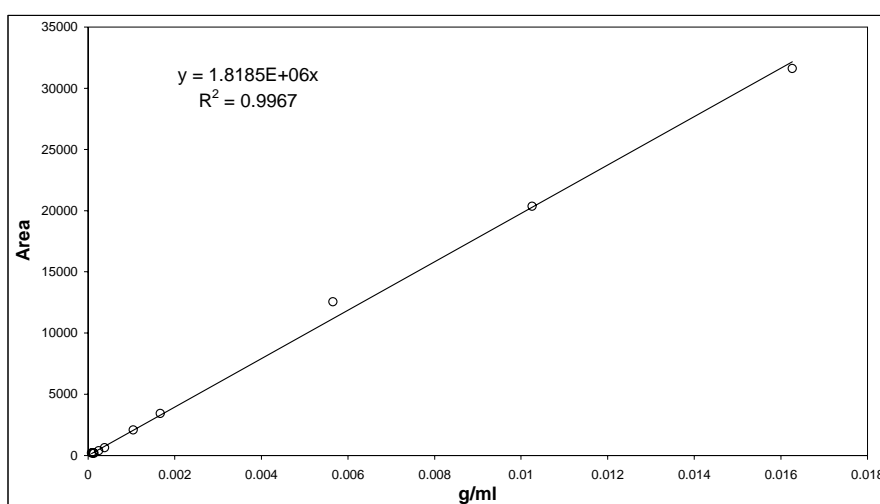


Figure 16. Tri-glycerides calibration curve. Method of quantification by areas.

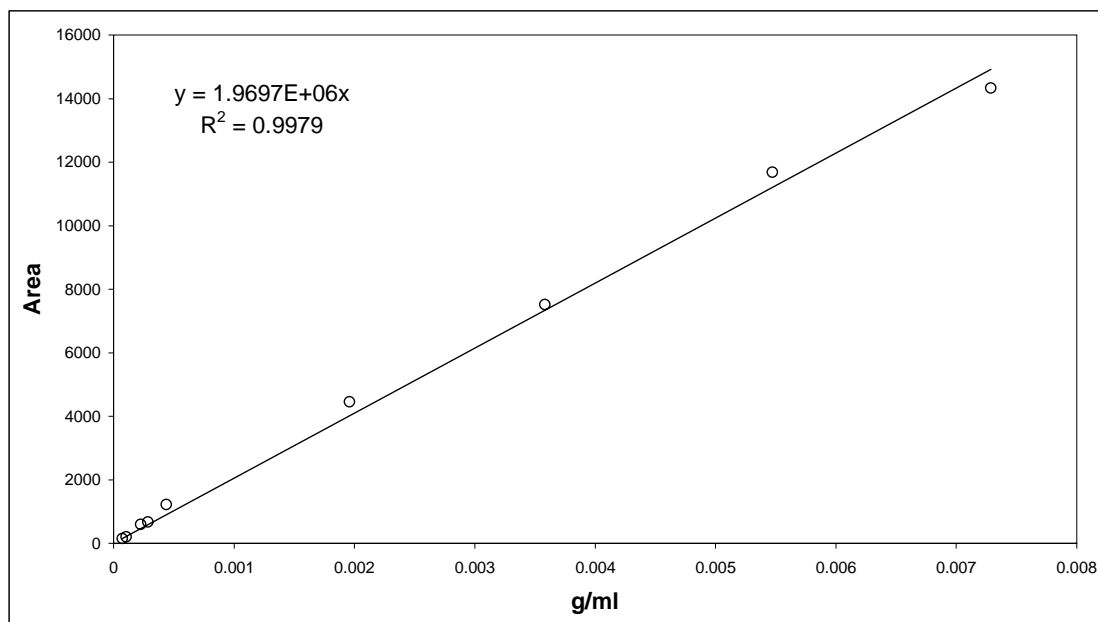


Figure 17. Di-glycerides calibration curve. Method of quantification by areas.

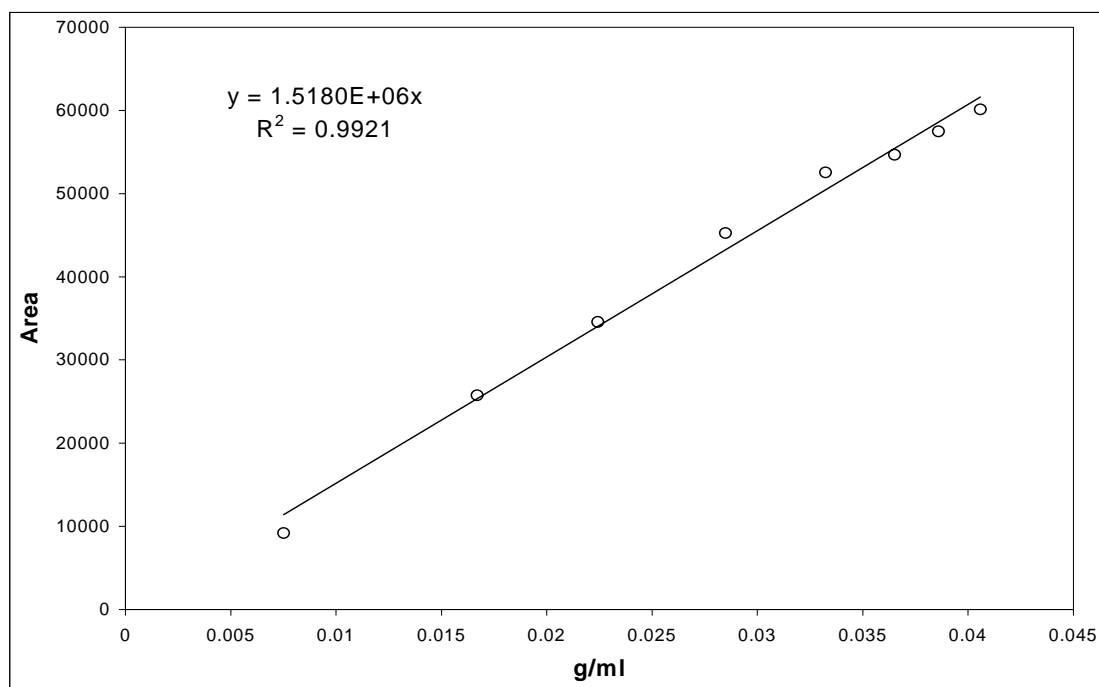


Figure 18. Methyl esters calibration curve. Method of quantification by areas.

XRF

X-ray fluorescence (XFR) was used to evaluate the weight percentage of potassium (catalyst) in samples at different process locations. Analyses were performed using ASOMA X-ray fluorescence analyzer, model 200-series. The samples were analyzed, filled the sample pan with eight milliliters and placed inside the equipment console.

SIE

A Potassium Selective Ion Electrode ORION coupled to one pH/mV meter ORION model 420A+ was used to complement catalyst studies by measurements in the glycerol phase.

KF

Water contents in oils were determined using a Karl Fisher Titrator 701 KF-Metrohm. A mixture of 50 (%vol.) of THF (co-solvent) and 50 (%vol.) of methanol was used as solvent and a Hydranal composite 5, analytical grade, as reagent.

ULTRASOUND INSTRUMENT

A BRANSON probe system used in this study operates at a frequency of 20 KHz. It has a digital wattmeter to measure the power applied to the transducer to maintain the amplitude for any given output control setting. As the load or pressure on the horn face increases, the power supply develops more power. The heart of the converter is a lead zirconate titanate electrostrictive element which, when subjected to an alternating voltage, expands and contracts. The converter vibrates in a longitudinal

direction and transmits this motion to the horn tip immersed in the solution, which causes cavitation.

WEIGHT AND VOLUME DETERMINATION

Weight determinations were made using calibrated analytical scales. Volume determinations were made using beakers, pipettes, burettes, flasks, and syringes calibrated ranging from 1 micro-liter to 300 ml. Special care was taken handling THF due to its rapid polymerization with plastic material; glass material is mandatory.

Experiment design

Soybean oil and Tallow were characterized in free fatty acid, iodine number, and water content. Identification of fatty acids was performed by GC-MS and the quantification of glycerides by HPLC.

Optimal conditions were determined by statistical screening of different reaction temperatures and molar ratios of alcohol to tri-glycerides using soybean oil as feedstock. For that the software Expert Design was employed. As response variable the weight percent of glycerides in the reactive mixture after two hours of reaction, assuming equilibrium conditions at this time was used.

A factorial 3^2 design confounded in three blocks and replicated twice was selected to tune the optimal conditions and considering the following aspects:

Three molar ratios MeOH/Oil (treatment B: 3:1, 4.5:1 and 6:1), and three reaction temperatures (treatment A: 25, 40 and 60 °C) were selected according to the literature review. Interactions between these two factors give useful information about

the transesterification process such as thermochemical data that permits to know if it is exothermic or endothermic, and if it is mass transfer or kinetically limited.

Experiments were programmed during three weeks per replicate, the minimal work time according to the personnel and laboratory availability constraints. Every week was considered a block where the operator, analytical equipment conditions, and experimental conditions were considered constants. The smallest sample size to perform an analysis of variance calculation is two replicates.

After the analysis of the information provided by the statistical design with soybean oil, the optimal conditions of molar ratio MeOH/Oil and reaction temperature were found and used to perform alkaline transesterifications of tallow with methanol along two hours of reaction using 1.5% KOH catalyst, further alkaline transesterifications of soybean with 2-propanol, 1-butanol, and ethanol were ran and evaluated only at equilibrium.

Sampling and Chemical Analysis

The experimentation consisted mainly of batches of alkaline transesterifications of triglycerides and alcohols using KOH as catalyst. Experimental conditions were determined according to literature review, except for the ultrasound parameters because there was not evidence of previous experimentation with ultrasound in this field.

One hundred and twenty grams of tri-glyceride, 1.8 grams of KOH (1.5% Kg/liter of feedstock) and the amount of alcohol required to get the desired molar ratio of alcohol/tri-glycerides, were fed into a cylindrical glass reactor during two hours. Ultrasound probe was introduced in the reactant mixture and turned on at an amplitude of 36%, a sound proof enclosure was used to reduce sound intensity at normal values.

Molecular weights of 862.74 and 892.86 for the soybean oil or yellow grease and tallow, were determined from the fatty acid percentages of the oil and tallow respectively and the required weight and volume of alcohol can be calculated by the corresponding molar ratio.

Reactants were heated until the reaction temperature selected while 1.8 g of KOH were dissolved in the prescribed amount of alcohol and then heated to the same temperature. Then, this solution was added to the reactor and the ultrasound probe system turned on. The reaction temperatures were controlled by water reflux through the external jacket of the reactor.

Samples were drawn from the middle of the reactor using sterile syringe of 10 cm³ and analyzed. Samples were taken at 0, 1, 2, 3, 4, 5, 8, 10, 12, 15, 20, 30, 40, 50, 60 and 120 minutes of reaction. Also, some samples were taken each hour during six hours to assure that the equilibrium was achieved (Borrero, 2002).

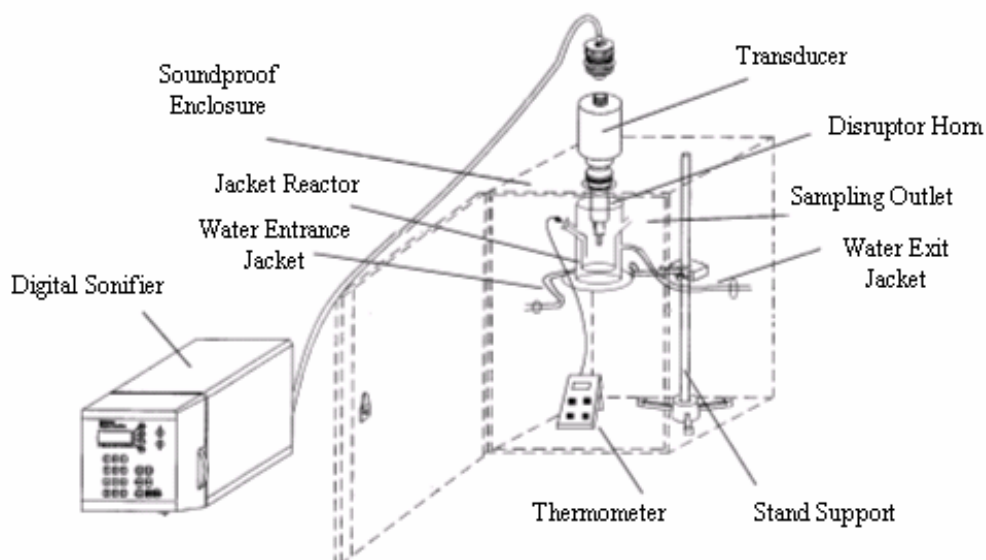


Figure 19. Experimental setup for transesterification of Biodiesel, Taken from Borrero (2002).

Each sample was analyzed by HPLC as mentioned above, quantifying Tri-glycerides, di-glycerides and a mix of mono-glycerides and methyl esters (Biodiesel).

About 400 mg of the sample mixture was placed in a vial and diluted with 10 ml of high-performance liquid chromatography grade tetrahydrofuran (THF). Then one drop of 0.6 N hydrochloric acid was added to neutralize the catalyst and stop the reaction. Samples were kept below 20 °C by refrigeration with ice until further analysis.

RESULTS

Optimal conditions

The following table of results shows the equilibrium conditions reached during the statistical screening performed at different temperatures – FACTOR A- and alcohol/oil molar ratios – FACTOR B-, the apparent yield in equilibrium – After two hours of reaction- was selected as response.

Table 4. Data obtained experimentally to perform the statistical screening of temperature and alcohol/oil molar ratio.

Codification	Run Number	Block Number	Factor A: Temperature	Factor B: A/O molar Ratio	Response: Apparent yield in eq.
2	1	1	25	3	90.78
18	2	1	60	6	99.5
16	3	1	40	6	99.8
1	4	1	25	3	91.01
9	5	1	40	4.5	98.56
11	6	1	60	4.5	98.14
15	7	3	40	6	99.82
17	8	2	60	6	99.42
3	9	2	40	3	90.57
14	10	2	25	6	99.78
10	11	3	40	4.5	98.5
6	12	3	60	3	90.42
5	13	3	60	3	90.45
4	14	3	40	3	90.54
8	15	2	25	4.5	98.41
13	16	2	25	6	99.77
12	17	2	60	4.5	98.3
7	18	3	25	4.5	98.35

After previous verification of residuals using the program Design Expert, as presented in the graph below, a coded model to predict the optimal apparent yield at equilibrium was found statistically.

DESIGN-EXPERT Plot
App. eq. yield

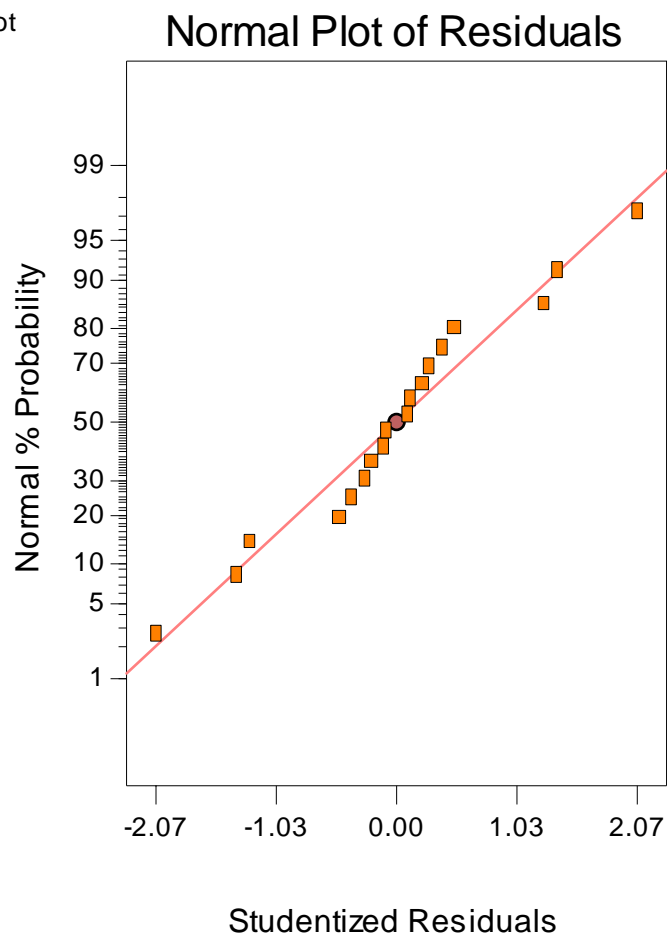


Figure 20. Studentized residuals obtained for the apparent equilibrium yield in the statistical screening.

The graph of residuals indicates that there is characteristic dispersion of constant variance in the data.

Respect to the optimal conditions the model reports values of 40 °C and a 9 for temperature and the alcohol-oil molar ratio respectively. However taking account technical and economic aspects such as the tallow melting point which is 42 °C and that

the industry prefers lower alcohol-oil molar ratios, the optimal conditions selected were 60 °C and a 6:1 alcohol-oil molar ratio.

According to the reversible consecutive reactions stoichiometry by Freedman et al. (1986), Darnoko and Cheryan (2000) for an alcohol-oil molar ratio of 6:1, the following stoichiometric table can be obtained:

Table 5. Stoichiometric table for the transesterification of oils with alcohol when an alcohol-oil molar ratio of 6:1 is used, z_i is the extent of the reaction i based on the initial moles of alcohol.

Species	Initial Concentration	Moles at extent z_i
Triglycerides	C_{TG0}	$C_{TG0} - z_1$
Diglycerides	C_{DG0}	$C_{DG0} + z_1 - z_2$
Monoglycerides	C_{MG0}	$C_{MG0} + z_2 - z_3$
Biodiesel	C_{ME0}	$C_{ME0} + z_1 + z_2 + z_3$
Monoglycerides+ Biodiesel	$C_{MG0} + C_{ME0}$	$C_{MG0} + C_{ME0} + z_1 + 2z_2$

Both the triglycerides and diglycerides molar balance can be used to find the values of z_1 and z_2 . These values were used to verify the numerical consistence of the data obtained by HPLC analysis because the analytical conditions selected for this instrument just reported the composition of triglycerides, diglycerides and the sum of monoglycerides and biodiesel.

Photographic analysis

In order to obtain a better understanding of mixing under ultrasound conditions, experiments with dyes were performed.

The methanol phase was dyed with phenolphthalein in order to show the behavior of the catalyst during the reaction and try to visualize a pattern flow. As shown below in the pictures the methanol was diminishing in the thickness along the reaction time and as it was expected the final location of the catalyst was in the glycerol product phase after turning off the sonicator. Note that the dye prefers the basic nature of the catalyst

Another important aspect to note is the wave form taken by the interface at larger reaction times. These experiments will be complemented in the near future with a sonoluminescence system.

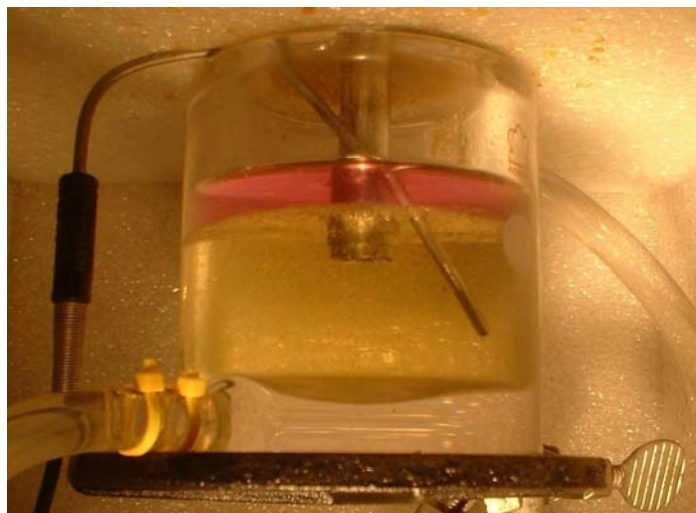


Figure 21. Reactant system before ultrasonic agitation, pure soybean oil and methanol-KOH at 40 °C

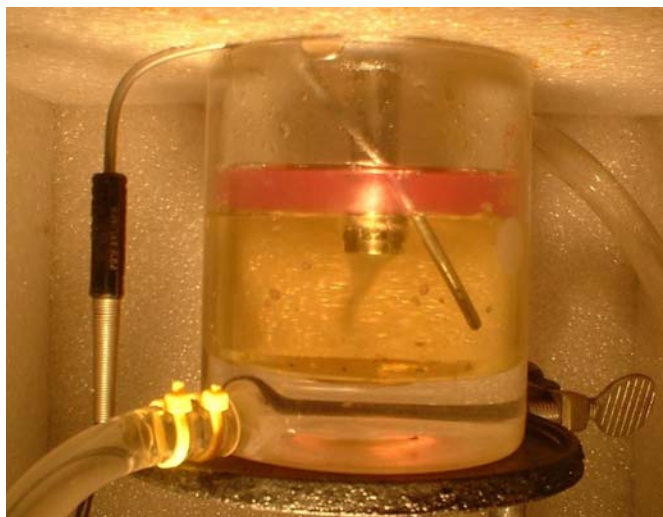


Figure 22. Reaction time of 3 minutes, pure soybean oil and methanol-KOH at 40 °C

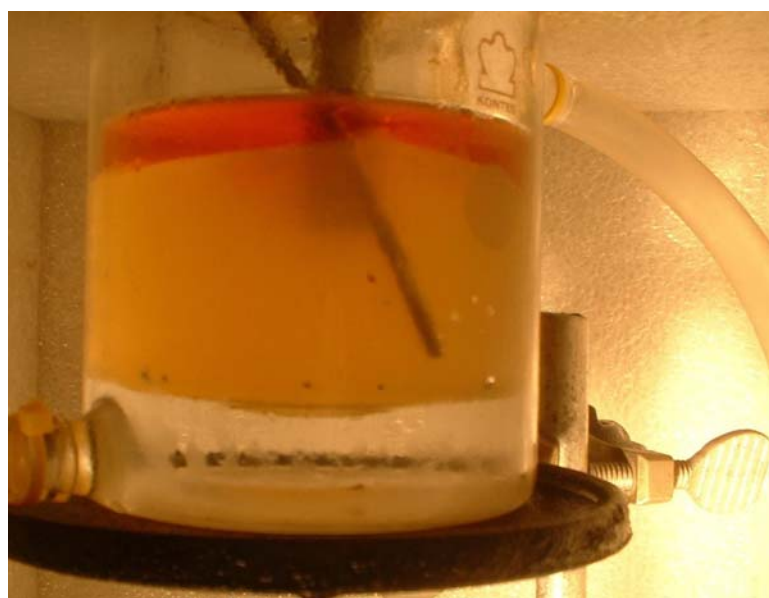


Figure 23. System operated a higher power intensities of 52 W for soybean oil and methanol at 40 °C.



Figure 24. End of reaction, reactants and products without ultrasonic agitation

Cavitation Model

According to the results obtained during the first stage of experimentation and analyzing experimental data supplied by other investigators as Darnoko and Cheryan (2000) and Freedman et al. (1986), it is clear the existence of a second order relationship between the initial rate of disappearance of triglyceride and the triglyceride concentration inside the reactor, which have been expressed as:

$$-\frac{d[TG]}{dt} = k[TG]^2 \quad (77)$$

where:

[TG] = Concentration of triglyceride, %wt

t	=	time, minutes
k	=	Overall pseudo rate constant, (wt%·min) ⁻¹

Usually the equation (77) is the result of the application of the excess method, assuming a quasi-constant concentration of alcohol, which drives the reaction to the forward direction. The kinetic constant is calculated by linear regression of the relationship between $\ln\left(\frac{d[TG]}{dt}\right)$ and $[TG]$, where the slope gives the order of the reaction and the intercept gives the value of the pseudo-kinetic constant. If experiments are performed at least at two different temperatures the energy of activation, E_a , also can be determined by the use of the Arrhenius equation.

Borrero (2002), Darnoko and Cheryan (2000), Freedman et al. (1986), and Eckey (1956) have found values of k for transesterification of vegetable oils with a molar ratio of oil/methanol of 1:6 at different temperatures. They assumed kinetic models to process the information obtained by experimentation.

This study proposes a mass transfer analysis to deal with the data obtained from the experimentation, given the evidence of mass transfer limitations presented in the data analysis of Borrero (2002) where a different temperatures the final equilibrium has not major significance over the reaction rate. However at the end, it is expected to find also a second order relationship between the rate of disappearance of triglyceride and the triglyceride concentration inside the reactor.

A preliminary approach to the explanation of this complex transesterification process has been made by the following simplifications:

At the beginning, by effect of the application of ultrasound a transient cavitation occurs and this stage is very short, perhaps microseconds. For there is not exchange of matter between the bubbles or cavities formed and the liquid surrounding.

Due to the violent collapse of the primary bubbles, the bubble walls raise their velocity reaching local values so high as the speed of the sound in liquid. These jets lead to the formation of drops of alcohol, which are dispersed into the oil phase forming an emulsion.

While the ultrasound is acting over the reaction an emulsion inside the reactor is visually observed, the model assume that break-up and coalescence occurs simultaneously due to the interaction among liquid drops and a size distribution is obtained. These different drop sizes can be represented by a mean drop diameter, which depends on the reaction conditions.

At initial reaction times, when the oil reaches the bubble surface, which consists mainly of methanol, this reactant is rapidly consumed forming methyl ester and diglyceride. The former remains inside the bubble or polar phase and the second migrates into the oil or non-polar phase.

Transient Cavitation

Equation (19) represents the most known mathematical approach in order to deal with the problem of bubble dynamics equation. Prasad et al. (1994) used it in modeling a batch sonochemical reactor for the ultrasonication of aqueous KI solution to describe the growth and collapse of a gas-vapour cavity.

In this case for the system methanol-oil, when this is irradiated with ultrasound, it is presumed that local pressures below the saturation vapor pressure of methanol induce the formation of cavities filled with solvent vapor.

The bubble is assumed to behave isothermally during its growth phase and a part of the collapsing phase. Then it is assumed to collapse adiabatically yielding high temperatures and pressures resulting in a well mix of the content of the bubble with the liquid surrounding.

Similar to the model described by Prasad et al. (1994) the following assumptions were made:

- The intensity of the sound field is constant.
- The bulk temperature itself is constant and it corresponds to the obtained experimental conditions.
- The gas and vapor present in the bubble behave ideally.
- The expansion phase and the initial part of collapsing phase of the bubble are isothermal, whereas the end part, of the collapsing phase, occurs adiabatically.
- The partial pressure of the vapor inside the bubble is equal to the vapor pressure of the liquid corresponding to the bulk liquid temperature during the isothermal periods.
- The transition from isothermal to adiabatic conditions in the collapsing phase occurs when partial pressure of gas and vapor in the bubble equalize.

- The end conditions of cavity collapse are in the point when the bubble wall velocity is equal to the sonic velocity in the liquid medium.
- The liquid is incompressible, and viscous forces are neglected.

Isothermal case

The following ordinary differential equations system, ODEs, must be solved by numerical methods to find a solution of the radius of bubble, R , as function of time from $t = 0$ until $t = t_{f1}$ where the radius of bubble reach a calculated radius of R_2 .

$$\frac{d\dot{R}}{dt} = \frac{1}{\rho} \left[P_{g0} \left(\frac{R_0^3}{R^4} \right) + \frac{P_v}{R} - \frac{2\sigma}{R^2} - \frac{(P_b - P_a \sin wt)}{R} \right] - \frac{3\dot{R}^2}{R} \quad (78)$$

$$P_{g0} = P_b - P_s + \frac{2\sigma}{R_0} \quad (79)$$

where:

$\frac{dR}{dt} = \dot{R}$; surface velocity of the bubble, m/s

$t =$ time, s

$\rho =$ Density of liquid, Kg/m³

$P_a =$ Acoustic pressure, N/m²

$P_b =$ Atmospheric pressure, N/m²

$P_{g0} =$ Initial gas pressure inside the bubble, N/m²

$P_s =$ Saturation vapour pressure of the liquid, N/m²

$P_v =$ Partial pressure of vapour in the bubble, N/m²

- $R_0 =$ Radius of the initial bubble, m
 $\sigma =$ Surface tension of the liquid, N/m
 $\omega =$ Angular frequency applied by ultrasound, rad/s

Initial conditions:

$$t = 0 \qquad R = R_0 \qquad \dot{R} = 0$$

Adiabatic case

The following ordinary differential equations system, ODEs, must be solved by numerical methods to find the second part of the solution of the radius of bubble as function of time for the adiabatic case from $t = t_{fl}$, where \dot{R} is known from the isothermal case, until $t = t_f$, when the wall of the bubble reach the velocity of sound in the liquid:

$$\frac{d\dot{R}}{dt} = \frac{1}{\rho} \left[2P_s \left(\frac{R_2^{3\gamma}}{R^{3\gamma+1}} \right) - \frac{2\sigma}{R^2} - \frac{(P_b - P_a \sin(\omega t))}{R} \right] - \frac{3\dot{R}^2}{2R} \quad (80)$$

$$\frac{dR}{dt} = \dot{R} \quad (81)$$

Intensity of power was calculated from the equation (26), applying the calorimetric method in the systems soybean oil – methanol and tallow – methanol without the presence of catalyst to avoid reaction interferences. After that acoustic pressure values were estimated for each system.

For soybean-methanol system simulations at 9.84 W and 15 W were performed and the results presented in the Figures 23, 24, 25, 26, 27 and 28.

For tallow-methanol system simulations at 12.54 W and 15 W were performed and the results presented in the Figures 29, 30, 31, 32, 33 and 34.

An initial bubble radius of 2 micrometers was considered for all simulations. In the case of soybean oil-methanol a temperature of 40 °C was introduced in the computer program, while for tallow-methanol 42 °C was the temperature chosen.

Numerical solution for isothermal and adiabatic cases were found by creating one program in mathcad, this includes a complete graphical solution from time equal to zero until the final time t_f where the bubble collapse.

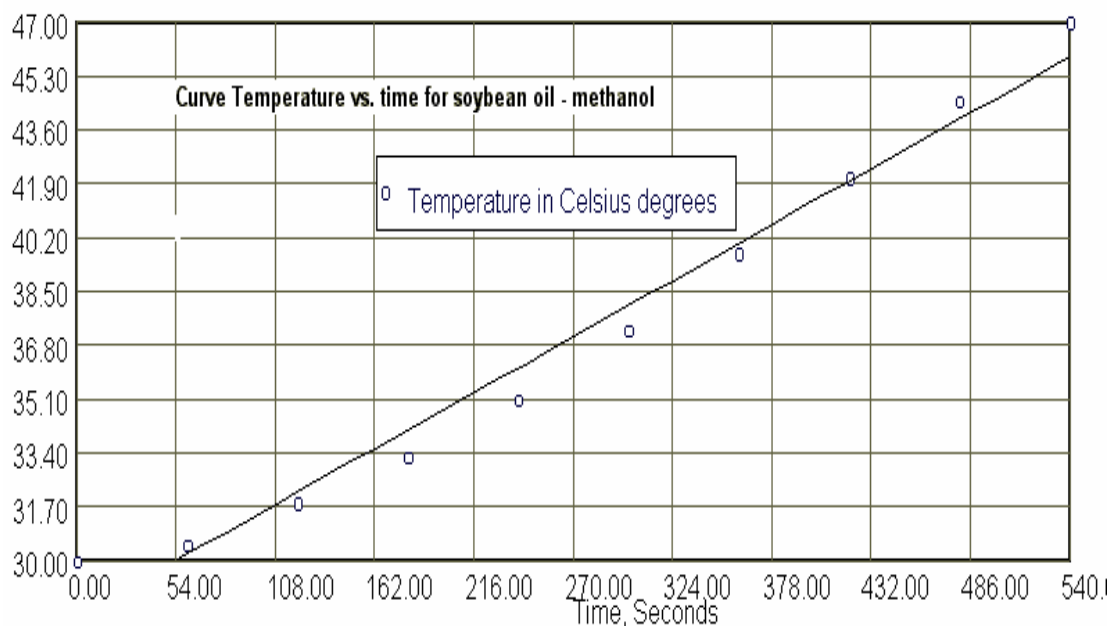


Figure 25. Experimental determination of dT/dt for the system methanol-soybean oil

POLYMATH Results
POLYMATH Report 09-19-2003

Linear Regression Report

Model: Temperature = a0 + a1*Time

<u>Variable</u>	<u>Value</u>	<u>95% confidence</u>
a0	28.301091	1.2796923
a1	0.0327071	0.0039951

General

Regression including free parameter
Number of observations = 10

Statistics

R² = 0.9780461
R²adj = 0.9753019
Rmsd = 0.267052
Variance = 0.8914594

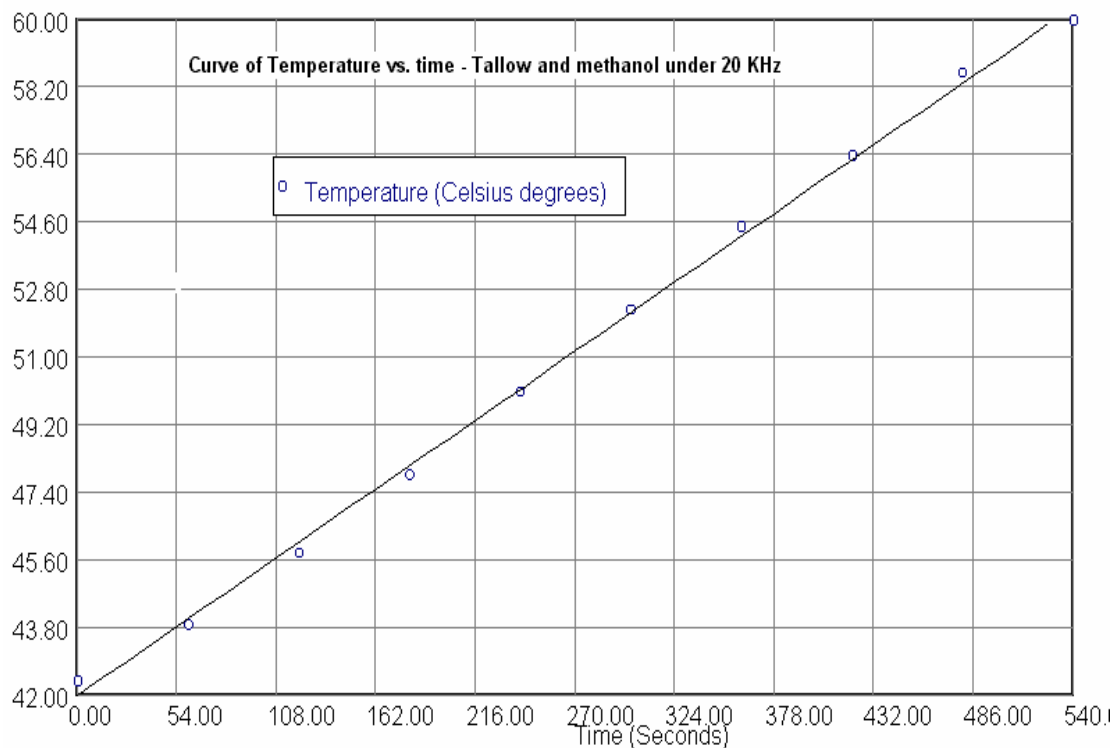


Figure 26. Experimental determination of dT/dt for the system methanol-tallow.

POLYMATH Results

No Title 09-19-2003

Linear Regression Report

Model: $\text{Temperature} = a_0 + a_1 \cdot \text{Time}$

<u>Variable</u>	<u>Value</u>	<u>95% confidence</u>
a0	42.018182	0.3738705
a1	0.0339697	0.0011672

General

Regression including free parameter

Number of observations = 10

Statistics

R ² =	0.998227
R ² adj =	0.9980054
Rmsd =	0.078021
Variance =	0.0760909

Table 6. Results obtained in simulations of power absorbed by the system methanol-soybean oil at 40 °C under ultrasound irradiation of 20,000 Hz using a molar ratio alcohol-oil of 6:1.

Intensity of Power (W)	Time of isothermal growth (ms)	Time of the collapse (ms)	Maximum Radius (mm)	Temperature of collapse (K)	Pressure of collapse (KPa)
9.84	57.03	139.18557	131.32987	2265.68	840,540
15	42.01	183.27234	415.611	273.5211	3.041

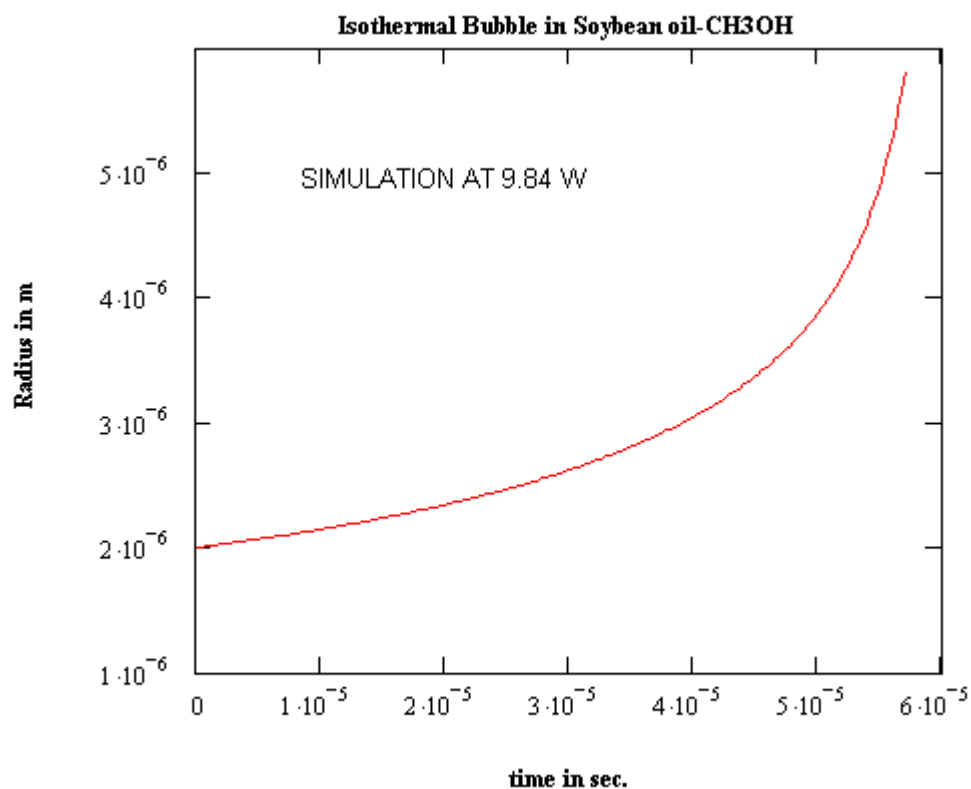


Figure 27. Isothermal bubble of methanol growing in soybean oil, results of simulation at 9.84 W of power absorbed by the system and 40 °C using mathcad.

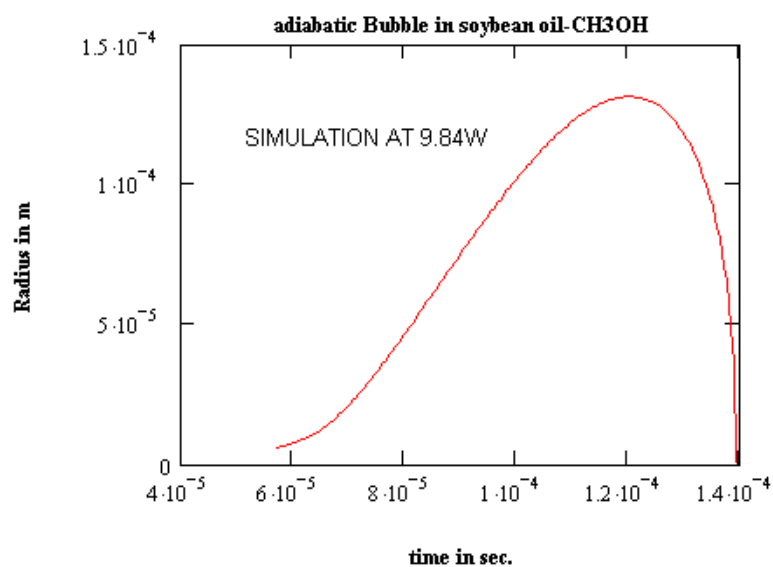


Figure 28. Adiabatic bubble of methanol growing in soybean oil and then collapsing, results of simulation at 9.84 W of power absorbed by the system and 40 °C using mathcad.

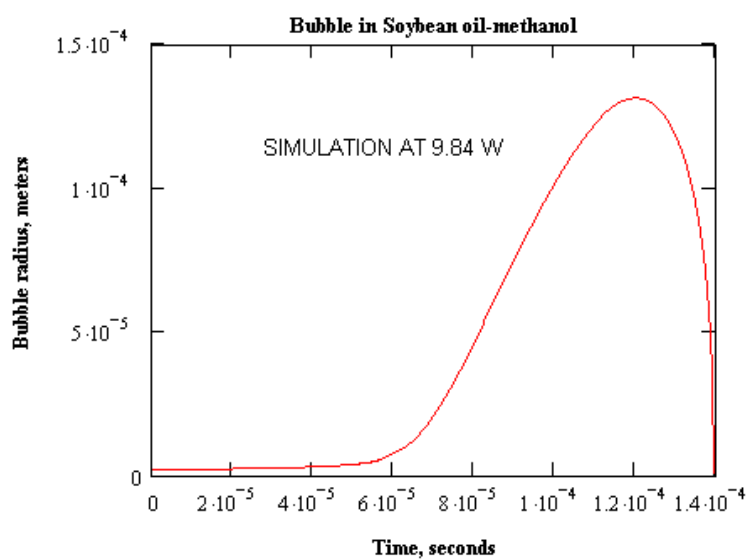


Figure 29. Dynamic of the bubble of methanol in soybean oil during its lifetime, results of simulation at 9.84 W of power absorbed by the system and 40 °C using mathcad.

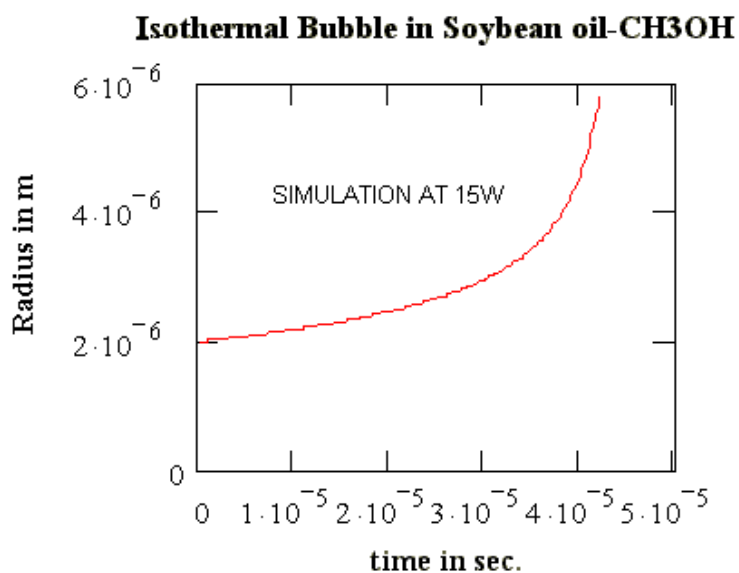


Figure 30. Isothermal bubble of methanol growing in soybean oil, results of simulation at 15 W of power absorbed by the system and 40 °C using mathcad.

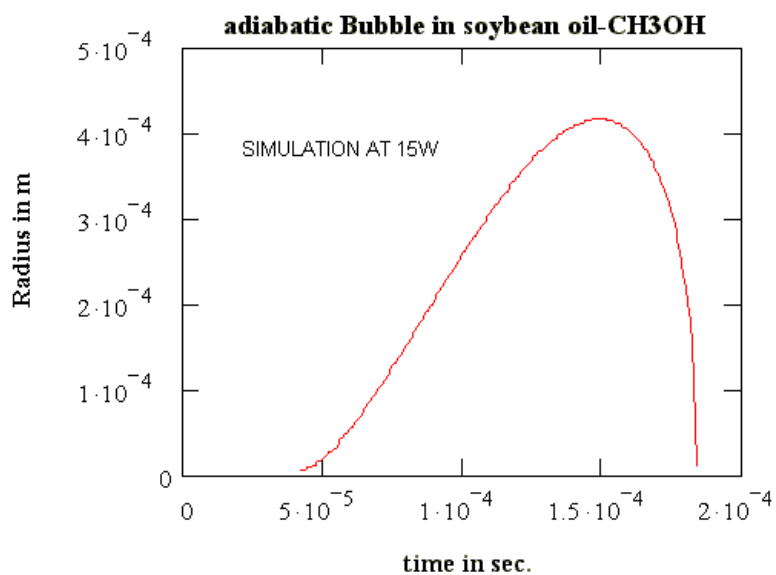


Figure 31. Adiabatic bubble of methanol growing in soybean oil and then collapsing, results of simulation at 15 W of power absorbed by the system and 40 °C using mathcad.

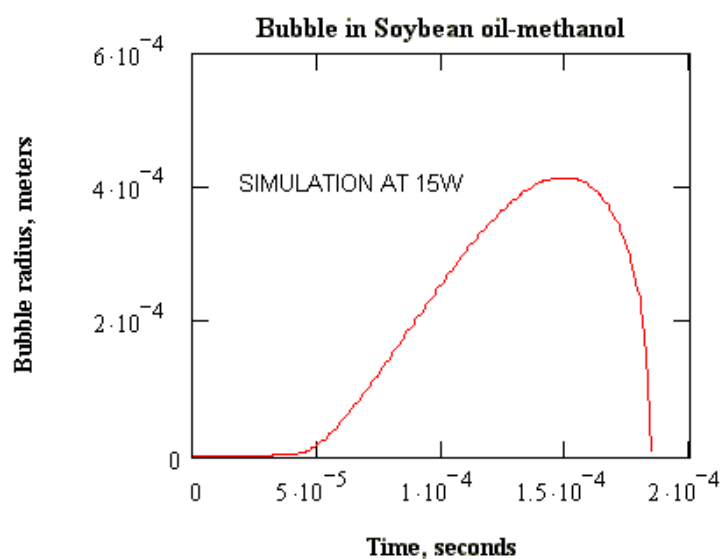


Figure 32. Dynamic of the bubble of methanol in soybean oil during its lifetime, results of simulation at 15 W of power absorbed by the system and 40 °C using mathcad.

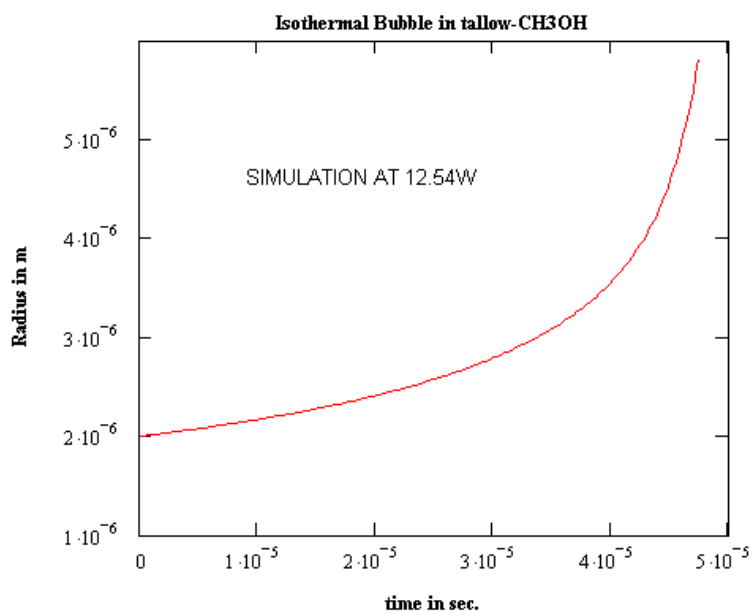


Figure 33. Isothermal bubble of methanol growing in tallow, results of simulation at 12.54 W of power absorbed by the system and 42 °C using mathcad.

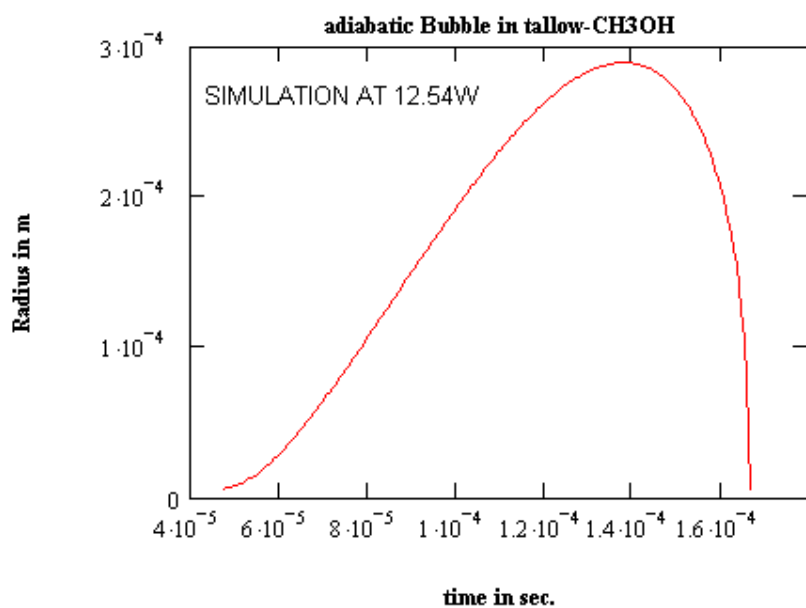


Figure 34. Adiabatic bubble of methanol growing in tallow and then collapsing, results of simulation at 12.54 W of power absorbed by the system and 42 °C using mathcad.

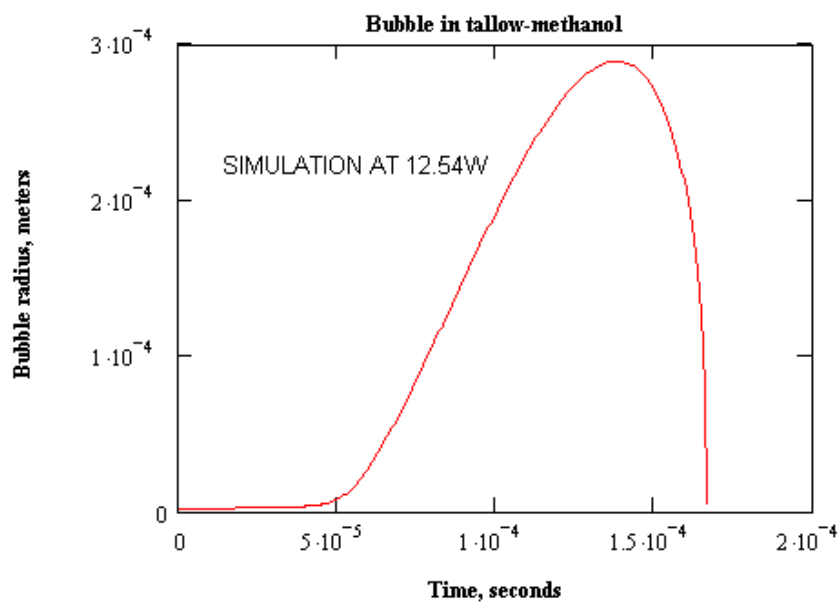


Figure 35. Dynamic of the bubble of methanol in tallow during its lifetime, results of simulation at 12.54 W of power absorbed by the system and 42 °C using mathcad.

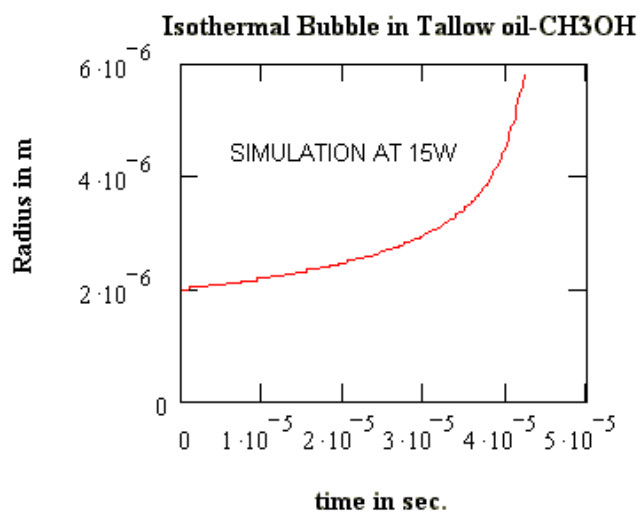


Figure 36. Isothermal bubble of methanol growing in tallow, results of simulation at 15 W of power absorbed by the system and 42 °C using mathcad.

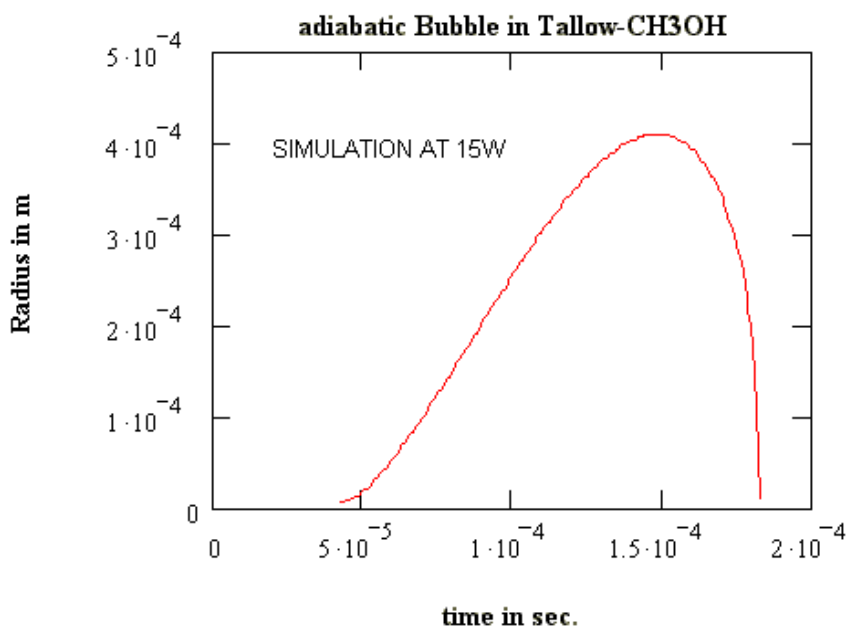


Figure 37. Adiabatic bubble of methanol growing in tallow and then collapsing, results of simulation at 15 W of power absorbed by the system and 42 °C using mathcad.

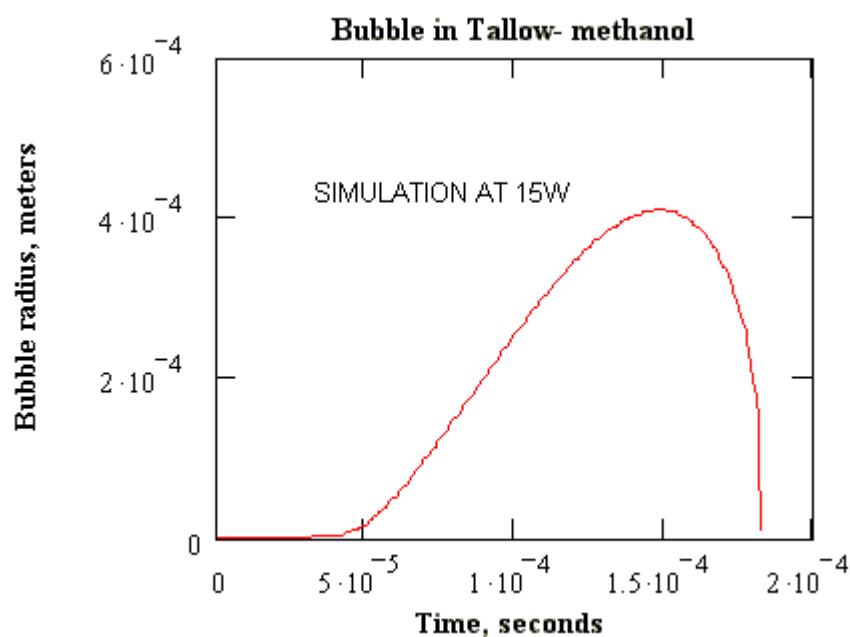


Figure 38. Dynamic of the bubble of methanol in tallow during its lifetime, results of simulation at 15 W of power absorbed by the system and 42 °C using mathcad.

Table 7. Results obtained in simulations of power absorbed by the system methanol-tallow at 42 °C under ultrasound irradiation of 20,000 Hz using a molar ratio alcohol-oil of 6:1.

Intensity of Power (W)	Time of isothermal growth (ms)	Time of the collapse (ms)	Maximum Radius (mm)	Temperature of collapse (K)	Pressure of collapse (KPa)
12.54	47.4	166.46222	289.201	426.57097	40.899
15	42.08	182.20786	409.735	277.999	3.32461

Note that the collapse conditions of the bubble are strongly dependent of the Intensity of Power. Experimental values of this characteristic of the system appear in

the first row of the data presented in the Tables 6 and 7 and the end conditions obtained in each case are contrasted with simulations made at 15 W of Intensity of Power.

Diffusion Model and mass transfer coefficient, k_{MT}

By definition of interfacial area for spherical drops, a_i , in m^2/m^3 , is represented by equation (26), but if we wish to calculate the interfacial area, in m^2 the following relationships are very useful:

For n spherical drops of methanol formed:

$$n = \frac{V_M}{(\pi D_p^3 / 6)} \quad (82)$$

where:

V_M = Volume of methanol at time t of reaction, m^3

D_p = Mean Drop diameter

Surface area generated by n spherical drops, a, will be given by:

$$a = n\pi D_p^2 \quad (83)$$

Then, combining Equations (82) and (83):

$$a = \frac{6V_M}{D_p} \quad (84)$$

If transesterification is a mass transfer limited reaction, the rate of disappearance of triglyceride must be equal to the rate of mass transfer of the triglyceride into the drop of methanol. This concept is expressed below in equation (85):

$$-\frac{dC_A}{dt} = k_{MT} a (C_A - C_A^*) \quad (85)$$

Where:

- C_A = Bulk concentration of triglyceride, %wt
 C_A^* = Concentration of triglyceride in the surface of the drop, %wt
 t = time, seconds
 k_{MT} = Mass transfer coefficient, m/s
 a = Surface Area, m²

Note that in this work we assume that $C_A^* \rightarrow 0$

By mass balance and assuming constant density:

$$V_M = V_M^0 - \text{volume of methanol consumed in reaction}$$

$$V_M = V_M^0 - \frac{MW_M}{\rho_M} (3(\text{initial moles of TG} - \text{moles of TG at time } t))$$

Multiplying by $\frac{MW_A m_T}{MW_A m_T}$, we obtain:

$$V_M = V_M^0 - 3 \frac{MW_M m_T}{MW_A \rho_M} (C_A^0 - C_A) \quad (86)$$

where:

- V_M = Volume of methanol at time t of reaction, m³
- V_M^0 = Initial volume of methanol at time t = 0, m³
- C_A = Bulk concentration of triglyceride, at time t of reaction, %wt
- C_A^0 = Bulk concentration of triglyceride at time t = 0, %wt
- MW_A = Molecular weight of methanol, Kg/Kg•mol
- MW_M = Molecular weight of triglyceride, Kg/Kg•mol
- ρ_M = Density of methanol, Kg/ m³
- m_T = Total mass of the system alcohol-triglyceride, Kg

Combining Equations (84), (85) and (86) we get:

$$-\frac{dC_A}{dt} = k_1 k_2 C_A + k_1 C_A^2 \quad (87)$$

where:

- C_A = Bulk concentration of triglyceride, at time t of reaction, %wt

$$k_1 = \frac{18k_{MT} MW_M m_T}{\rho_M D_P MW_A}, \text{ given in (wt-s)}^{-1} \quad (88)$$

$$k_2 = \frac{V_M^0 MW_A \rho_M}{3MW_M m_T} - C_A^0, \text{ given in %wt} \quad (89)$$

Equation (87) can be solved analytically by partial fractions:

$$\int_{C_A^0}^{C_A} \frac{dC_A}{k_1 k_2 C_A + k_1 C_A^2} = \int_0^t -dt \quad (90)$$

Making the following transformation:

$$\int_{C_A^0}^{C_A} \frac{dC_A}{k_1 C_A (k_2 + C_A)} = \int_{C_A^0}^{C_A} \frac{X dC_A}{k_1 C_A} + \int_{C_A^0}^{C_A} \frac{Y dC_A}{k_2 + C_A} \quad (91)$$

From Equation (91), two algebraic expressions are obtained:

$$X k_2 = 1 \quad (92)$$

$$C_A (X + k_1 Y) = 0 \quad (93)$$

And X and Y are found:

$$X = \frac{1}{k_2} \quad (94)$$

$$Y = -\frac{1}{k_1 k_2} \quad (95)$$

Substituting X, Y and solving the integrals in Equation (91):

$$\frac{1}{k_1 k_2} \text{Ln} \frac{C_A}{C_A^0} - \frac{1}{k_1 k_2} \text{Ln} \left(\frac{k_2 + C_A}{k_2 + C_A^0} \right) = -t \quad (96)$$

Then:

$$\text{Ln} \left(\frac{C_A (k_2 + C_A^0)}{C_A^0 (k_2 + C_A)} \right) = -k_1 k_2 t \quad (97)$$

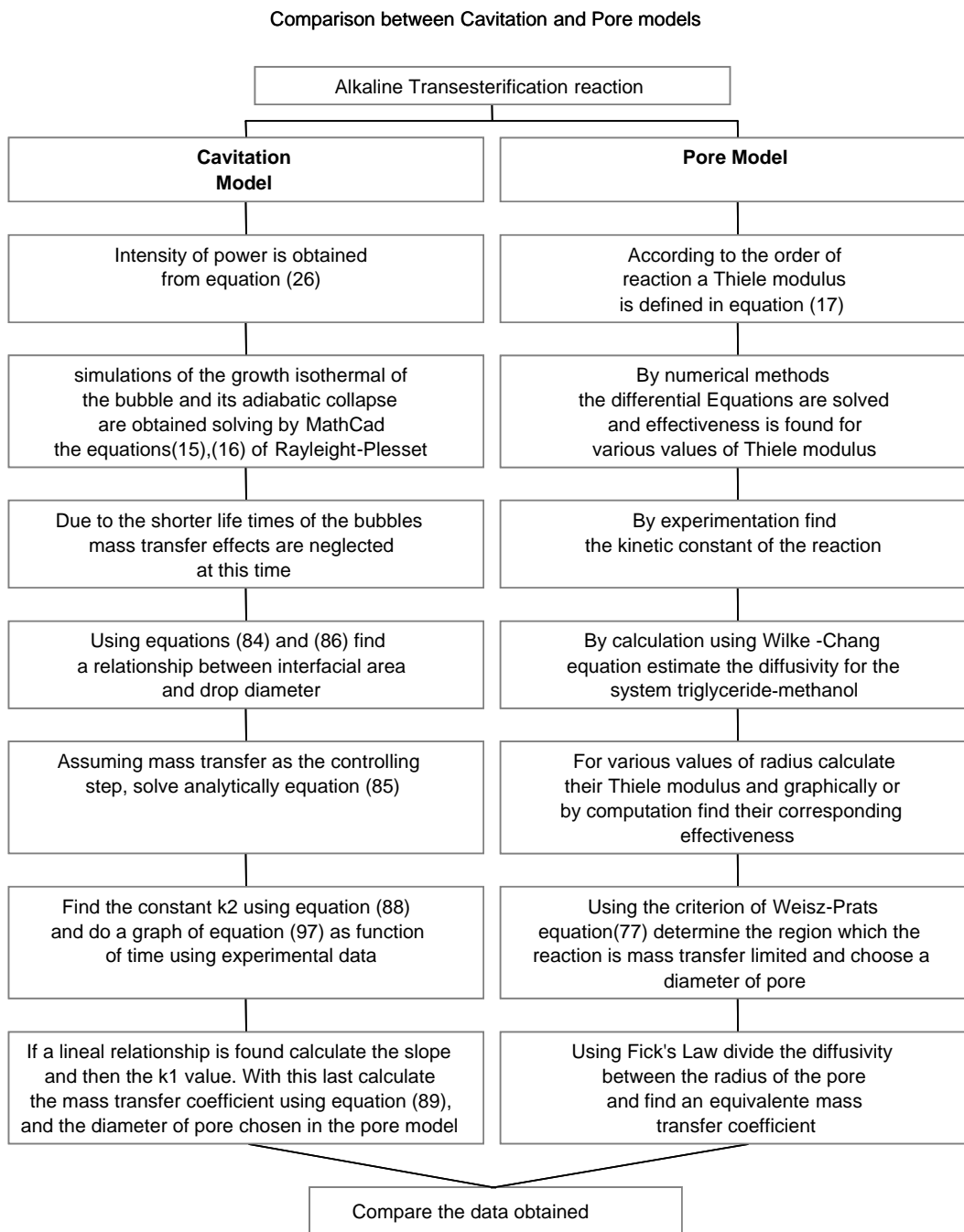


Figure 39. Procedure to develop a mathematical model in order to predict the mass transfer coefficients in the alkaline transesterification of soybean oil with methanol.

All Terms on the left side in equation (97) are known from the experimentation and can be plotted vs. time. If a linear expression crossing the origin is obtained, k_1 is calculated from the slope.

Using a calculated value of -0.978 for k_2 , the experimental data of transesterification for Soybean Oil at 25 Celsius and an Alcohol-Oil molar ratio of 6:1, a graph of Equation (60) is obtained. See Table 8 and Figure 40.

Table 8. Data used to calculate k_1 from experiments with soybean oil at 25 °C, an alcohol-oil molar ratio of 6:1.

t, sec	$Ln\left(\frac{C_A(k_2 + C_A^0)}{C_A^0(k_2 + C_A)}\right)$
0	0
60	0.009637523
120	0.01436694
180	0.020748274
240	0.033323025
300	0.042249516
480	0.050368931
600	0.058443445
720	0.065391386
1200	0.065525659
1800	0.139714683
2400	0.172140578
3000	0.220015355
3600	0.300415924

Constant k_1 for these experimental conditions is 0.00838, note the fit reached during the first 12 minutes of reaction. For a D_p of 10 mm, or a radius of 5×10^{-4} m a value of 6.5×10^{-4} m/s is obtained for k_{MT} .

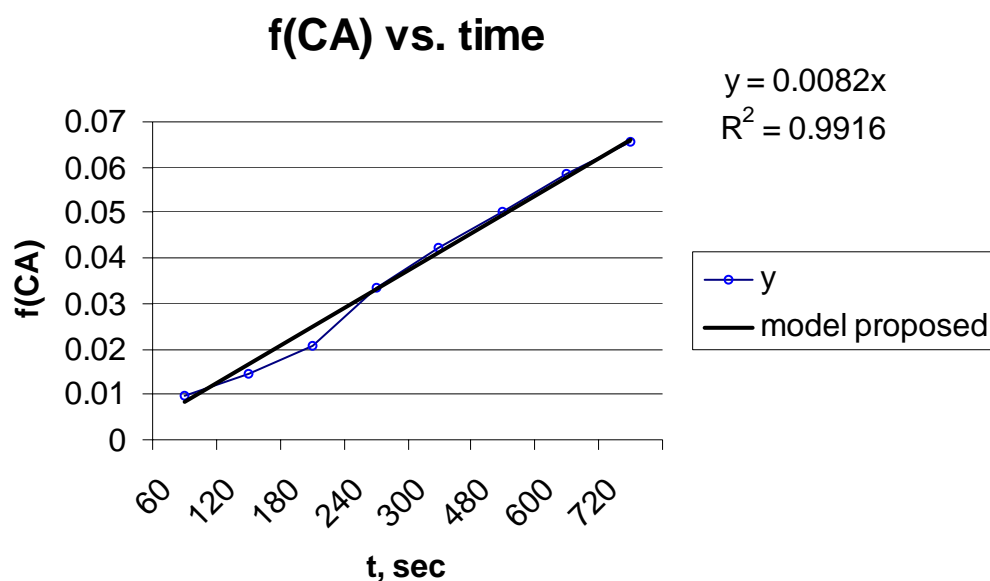


Figure 40. Graphical determination of constants of the model proposed for ultrasonic transesterification of Soybean Oil at 25 °C, and an alcohol-oil molar ratio of 6:1.

Pore model for mass transfer and reaction rate limiting the chemical reaction.

To describe both diffusion and kinetic as limiting steps in the chemical reaction of second order, the pore model studied before is developed at different Thiele modulus values. At low values is expected that the reaction be limited by reaction rate, while at high values the behavior observed corresponds a cases where the internal diffusion is the limiting step.

For the case of \bullet equal to 0.5, the numerical code and the solution obtained by a program made in mathcad is presented below, this include a solution for the concentration profile of the triglyceride within the methanol drop. Figure 41 presents all

results obtained for the calculation of Effectiveness from the Thiele modulus values evaluated utilizing the equation (56)

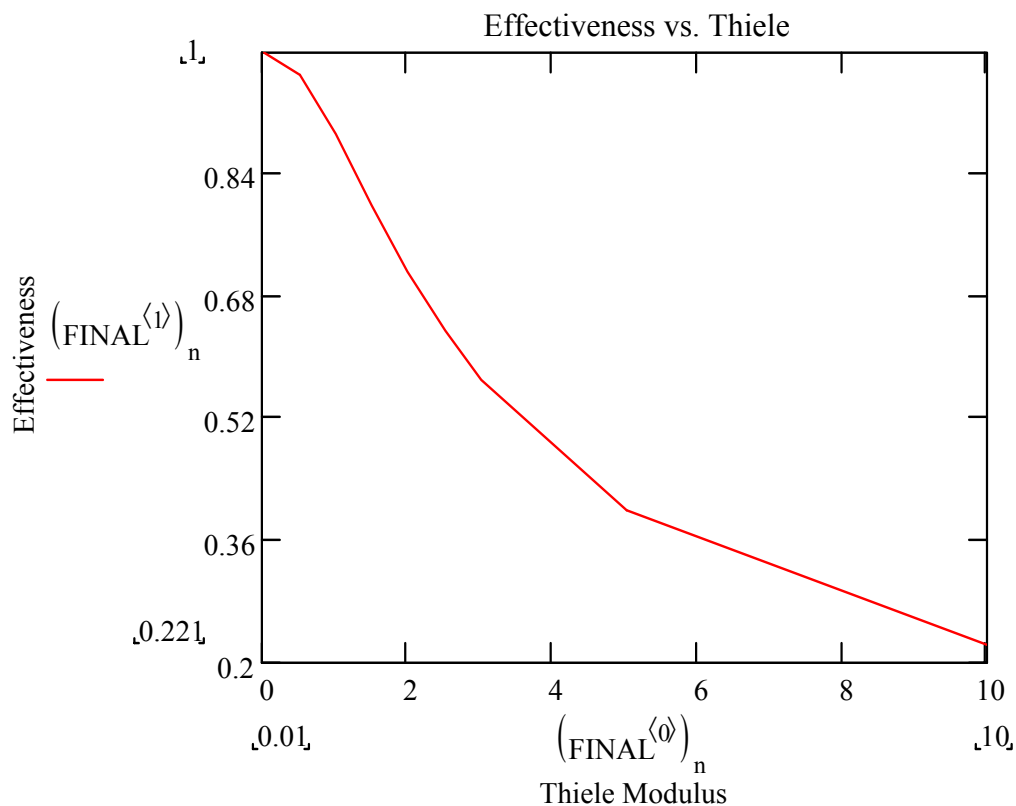


Figure 41. Effectiveness versus Thiele modulus for a second order reaction in an spherical drop.

Sensitivity of the Thiele modulus with the drop diameter was determined by derivation of the Thiele modulus respect to different diffusivity and drop size values as presented in the Figure 42 below:

Note that at small drop diameters the Thiele modulus is constant at different diffusivities. This implies that the reaction is kinetically controlled within typical diffusivities. At higher drop diameters – greater than 50 micrometers - a very strong

dependence of the Thiele modulus versus diffusivity is observed. It should be mentioned that usually in mechanical agitation systems typical drop diameters range from 100 micrometers to 2 mm. In ultrasound systems two orders of magnitude reductions in drop sizes are common (McCabe et al., 1985), (Kimmel, et al., 2000).

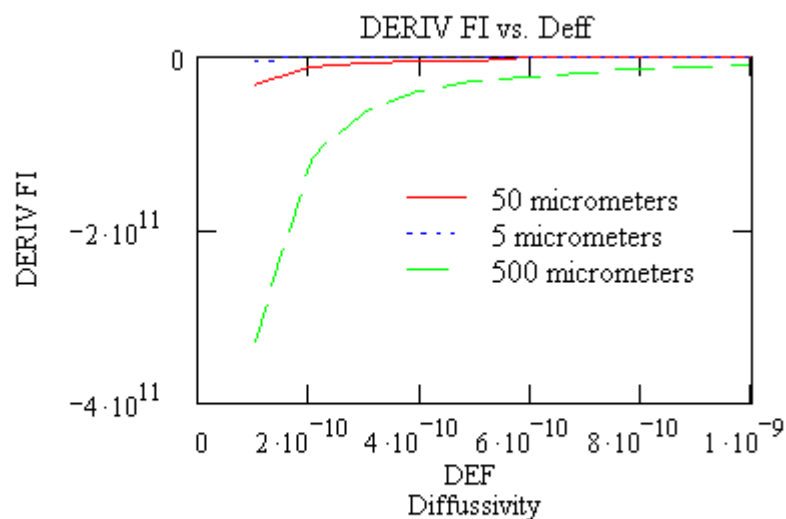


Figure 42. Sensitivity of the Thiele modulus to variations of drop size and diffusivities.

Diffusivity of triglycerides as tristearin in methanol was calculated from the Wilke-Chang equation and a value of $7.38 \cdot 10^{-10} \text{ m}^2/\text{s}$ was found. Tristearin molecule has 57 carbon, 110 hydrogen and 6 oxygen atoms whose contribution in the equation are 14.8/1000, 3.7/1000 and 11/1000 respectively; an approach of the molar volume of the triglyceride at boiling point was used (Geankoplis, 1983).

If we use a value of $0.00067 \text{ (wt.s)}^{-1}$ found by Borrero (2002) for the pseudo kinetic constant in the triglyceride-methyl ester reaction at 40 Celsius, k_{kinetic} in equation

(56), the Thiele modulus for 5, 50, 100, 500 and 1000 micrometers can be calculated from the definition made previously of this parameter. The other one experimental data necessary for this computation is the initial concentration of the triglyceride, which must be less or equal to the solubility of the compound in methanol due to immiscibility of the reactants. Boocock (2003) reported a value of 5.7 g/L after vigorous stirring of soybean in methanol for several minutes (Borrero, 2002), (Fogler, 1999).

For each Thiele modulus determined a corresponding effectiveness value is computed by using the diffusion model of spherical pore and the criterion of Weisz-Prater is used to predict whether the reaction is mass transfer limited or not. Besides the diameter corresponding to the confuse region for the criterion of Weisz-Prater equal to one was found by trial and error, Table 9 below presents the results obtained (Fogler, 1999).

Table 9. Analysis of rate controlling by Weisz-Prater criterion for alkaline transesterification of soybean oil catalyzed by potassium hydroxide.

Parameter	5 μm	50 μm	100 μm	500 μm	1000 μm	13 mm
• Thiele modulus	0.000404	0.00404	0.00808	0.0404	0.0808	1.066
• Effectiveness	1	1	1	0.9998	0.9991	0.8796
C_{wp}						
Weisz-Prater	1.63e-7	1.63e-5	6.53e-5	1.63e-3	6.47e-3	1

According to the results obtained we observe a reaction limited by kinetic when the drop size is less than 50 micrometers and some mass transfer limited at above of 10

millimeters, being 13 millimeters the limit value where there is not a clear predominant limiting step.

Table 10. Mass transfer and type of agitation estimated at different size of drops.

Particle Diameter (μm)	k_{mt} by cavitation model (m/s)	Typical agitation type
5	3.27e-7	Ultrasound
50	3.27e-6	Ultrasound
100	6.55e-6	Ultrasound-Mechanical
209	1.36e-5	Mechanical
500	3.27e-5	Mechanical
1000 and up	65.48	Mechanical

For a system without ultrasound mixing the liquid drops could be stand in an emulsion where the pure diffusion of triglyceride in methanol would produce a mass transfer coefficient of $1.476\text{e-}6$ m/s for an equivalent radius drop distribution of 500 micrometers using Fick's Law. Thus, for a methanol drop immersed in oil with a radius of 500 micrometers the ultrasonic mixing increases the mass transfer about 450 times the pure diffusion if the cavitation model proposed in this study is used.

As a first approach in the validation of the cavitation model, a value of 0.0003 (wt-s)⁻¹ reported by Darnoko and Cheryan (2000) with alkaline transesterification of palm oil with methanol and KOH at 50 celsius degrees was used in order to calculate the Thiele modulus, effectiveness and the Weisz-Prater parameter, a value of 12.97 mm for the radius corresponds to a value of 1 for the Weisz-Prater criterion. Hence we can say that the values calculated by Darnoko and Cheryan (2000) can be valid values due to his assumption of a kinetic controlled reaction, which can be reached easily by mechanical stirring. According to the pore model drop sizes less than 1 mm hold the system under the kinetic control.

CONCLUSIONS AND RECOMMENDATIONS

The main conclusions, observations and recommendations for this project are the following:

Ultrasonic mixing in immiscible systems has a special flow pattern where the equations developed for mechanical mixing can not be used to predict the relationship between drop size distribution and intensity of power applied.

Alkaline transesterification reaction of soybean oil and tallow with alcohols catalyzed by potassium hydroxide within an ultrasonic reactor is a complex reaction where the mass transfer approach through the shrinking and pore diffusion models permits to account for the importance of the interfacial contact required to get high apparent yields of biodiesel.

Images of the alkaline transesterification with the alcohol-catalyst phase dyed with phenolphthalein were very helpful in the understanding of the function of the catalyst, in this study the analysis made by X-Ray in order to determine the final location of the potassium hydroxide was verified by photography.

A model and a program in mathcad was developed and tested in order to find numerically the collapse conditions of bubbles of oil and methanol.

Transient cavitation of the soybean oil in the alkaline transesterification reaction has been studied according to the Rayleigh-Plesset equations neglecting viscous effects and the presence of hot spots at 2265.68 K and 840,540 Pa seems to be responsible of the heating effect of the reactant system.

Cavitation model could be useful in the determination of mass transfer coefficients if the characteristic diameter of the drops formed during the emulsification stage could be measured or inferred.

Pore model diffusion is a strong tool of research when is used in the determination of the step controlling in a reaction with two immiscible liquids.

It is recommended that measurements of the gas-vapor bubbles and liquid drops diameter distribution must be included in the analysis of the alkaline transesterification reaction in order to get a better characterization of the emulsion formed during the application of ultrasound. This should include viscous effects.

Measurements of the gas-vapor bubbles and liquid drops diameter distribution must be included in the analysis of the alkaline transesterification reaction in order to get a better estimation of mass transfer coefficient. Viscous effects must be evaluated for the bubble collapsing conditions in order to improve the initial approach made in this study.

Hot spots found by the mathematical model used in this study must be verified using other analytical techniques such as sonoluminescence, use of hydrophones or electrochemical studies. Overall, energetic aspects of the bubble collapse must be linked to the diffusion model in order to obtain a better understanding of the ultrasonic effects in the transesterification and other two-phase reactions.

BIBLIOGRAPHY

- Abismail, B., J.P. Canselier, A.M. Wilhelm, H. Delmas and C. Gourdon, *Ultrasonics Sonochemistry*, **6**, 75 (1999).
- Adeyuyi, Y.G., *Sonochemistry: Environmental Science and Engineering Applications*, *Ind. Eng. Chem. Res.* **2001**, *40*, p. 4681-4715
- Astarita, G., *Mass transfer with chemical reaction*, Elsevier publishing company, Amsterdam, 1967
- Batchelor, G.K., *Proc. Cambridge Phil. Soc.* **47**, 359 (1951).
- Beyer, R.T., Stephen Letcher, *Physical Ultrasonics*, pp 235-237 . Academic Press, New York, 1969.
- Boocock, D., short personal communication, University of Toronto-Canada, October of 2003.
- Borrero, E., "Optimization studies for the alkaline transesterification biodiesel reaction using ultrasound mixing", Master Thesis. University of Puerto Rico, Mayaguez, 2002.
- BRANSON ULTRASONIC CORPORATION, *Models 250 & 450 User's Manual*. Connecticut U.S.A. , 1998.
- Brendel, M., Mhandi, A. and Marquardt, W., "Estimation of reaction and mass transfer in multi-phase reactors". Internal report. RWTH AACHEN, Germany, 2002.
- Calderbank, P.H., Moo-Yung, M.B. and Ribby, R., "Coalescence in bubble reactors and absorbers". Third European Sym. Chem. Reactors Eng.. Pergamon press, Oxford, 1965.
- Carlin, B., *Ultrasonica* , Ediciones URMO, Spain, 1972.
- Crank, J., *The mathematics of diffusion*. Oxford University Press, New York, 1979.
- Darnoko, D. and Cheryan M., "Continuous Production of Palm Methyl Esters". *JAACS*, pp. 1269-1272, **77**, 12, 2000.
- Darnoko, D. and Cheryan M., "Kinetics of Palm Oil Transesterification in a Batch Reactor". *JAACS*, pp. 1263-1267, **77**, No. 12, 2000.

- Deuel, H., "The lipids: Their chemistry and Biochemistry". Interscience publishers Inc, New York, 1951.
- Eckey, E.W., "Esterification and interesterification". *JAACS*, pp. 576-579, **33**, 1956.
- Fangrui, M., Hanna M.A., *Bioresource Technology*, pp. 1-15, **70**, 1999.
- Fogler, H.S., Elements of Chemical Reaction Engineering. Prentice Hall, Third Edition, New Jersey, 1999
- Freedman, B., Butterfield, R.O., Pryde, E.H., "Transesterification kinetics of soybean oil". *JAACS.*, 1986, **63**, pp. 1375-1380
- Geankoplis, C.J., Transport Processes: momentum, heat and mass. Allyn and Bacon Series in Engineering, Newton Massachussets, 1983
- Goodrum, J.W., Biodiesel bus demonstration in Atlanta '96 Olympics. Thermal techniques for detecting biodiesel fuel quality. Dept. of Biological and Agricultural Engineering, Univ. of Georgia, Athens, Ga, 1996
- Gondexdron, N., Renaudin, V., Petrier, C., Clement, M., Boldo, P., Gonthier, Y. and Bernies, A., "Experimental study of the hydrodynamic behaviour of a high frequency ultrasonic reactor". *Ultrasonics sonochemistry* **1998**, 5, pp. 1-6
- Graboski, M. and McCormick L., "Combustion of Fat and Vegetable Oil Derived Fuels in Diesel Engines". *Prog. Energy Combust. Sci.*, **24**, p.125-164, 1998
- Harkin, A., Nadim, A., and Kaper, T.J., *Phys. Fluids*, **11**, 2, p. 274-287, 1999.
- Hill, C.G. jr., An Introduction of Chemical Engineering Kinetics and Reactor Design. John Wiley, New York, 1977
- Kanakci, M., "Production of Biodiesel from feedstocks with high free fatty acids and its effect on diesel engine performance and emissions", Doctoral dissertation. Iowa State University, Ames, 2001
- Kann, J., Rang, H., and Kriis, J., *Proc. Stonian Acad. Sci. Chem.*, **51**, 2, p. 75-117, 2002.
- Keshavamurthy, H.C., and Sridhar S., "Novel Capacitor fluid from vegetable oil". Conference record of the 1998 IEEE international symposium on Electrical insulation, Arlington, Virginia, USA, 1998.

- Kimmel, T., Joshi, M., and Schomäcker, R., "The influence of the liquid-liquid interphase on the kinetics of the transesterification of methyl esters of fatty acids with glycerol In-situ measurement of drop size distribution at high volume fractions of dispersed phase". Proposal of research, *Institut für Technische Universität Berlin*, 2000
- Kings, F.R., *JAACS*, 1985, **62**, pp. 815-818
- Kolmogoroff, A.N., *Compt. Rend. Acad. Sci. U.S.S.R.* **30**, 301 (1941).
- Kusdiana, D., and Saka, S., "Methyl esterification of free fatty acids of rapeseed oil as treated in supercritical methanol". *Journal of Chemical Engineering of Japan*, Vol. 34, No. 3, pp. 383-387, 2001
- Lee I., Johnson, L.A., Hammond E.G., "Use of branched-chain esters to reduce the crystallization temperature of biodiesel". *JAACS*, 1995, **72**, pp. 1155-1160
- Levenspiel, O., *Chemical reaction engineering*, John Wiley & Sons, Inc., Second Edition, New York, 1972
- Löning, J.M., Horst, C., Hoffmann, U., *Ultrasonics sonochemistry* **2002**, *9*, pp. 169-179
- Mason, T.J., "Sonochemistry", Oxford University Press, New York, 1999.
- McCabe, W.L., Smith, J.C., and Harriot, P., *Unit Operations in Chemical Engineering*, McGraw Hill International Editions, Fourth Edition, New York, 1985
- Microsoft Corporation, Microsoft® Encarta® Online Encyclopedia, "Internal-Combustion Engine", web page: <http://encarta.msn.com> © 1997-2002
- Millich, F., and Carraher C.E. Jr., *Interfacial Synthesis: Vol. I*, Marcell Dekker Inc, New York, 1977.
- Noble, T., Ultrasound: Coming Over Loud and Clear, *Chemical Engineering Progress*, **98**, *9*, p. 10-12, 2002
- Peterson, C.L., and Auld, D.L., Technical overview of vegetable oils as a transportation fuel, *Solid fuel conversion for the transportation section, FACT-* **12**, ASME, 1991
- Prasad, D.V., Rajan, R., Kumar, R., Gandhi, K.S., Arakeri, V.H. and Chandrasekaran, S., "Modelling a Batch Sonochemical Reactor". *Chemical Engineering Science*, **49**, *6*, pp.877-888, 1994.

- Shinnar, R. and Church, M., "Predicting particle size in agitated dispersion". *Industrial and Engineering Chemistry*, **52**, 3, pp.253-256, 1960.
- Shutilov, V.A., Fundamentals physics of ultrasound, Gordon and Breach science publishers, Amsterdam, 1988.
- SONICSYSTEMS, Power ultrasonic equipment, practice and application, <http://www.sonicystems.co.uk/sonic.htm>, Based on a paper presented at the Sonochemistry Symposium, Annual Chemical Congress, held at Warwick University, UK, 8-11 April 1986.
- Treybal, R. E., Mass-Transfer Operations, McGraw Hill chemical engineering series, Third Edition, New York, 1980.
- Uhl, V.W., Gray, J.B., "Mixing: Theory and Practice Vol. 2", Academic Press, London, 1967.
- Van Gerpen, J., Johnson, L., Hammond, E.J., and Marley, S.J., "Determining the Optimum Composition of a Biodiesel Fuel". Report prepared for the Iowa Soybean Promotion Board. Iowa State University, 1995.
- Vichare, N.P., Gogate, P.R., Dindore, V.Y., Pandit A.B., Mixing time analysis of a sonochemical reactor, *Ultrasonics sonochemistry* **2001**, 8, p. 23-33.
- Walas, S.M., Modeling with Differential Equations in Chemical Engineering. Howard Brenner, Boston, 1991
- Young, R. "Cavitation," McGraw Hill, London, 1989.

**APPENDIX 1 : Bubble Dynamic Simulations for the system soybean
oil-methanol at 15 W**

ULTRASONIC Soybean Oil - methanol (Simulation at 15W)

A. General Data (Inputs)

$$\text{Speed} := 1460 \frac{\text{m}}{\text{s}} \quad \text{Pot} := 15 \quad \text{Watts} \quad \text{R0} := 2 \cdot 10^{-6} \text{ m} \quad \text{Ps} := 5332 \quad \text{Pa}$$

$$\text{DiameterReactor} := 0.05 \quad \text{m} \quad \text{Alpha} := 1 \quad \text{isothermal} \quad \text{sigma} := 0.0358 \quad \frac{\text{N}}{\text{m}}$$

$$\text{Temp} := 338 \quad \text{K} \quad \text{Dl} := 899 \quad \frac{\text{Kg}}{\text{m}^3} \quad \text{Pb} := 101325 \quad \text{Pa}$$

$$\text{GAMMA} := 1.203 \quad \text{Adiabatic Cp/Cv} \quad \text{f} := 20000 \quad \text{s}^{-1} \quad \text{Frequency of the ultrasound}$$

DETERMINATION OF MAIN VARIABLES

$$\text{Area} := \frac{\pi}{4} \cdot \text{DiameterReactor}^2 \quad \text{Area} = 0.001963495408494 \quad \text{m}^2$$

$$\text{I} := \frac{\text{Pot}}{\text{Area}} \quad \text{I} = 7639.43726841098 \quad \frac{\text{W}}{\text{m}^2}$$

$$\text{PGO} := \text{Pb} + 2 \cdot \frac{\text{sigma}}{\text{R0}} - \text{Ps} \quad \text{PGO} = 131793 \quad \text{Pascal}$$

$$\mathbf{Pa} := (2 \cdot \mathbf{Dl} \cdot \mathbf{Speed} \cdot \mathbf{I})^{0.5} \quad \mathbf{Pa} = 141612.619439654 \quad \mathbf{Pa} \quad \mathbf{R2} := \mathbf{R0} \cdot \left(\frac{\mathbf{PGO}}{\mathbf{Ps}} \right)^{\frac{1}{3}}$$

$$\mathbf{R2} = 0.000005825913919$$

$$\mathbf{Rc} := 4 \cdot \frac{\mathbf{sigma}}{[3 \cdot [\mathbf{Ps} - (\mathbf{Pb} - \mathbf{Pa})]]} \quad \mathbf{Rc} = 0.00000104633344 \quad \mathbf{meters}$$

The smallest bubble at the lowest pressure of the system

$$\mathbf{F(RI)} := \left[\frac{[3 \cdot (\mathbf{Pb} - \mathbf{Ps}) \cdot \mathbf{RI}^3 + 6 \cdot \mathbf{sigma} \cdot \mathbf{RI}^2]}{2 \cdot \mathbf{sigma}} \right]^{0.5} - \mathbf{Rc}$$

$$\mathbf{z} := 1 \cdot 10^{-6}$$

$$\mathbf{RI} := \mathbf{root}(\mathbf{F(z)}, \mathbf{z})$$

$$\mathbf{RI} = 0.000000530472745 \quad \mathbf{meters}$$

Estimating R0 to compare it with the value assumed or introduced in the Input data Section

B. Bubble grows Isothermally

$$\mathbf{EP1} := 42.01 \cdot 10^{-6}$$

End Point of Exploration (Trial and Error)

$$\mathbf{td} := 2 \cdot 10^{-8}, 3 \cdot 10^{-8} \dots \mathbf{EP1}$$

Solve

$$D(x, y) := \left[\left[\left[\frac{1}{DI} \left[\frac{-Pb}{y_0} + Pa \cdot \frac{\sin(f \cdot x)}{y_0} + PGO \cdot \frac{(R0)^{(3 \cdot Alpha)}}{(y_0)^{[(3 \cdot Alpha) + 1]}} + \frac{Ps}{y_0} - 2 \cdot \frac{\sigma}{(y_0)^2} \right] - 1.5 \cdot \frac{(y_1)^2}{y_0} \right] \right] \right]$$

$$P(td) := \text{rkfixed} \left[\begin{pmatrix} R0 \\ 0 \end{pmatrix}, 0, td, 200, D \right] \quad n := 0, 1..200$$

$$Diff(td) := \left[\left[R2 - (P(td)^{\langle 1 \rangle})_{200} \right] \right] \quad \text{Optimization function}$$

$$t := EP1$$

Initial value for the search of the optimal

$$\text{root}(Diff(t), t) = 0.00004200239887$$

$$\text{soln} := \text{root}(Diff(t), t)$$

$$\text{round}(\text{soln}, 7) = 0.000042$$

$$\text{xx} := \text{round}(\text{soln}, 7) \quad \text{xx} = 0.000042$$

time necessary to reach a radius of R2 by optimization

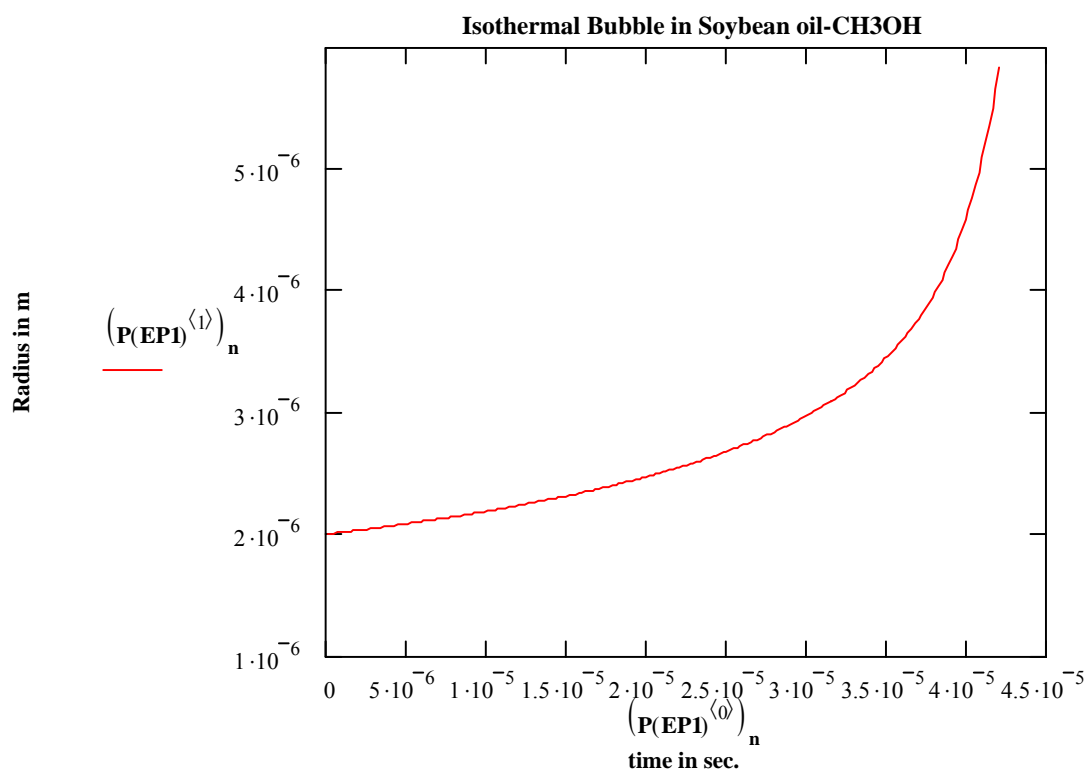
$$EP1 = 0.00004201$$

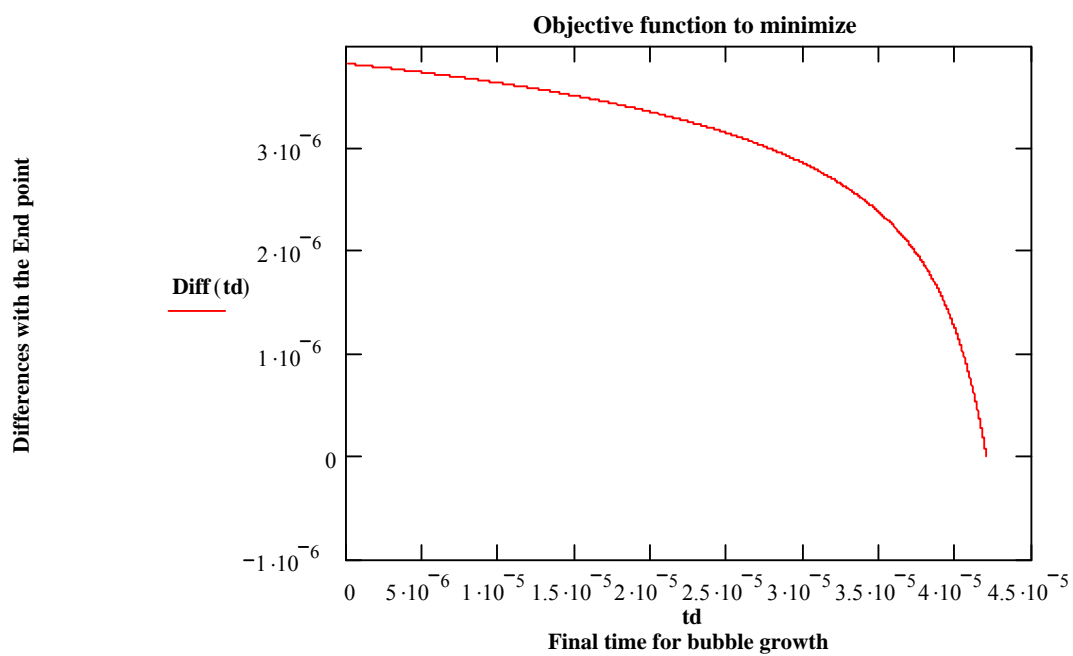
time necessary to reach a radius of R2 by Trial and error

$$\left(\mathbf{P}(\mathbf{EPI})^{(1)}\right)_{200} = 0.000005832828824$$

$$\left(\mathbf{P}(\mathbf{xx})^{(1)}\right)_{200} = 0.000005824393306$$

Checking the solution for Isothermal growing of the bubble





C. Bubble falling in adiabatic collapse

$$dRdt := \left(P(EP1)^{(2)} \right)_{200}$$

$$dRdt = 0.845030420864392$$

Initial condition for the first derivate is a result from part B

$$EP := 183.2723410^{-6}$$

End Point of Exploration (Trial and Error)

$$tf := EP$$

Iteration for life time of bubble

Solve

$$\mathbf{D}(\mathbf{x}, \mathbf{y}) := \left[\left[\left[\frac{1}{\mathbf{DI}} \cdot \left[\frac{-\mathbf{Pb}}{\mathbf{y}_0} + \mathbf{Pa} \cdot \frac{(\sin(\mathbf{f} \cdot \mathbf{x}))}{\mathbf{y}_0} + 2 \cdot \mathbf{Ps} \cdot \frac{\mathbf{R2}^{(3 \cdot \mathbf{Alpha})}}{(\mathbf{y}_0)^{[(3 \cdot \mathbf{Alpha}) + 1]}} - 2 \cdot \frac{\mathbf{sigma}}{(\mathbf{y}_0)^2} \right] - 1.5 \cdot \frac{(\mathbf{y}_1)^2}{\mathbf{y}_0} \right] \right] \right]$$

$$\mathbf{Q}(\mathbf{tf}) := \text{rkfixed} \left[\begin{pmatrix} \mathbf{R2} \\ \mathbf{dRdt} \end{pmatrix}, \mathbf{EP1}, \mathbf{tf}, 200, \mathbf{D} \right] \quad \mathbf{n} := 0, 1..200$$

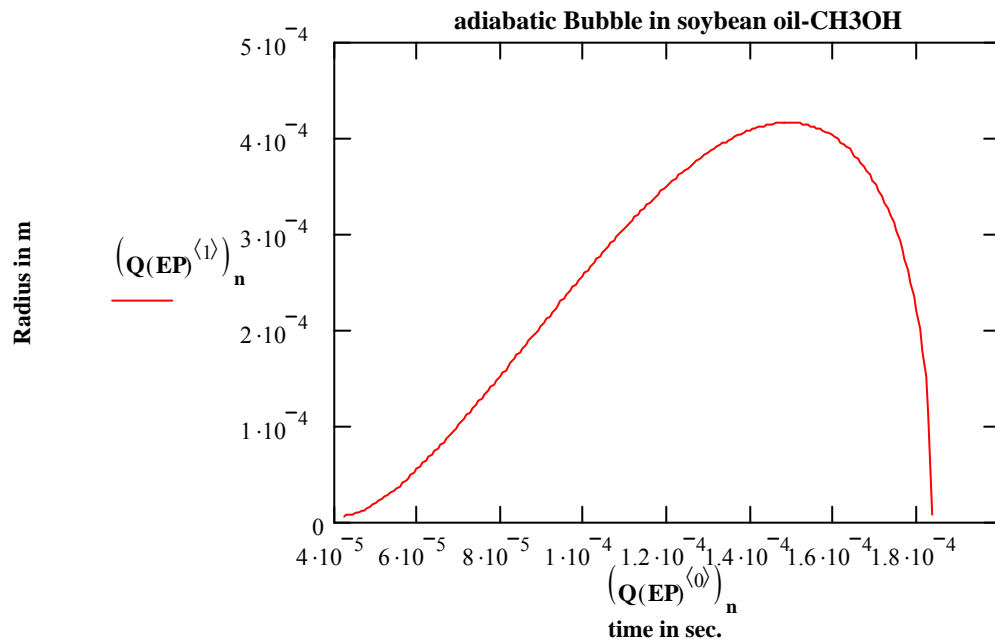
$$\mathbf{Diff2}(\mathbf{tf}) := \left[\text{Speed} - \left| \left(\mathbf{Q}(\mathbf{tf})^{(2)} \right)_{200} \right| \right] \quad \text{Optimization function}$$

$$\mathbf{Diff2}(\mathbf{EP}) = -0.553839204404085$$

$$\left(\mathbf{Q}(\mathbf{EP})^{(1)} \right)_{200} = 0.000008247257921 \quad \text{meters, bubble radius at collapse}$$

$$\left(\mathbf{Q}(\mathbf{EP})^{(2)} \right)_{200} = -1460.5538392044 \quad \text{Speed of the wall bubble at collapse in m/s}$$

Checking the solution for adiabatic collapse of the bubble



$$Rf(EP) := (Q(EP)^{\langle 1 \rangle})_{200}$$

$$Rf(EP) = 0.000008247257921$$

$$TEMPf := Temp \left(\frac{R2}{Rf(EP)} \right)^{3 \cdot (GAMMA - 1)}$$

$$TEMPf = 273.52113042377$$

Temperature at collapse in Kelvin

$$PRESSf := \left(\left(\frac{R2}{Rf(EP)} \right) \right)^{3 \cdot GAMMA} \cdot (2 \cdot Ps)$$

PRESSf = 3041.98997759494

Pressure at collapse in Pascal

RMAX := $\max(Q(EP)^{\langle 1 \rangle})$

RMAX = 0.000415611707025 **meters**

Maximum Radius of the bubble

D. Final Solution for isothermal growing and adiabatic collapse of the bubble

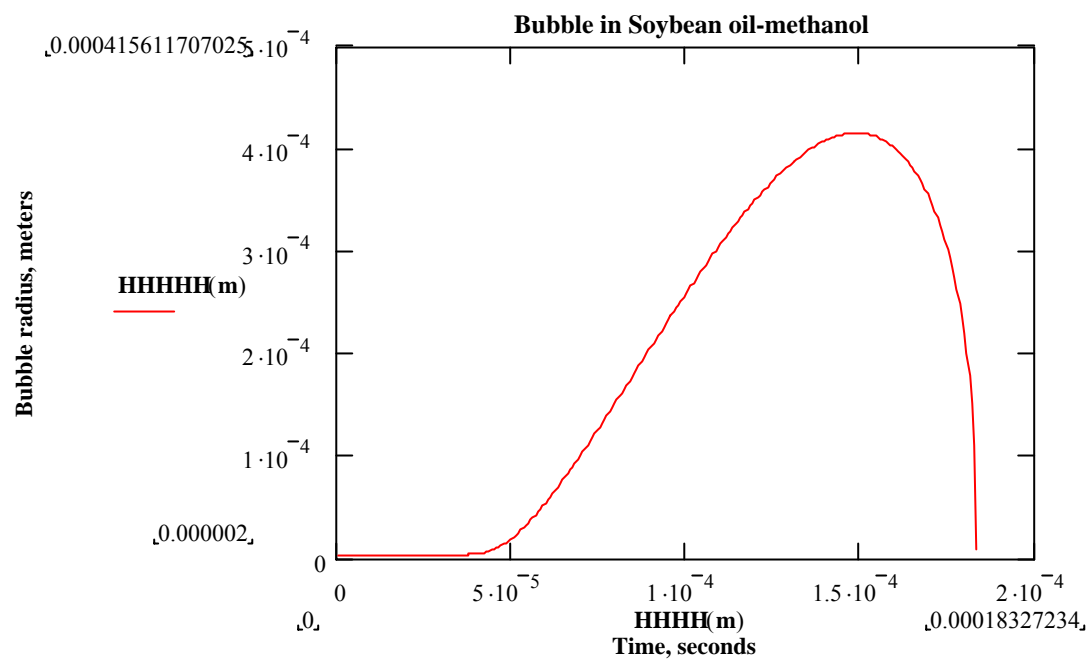
m := 0, 1 .. 401

HH := $\text{stack}[(P(EP1)^{\langle 0 \rangle}), (Q(EP)^{\langle 0 \rangle})]$

HHH := $\text{stack}[(P(EP1)^{\langle 1 \rangle}), (Q(EP)^{\langle 1 \rangle})]$

HHHH(m) := $[(m \leq 200) \cdot \mathbf{HH}_m + (m > 200) \cdot \mathbf{HH}_{m+1}]$ Axis X

HHHHH(m) := $[(m \leq 200) \cdot \mathbf{HHH}_m + (m > 200) \cdot \mathbf{HHH}_{m+1}]$ Axis Y



**APPENDIX 2 : Bubble Dynamic Simulations for the system soybean
oil-methanol at 9.84 W**

ULTRASONIC Soybean Oil - methanol (Simulation at 9.84 W)
Experimental Conditions of Intensity of Power

A. General Data (Inputs)

$$\text{Speed} := 1460 \frac{\text{m}}{\text{s}} \quad \text{Pot} := 9.84 \text{ Watts} \quad \text{R0} := 2 \cdot 10^{-6} \text{ m} \quad \text{Ps} := 5332 \text{ Pa}$$

$$\text{DiameterReactor} := 0.05 \text{ m} \quad \text{Alpha} := 1 \text{ isothermal} \quad \text{sigma} := 0.0358 \frac{\text{N}}{\text{m}}$$

$$\text{Temp} := 338 \text{ K} \quad \text{Dl} := 899 \frac{\text{Kg}}{\text{m}^3} \quad \text{Pb} := 101325 \text{ Pa}$$

$$\text{GAMMA} := 1.203 \text{ Adiabatic Cp/Cv} \quad \text{f} := 20000 \text{ s}^{-1} \text{ Frequency of the ultrasound}$$

DETERMINATION OF MAIN VARIABLES

$$\text{Area} := \frac{\pi}{4} \cdot \text{DiameterReactor}^2 \quad \text{Area} = 0.001963495408494 \text{ m}^2$$

$$\text{I} := \frac{\text{Pot}}{\text{Area}} \quad \text{I} = 5011.4708480776 \frac{\text{W}}{\text{m}^2}$$

$$\text{PGO} := \text{Pb} + 2 \cdot \frac{\text{sigma}}{\text{R0}} - \text{Ps} \quad \text{PGO} = 131793 \text{ Pascal}$$

$$\mathbf{Pa} := (2 \cdot \mathbf{DI} \cdot \mathbf{Speed} \cdot \mathbf{I})^{0.5} \quad \mathbf{Pa} = 114697.479893289 \quad \mathbf{Pa} \quad \mathbf{R2} := \mathbf{R0} \cdot \left(\frac{\mathbf{PGO}}{\mathbf{Ps}} \right)^{\frac{1}{3}}$$

$$\mathbf{R2} = 0.000005825913919$$

$$\mathbf{Rc} := 4 \cdot \frac{\mathbf{sigma}}{[3 \cdot [\mathbf{Ps} - (\mathbf{Pb} - \mathbf{Pa})]]} \quad \mathbf{Rc} = 0.000002551973303 \text{ meters}$$

The smallest bubble at the lowest pressure of the system

$$\mathbf{F}(\mathbf{RI}) := \left[\frac{[3 \cdot (\mathbf{Pb} - \mathbf{Ps}) \cdot \mathbf{RI}^3 + 6 \cdot \mathbf{sigma} \cdot \mathbf{RI}^2]}{2 \cdot \mathbf{sigma}} \right]^{0.5} - \mathbf{Rc}$$

$$\mathbf{z} := 1 \cdot 10^{-6}$$

$$\mathbf{RI} := \mathbf{root}(\mathbf{F}(\mathbf{z}), \mathbf{z})$$

$$\mathbf{RI} = 0.000000971322573 \text{ meters}$$

Estimating R0 to compare it with the value assumed or introduced in the Input data Section

B. Bubble grows Isothermally

$$\mathbf{EP1} := 57.03 \cdot 10^{-6}$$

End Point of Exploration (Trial and Error)

$$\mathbf{td} := 2 \cdot 10^{-8}, 3 \cdot 10^{-8} \dots \mathbf{EP1}$$

Solve

$$D(x, y) := \left[\left[\left[\frac{1}{DI} \left[\frac{-Pb}{y_0} + Pa \cdot \frac{\sin(f \cdot x)}{y_0} + PGO \cdot \frac{(R0)^{(3 \cdot Alpha)}}{(y_0)^{[(3 \cdot Alpha) + 1]}} + \frac{Ps}{y_0} - 2 \cdot \frac{\sigma}{(y_0)^2} \right] - 1.5 \cdot \frac{(y_1)^2}{y_0} \right] \right] \right]$$

$$P(td) := \text{rkfixed} \left[\begin{pmatrix} R0 \\ 0 \end{pmatrix}, 0, td, 200, D \right] \quad n := 0, 1..200$$

$$Diff(td) := \left[\left[R2 - (P(td))_{200}^{(1)} \right] \right] \quad \text{Optimization function}$$

$$t := EP1$$

Initial value for the search of the optimal

$$\text{root}(Diff(t), t) = 0.000057037741069$$

$$\text{soln} := \text{root}(Diff(t), t)$$

$$\text{round}(\text{soln}, 7) = 0.000057$$

$$\text{xx} := \text{round}(\text{soln}, 7) \quad \text{xx} = 0.000057$$

time necessary to reach a radius of R2 by optimization

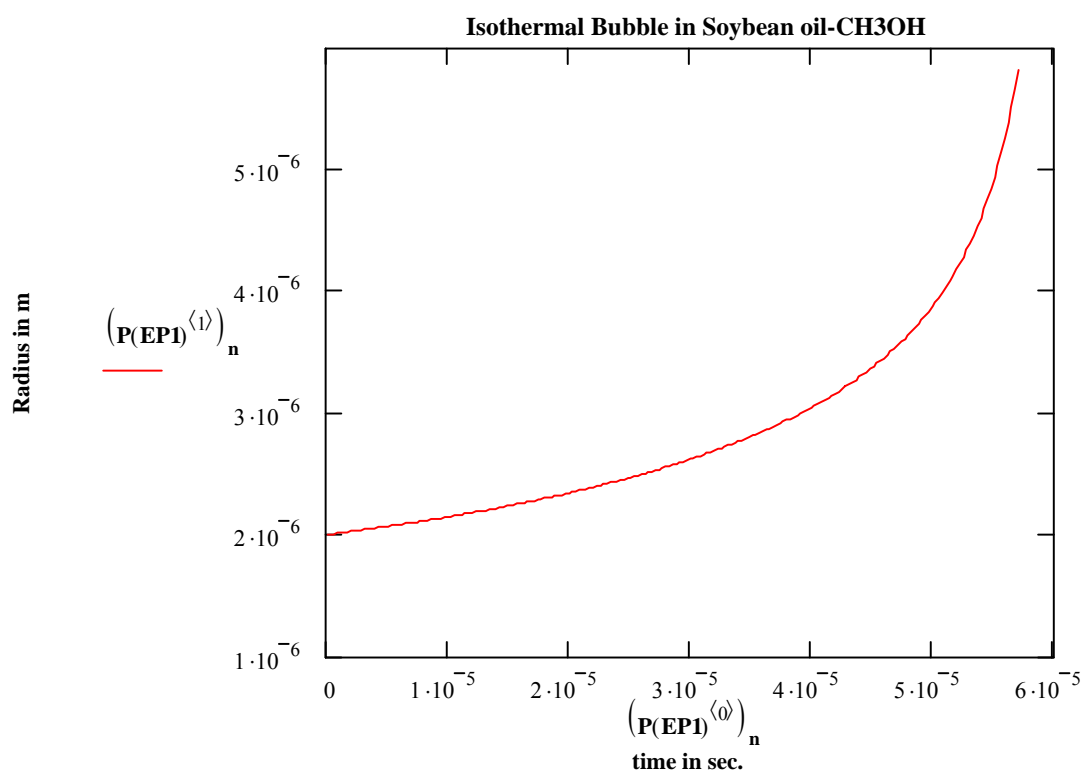
$$EP1 = 0.00005703$$

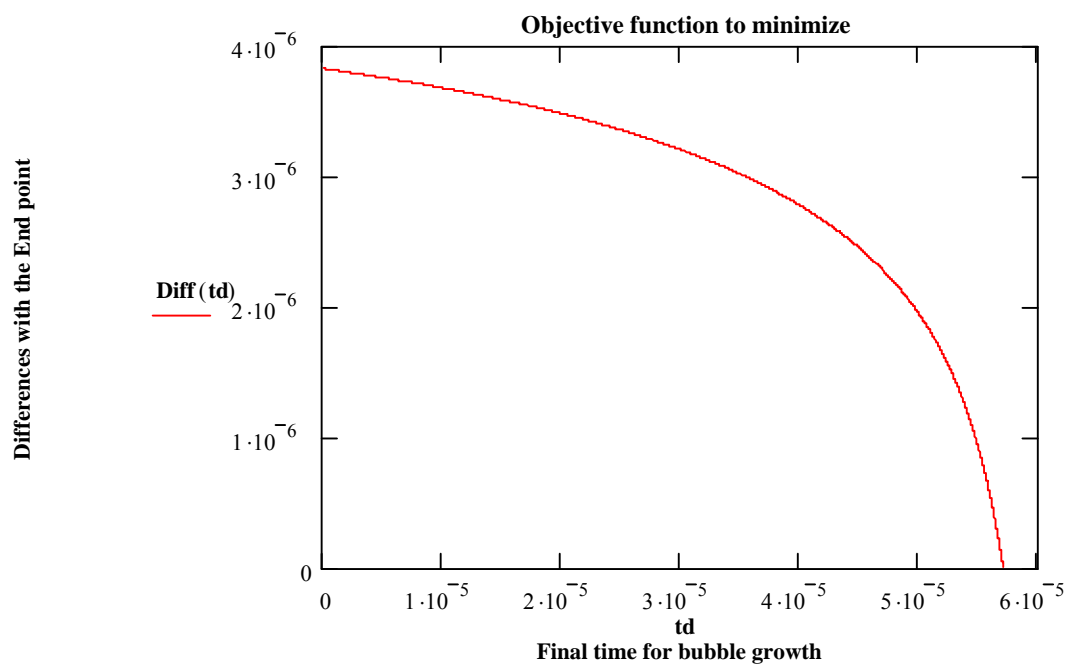
time necessary to reach a radius of R2 by Trial and error

$$\left(\mathbf{P}(\mathbf{E}\mathbf{P}\mathbf{1})^{\langle 1 \rangle}\right)_{200} = 0.000005821070459$$

$$\left(\mathbf{P}(\mathbf{x}\mathbf{x})^{\langle 1 \rangle}\right)_{200} = 0.000005803841199$$

Checking the solution for Isothermal growing of the bubble





C. Bubble falling in adiabatic collapse

$$dRdt := \left(P(EP1)^{\langle 2 \rangle} \right)_{200}$$

$$dRdt = 0.576739425667973$$

Initial condition for the first derivate is a result from part B

$$EP := 139.1855710^{-6}$$

End Point of Exploration (Trial and Error)

$$tf := EP$$

Iteration for life time of bubble

Solve

$$\mathbf{D}(\mathbf{x}, \mathbf{y}) := \begin{bmatrix} y_1 \\ \left[\frac{1}{\mathbf{DI}} \cdot \left[\frac{-\mathbf{Pb}}{y_0} + \mathbf{Pa} \cdot \frac{(\sin(\mathbf{f} \cdot \mathbf{x}))}{y_0} + 2 \cdot \mathbf{Ps} \cdot \frac{\mathbf{R2}^{(3 \cdot \mathbf{Alpha})}}{(y_0)^{[(3 \cdot \mathbf{Alpha}) + 1]}} - 2 \cdot \frac{\mathbf{sigma}}{(y_0)^2} \right] - 1.5 \cdot \frac{(y_1)^2}{y_0} \right] \end{bmatrix}$$

$$\mathbf{Q}(\mathbf{tf}) := \text{rkfixed} \left[\begin{pmatrix} \mathbf{R2} \\ \mathbf{dRdt} \end{pmatrix}, \mathbf{EP1}, \mathbf{tf}, 200, \mathbf{D} \right] \quad \mathbf{n} := 0, 1..200$$

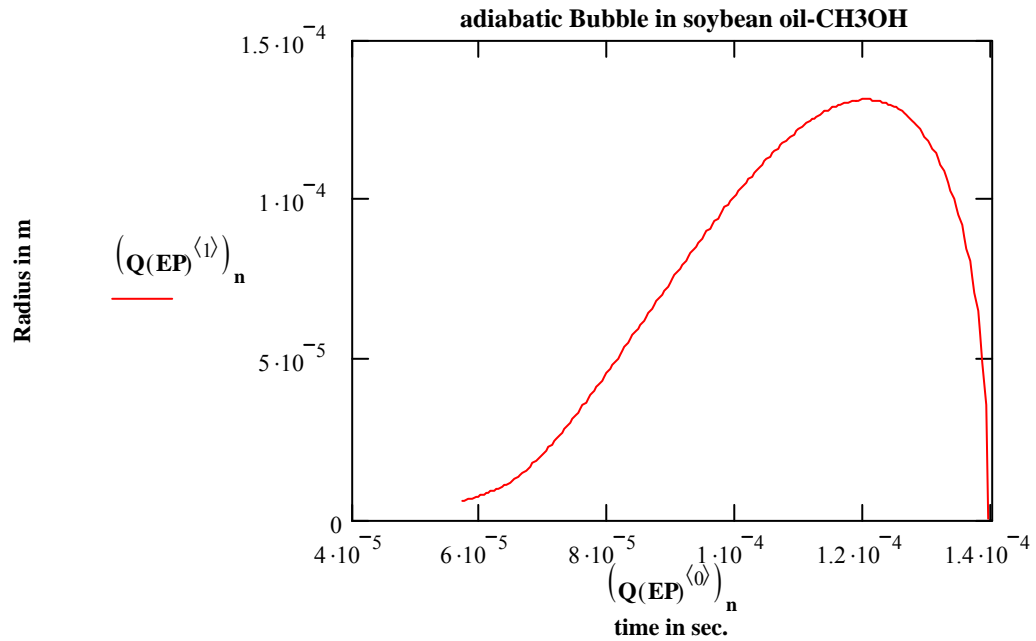
$$\mathbf{Diff2}(\mathbf{tf}) := \left[\text{Speed} - \left| \left(\mathbf{Q}(\mathbf{tf})^{(2)} \right)_{200} \right| \right] \quad \text{Optimization function}$$

$$\mathbf{Diff2}(\mathbf{EP}) = -0.267478783154047$$

$$\left(\mathbf{Q}(\mathbf{EP})^{(1)} \right)_{200} = 0.000000256199692 \quad \text{meters, bubble radius at collapse}$$

$$\left(\mathbf{Q}(\mathbf{EP})^{(2)} \right)_{200} = -1460.26747878315 \quad \text{Speed of the wall bubble at collapse in m/s}$$

Checking the solution for adiabatic collapse of the bubble



$$Rf(EP) := (Q(EP)^{\langle 1 \rangle})_{200}$$

$$Rf(EP) = 0.000000256199692$$

$$TEMPf := Temp \left(\frac{R2}{Rf(EP)} \right)^{3 \cdot (GAMMA - 1)}$$

$$TEMPf = 2265.6824759863$$

Temperature at collapse in Kelvin

$$PRESSf := \left(\left(\frac{R2}{Rf(EP)} \right) \right)^{3 \cdot GAMMA} \cdot (2 \cdot Ps)$$

PRESSf = 840540923.13778

Pressure at collapse in Pascal

RMAX := $\max(Q(EP)^{\langle 1 \rangle})$

RMAX = 0.000131329877013 **meters**

Maximum Radius of the bubble

D. Final Solution for isothermal growing and adiabatic collapse of the bubble

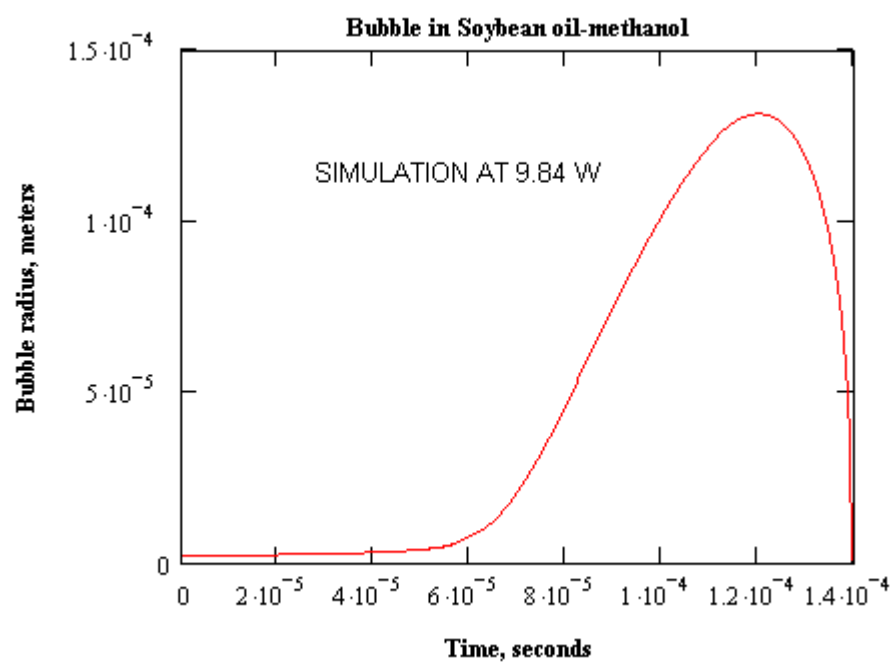
m := 0, 1 .. 401

HH := $\text{stack}[(P(EP1)^{\langle 0 \rangle}), (Q(EP)^{\langle 0 \rangle})]$

HHH := $\text{stack}[(P(EP1)^{\langle 1 \rangle}), (Q(EP)^{\langle 1 \rangle})]$

HHHH(m) := $[(m \leq 200) \cdot \mathbf{HH}_m + (m > 200) \cdot \mathbf{HH}_{m+1}]$ Axis X

HHHHH(m) := $[(m \leq 200) \cdot \mathbf{HHH}_m + (m > 200) \cdot \mathbf{HHH}_{m+1}]$ Axis Y



**APPENDIX 3: Bubble Dynamic Simulations for the system tallow-
methanol at 15 W**

ULTRASONIC Tallow - methanol (Simulation at 15W)

A. General Data (Inputs)

$$\text{Speed} := 1460 \frac{\text{m}}{\text{s}} \quad \text{Pot} := 15 \quad \text{Watts} \quad \text{R0} := 2 \cdot 10^{-6} \text{ m} \quad \text{Ps} := 5332 \quad \text{Pa}$$

$$\text{DiameterReactor} := 0.05 \quad \text{m} \quad \text{Alpha} := 1 \quad \text{isothermal} \quad \text{sigma} := 0.0342 \quad \frac{\text{N}}{\text{m}}$$

$$\text{Temp} := 340 \quad \text{K} \quad \text{Dl} := 886 \quad \frac{\text{Kg}}{\text{m}^3} \quad \text{Pb} := 101325 \quad \text{Pa}$$

$$\text{GAMMA} := 1.203 \quad \text{Adiabatic Cp/Cv} \quad \text{f} := 20000 \quad \text{s}^{-1} \quad \text{Frequency of the ultrasound}$$

DETERMINATION OF MAIN VARIABLES

$$\text{Area} := \frac{\pi}{4} \cdot \text{DiameterReactor}^2 \quad \text{Area} = 0.001963495408494 \quad \text{m}^2$$

$$\text{I} := \frac{\text{Pot}}{\text{Area}} \quad \text{I} = 7639.43726841098 \quad \frac{\text{W}}{\text{m}^2}$$

$$\text{PGO} := \text{Pb} + 2 \cdot \frac{\text{sigma}}{\text{R0}} - \text{Ps} \quad \text{PGO} = 130193 \quad \text{Pascal}$$

$$Pa := (2 \cdot DI \cdot Speed \cdot I)^{0.5}$$

$$Pa = 140584.995450622 \quad Pa$$

$$R2 := R0 \cdot \left(\frac{PGO}{Ps} \right)^{\frac{1}{3}}$$

$$R2 = 0.000005802241846$$

$$Rc := 4 \cdot \frac{\sigma}{3 \cdot [Ps - (Pb - Pa)]}$$

$$Rc = 0.000001022605056 \text{ meters}$$

The smallest bubble at the lowest pressure of the system

$$F(RI) := \left[\frac{3 \cdot (Pb - Ps) \cdot RI^3 + 6 \cdot \sigma \cdot RI^2}{2 \cdot \sigma} \right]^{0.5} - Rc$$

$$z := 1 \cdot 10^{-6}$$

$$RI := \text{root}(F(z), z)$$

$$RI = 0.000000521675889 \text{ meters}$$

Estimating R0 to compare it with the value assumed or introduced in the Input data Section

B. Bubble grows Isothermally

$$EP1 := 42.08 \cdot 10^{-6}$$

End Point of Exploration (Trial and Error)

$$td := 2 \cdot 10^{-8}, 3 \cdot 10^{-8} \dots EP1$$

Solve

$$D(x, y) := \left[\left[\left[\frac{1}{DI} \left[\frac{-Pb}{y_0} + Pa \cdot \frac{\sin(f \cdot x)}{y_0} + PGO \cdot \frac{(R0)^{(3 \cdot Alpha)}}{(y_0)^{[(3 \cdot Alpha) + 1]}} + \frac{Ps}{y_0} - 2 \cdot \frac{\sigma}{(y_0)^2} \right] - 1.5 \cdot \frac{(y_1)^2}{y_0} \right] \right] \right]$$

$$P(td) := \text{rkfixed} \left[\begin{pmatrix} R0 \\ 0 \end{pmatrix}, 0, td, 200, D \right] \quad n := 0, 1..200$$

$$Diff(td) := \left[\left[R2 - (P(td)^{\langle 1 \rangle})_{200} \right] \right] \quad \text{Optimization function}$$

t := EP1

Initial value for the search of the optimal

$$\text{root}(Diff(t), t) = 0.000042072571743$$

$$\text{soln} := \text{root}(Diff(t), t)$$

$$\text{round}(\text{soln}, 7) = 0.0000421$$

$$\text{xx} := \text{round}(\text{soln}, 7) \quad \text{xx} = 0.0000421$$

time necessary to reach a radius of R2 by optimization

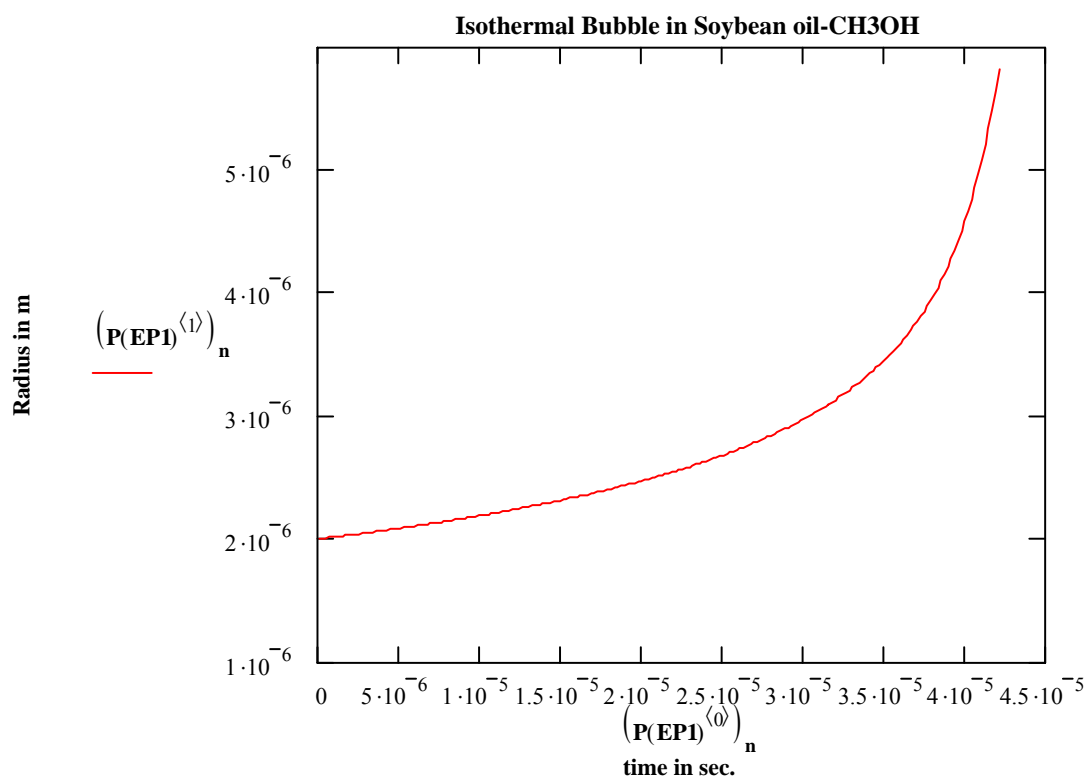
$$\text{EP1} = 0.00004208$$

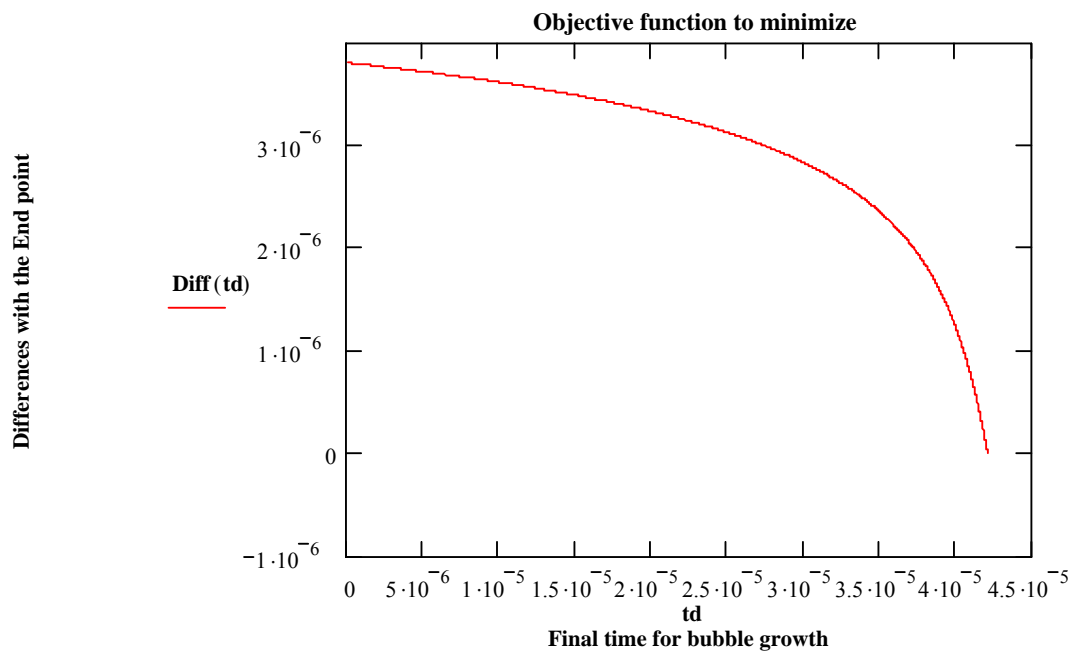
time necessary to reach a radius of R2 by Trial and error

$$\left(\mathbf{P}(\mathbf{EP1})^{(1)}\right)_{200} = 0.00000580884263$$

$$\left(\mathbf{P}(\mathbf{xx})^{(1)}\right)_{200} = 0.000005825416081$$

Checking the solution for Isothermal growing of the bubble





C. Bubble falling in adiabatic collapse

$$dRdt := \left(P(EP1)^{\langle 2 \rangle} \right)_{200}$$

$$dRdt = 0.825801424063212$$

Initial condition for the first derivate is a result from part B

$$EP := 182.2078610^{-6}$$

End Point of Exploration (Trial and Error)

$$tf := EP$$

Iteration for life time of bubble

Solve

$$\mathbf{D}(\mathbf{x}, \mathbf{y}) := \left[\left[\left[\frac{1}{\mathbf{DI}} \cdot \left[\frac{-\mathbf{Pb}}{y_0} + \mathbf{Pa} \cdot \frac{(\sin(f \cdot x))}{y_0} + 2 \cdot \mathbf{Ps} \cdot \frac{R2^{(3 \cdot \mathbf{Alpha})}}{(y_0)^{[(3 \cdot \mathbf{Alpha}) + 1]}} - 2 \cdot \frac{\mathbf{sigma}}{(y_0)^2} \right] - 1.5 \cdot \frac{(y_1)^2}{y_0} \right] \right] \right]$$

$$\mathbf{Q}(\mathbf{tf}) := \text{rkfixed} \left[\begin{pmatrix} \mathbf{R2} \\ \mathbf{dRdt} \end{pmatrix}, \mathbf{EP1}, \mathbf{tf}, 200, \mathbf{D} \right] \quad \mathbf{n} := 0, 1..200$$

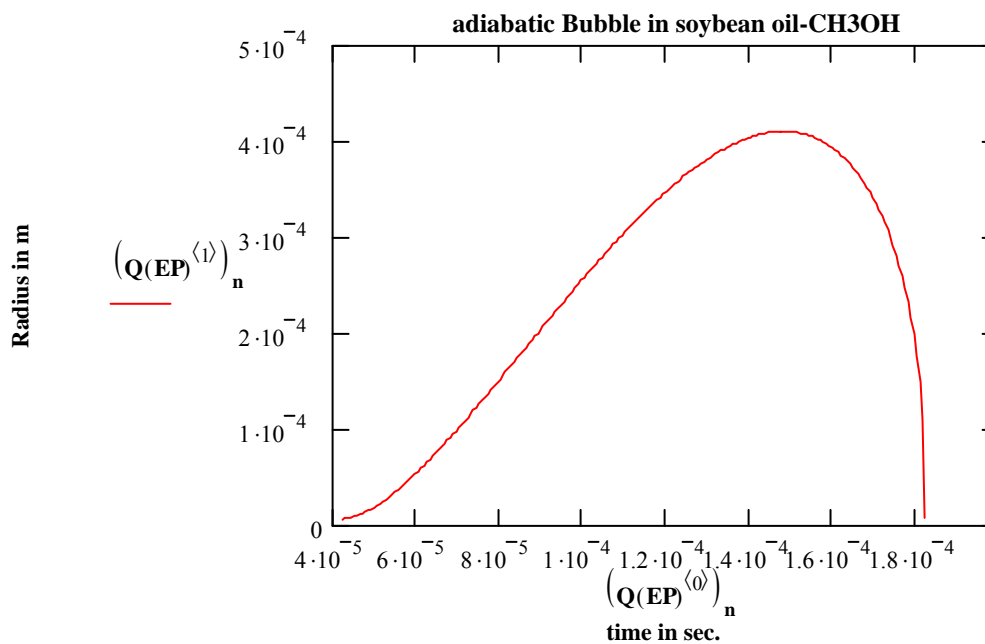
$$\mathbf{Diff2}(\mathbf{tf}) := \left[\text{Speed} - \left| \left(\mathbf{Q}(\mathbf{tf})^{(2)} \right)_{200} \right| \right] \quad \text{Optimization function}$$

$$\mathbf{Diff2}(\mathbf{EP}) = -0.16008341569318$$

$$\left(\mathbf{Q}(\mathbf{EP})^{(1)} \right)_{200} = 0.000008075462155 \quad \text{meters, bubble radius at collapse}$$

$$\left(\mathbf{Q}(\mathbf{EP})^{(2)} \right)_{200} = -1460.16008341569 \quad \text{Speed of the wall bubble at collapse in m/s}$$

Checking the solution for adiabatic collapse of the bubble



$$Rf(EP) := (Q(EP)^{\langle 1 \rangle})_{200}$$

$$Rf(EP) = 0.000008075462155$$

$$TEMPf := Temp \left(\frac{R2}{Rf(EP)} \right)^{3 \cdot (GAMMA - 1)}$$

$$TEMPf = 277.999386456059$$

Temperature at collapse in Kelvin

$$PRESSf := \left(\left(\frac{R2}{Rf(EP)} \right) \right)^{3 \cdot GAMMA} \cdot (2 \cdot Ps)$$

PRESSf = 3234.22611037275

Pressure at collapse in Pascal

RMAX := $\max(Q(EP)^{\langle 1 \rangle})$

RMAX = 0.000409734992994 **meters**

Maximum Radius of the bubble

D. Final Solution for isothermal growing and adiabatic collapse of the bubble

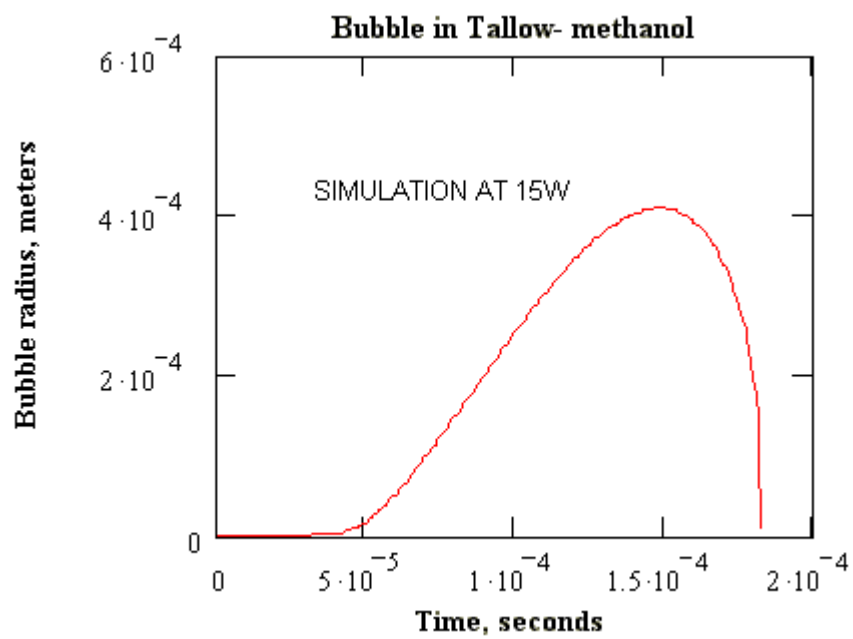
m := 0, 1 .. 401

HH := $\text{stack}[(P(EP1)^{\langle 0 \rangle}), (Q(EP)^{\langle 0 \rangle})]$

HHH := $\text{stack}[(P(EP1)^{\langle 1 \rangle}), (Q(EP)^{\langle 1 \rangle})]$

HHHH(m) := $[(m \leq 200) \cdot \mathbf{HH}_m + (m > 200) \cdot \mathbf{HH}_{m+1}]$ Axis X

HHHHH(m) := $[(m \leq 200) \cdot \mathbf{HHH}_m + (m > 200) \cdot \mathbf{HHH}_{m+1}]$ Axis Y



**APPENDIX 4: Bubble Dynamic Simulations for the system tallow-
methanol at 12.54 W**

ULTRASONIC Tallow - methanol (Simulation at 12.54W)

A. General Data (Inputs)

$$\text{Speed} := 1460 \frac{\text{m}}{\text{s}} \quad \text{Pot} := 12.54 \text{ Watts} \quad \text{R0} := 2 \cdot 10^{-6} \text{ m} \quad \text{Ps} := 5332 \text{ Pa}$$

$$\text{DiameterReactor} := 0.05 \text{ m} \quad \text{Alpha} := 1 \quad \text{isothermal} \quad \text{sigma} := 0.0342 \frac{\text{N}}{\text{m}}$$

$$\text{Temp} := 340 \text{ K} \quad \text{DI} := 886 \frac{\text{Kg}}{\text{m}^3} \quad \text{Pb} := 101325 \text{ Pa}$$

$$\text{GAMMA} := 1.203 \text{ Adiabatic Cp/Cv} \quad \text{f} := 20000 \text{ s}^{-1} \text{ Frequency of the ultrasound}$$

DETERMINATION OF MAIN VARIABLES

$$\text{Area} := \frac{\pi}{4} \cdot \text{DiameterReactor}^2 \quad \text{Area} = 0.001963495408494 \text{ m}^2$$

$$\text{I} := \frac{\text{Pot}}{\text{Area}} \quad \text{I} = 6386.56955639158 \frac{\text{W}}{\text{m}^2}$$

$$\text{PGO} := \text{Pb} + 2 \cdot \frac{\text{sigma}}{\text{R0}} - \text{Ps} \quad \text{PGO} = 130193 \text{ Pascal}$$

$$Pa := (2 \cdot DI \cdot Speed \cdot I)^{0.5}$$

$$Pa = 128541.128946076 \quad Pa$$

$$R2 := R0 \cdot \left(\frac{PGO}{Ps} \right)^{\frac{1}{3}}$$

$$R2 = 0.000005802241846$$

$$Rc := 4 \cdot \frac{\sigma}{3 \cdot [Ps - (Pb - Pa)]}$$

$$Rc = 0.000001401002192 \text{ meters}$$

The smallest bubble at the lowest pressure of the system

$$F(RI) := \left[\frac{3 \cdot (Pb - Ps) \cdot RI^3 + 6 \cdot \sigma \cdot RI^2}{2 \cdot \sigma} \right]^{0.5} - Rc$$

$$z := 1 \cdot 10^{-6}$$

$$RI := \text{root}(F(z), z)$$

$$RI = 0.000000630540703 \text{ meters}$$

Estimating R0 to compare it with the value assumed or introduced in the Input data Section

B. Bubble grows Isothermally

$$EP1 := 47.4 \cdot 10^{-6}$$

End Point of Exploration (Trial and Error)

$$td := 2 \cdot 10^{-8}, 3 \cdot 10^{-8} \dots EP1$$

Solve

$$D(x, y) := \left[\left[\left[\frac{1}{DI} \left[\frac{-Pb}{y_0} + Pa \cdot \frac{\sin(f \cdot x)}{y_0} + PGO \cdot \frac{(R0)^{(3 \cdot Alpha)}}{(y_0)^{[(3 \cdot Alpha) + 1]}} + \frac{Ps}{y_0} - 2 \cdot \frac{\sigma}{(y_0)^2} \right] - 1.5 \cdot \frac{(y_1)^2}{y_0} \right] \right] \right]$$

$$P(td) := \text{rkfixed} \left[\begin{pmatrix} R0 \\ 0 \end{pmatrix}, 0, td, 200, D \right] \quad n := 0, 1..200$$

$$Diff(td) := \left[\left[R2 - (P(td)^{\langle 1 \rangle})_{200} \right] \right] \quad \text{Optimization function}$$

$$t := EP1$$

Initial value for the search of the optimal

$$\text{root}(Diff(t), t) = 0.000047374348504$$

$$\text{soln} := \text{root}(Diff(t), t)$$

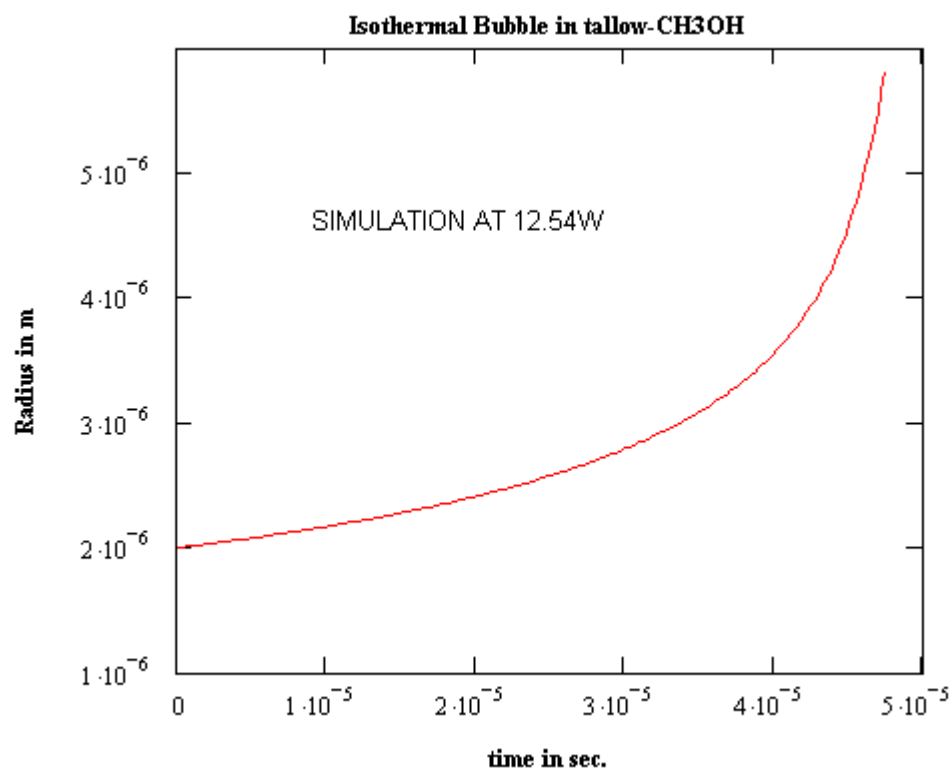
$$\text{round}(\text{soln}, 7) = 0.0000474$$

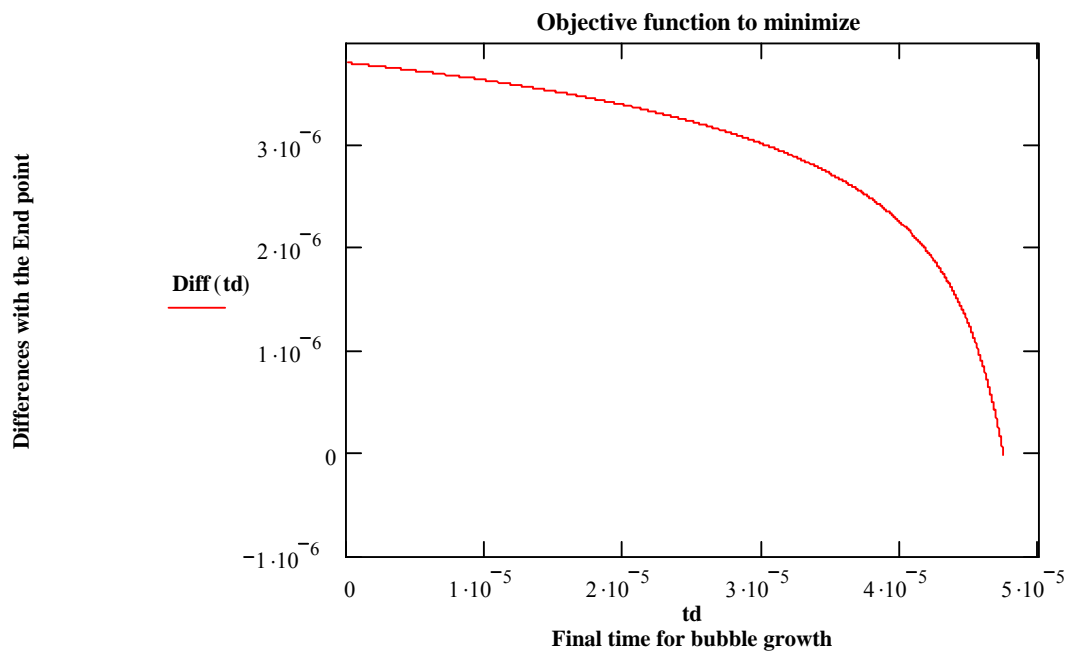
$$\text{xx} := \text{round}(\text{soln}, 7) \quad \text{xx} = 0.0000474$$

time necessary to reach a radius of R2 by optimization

$$EP1 = 0.0000474$$

time necessary to reach a radius of R2 by Trial and error





C. Bubble falling in adiabatic collapse

$$dRdt := \left(P(EP1)^{\langle 2 \rangle} \right)_{200}$$

$$dRdt = 0.734333636550302$$

Initial condition for the first derivate is a result from part B

$$EP := 166.4622210^{-6}$$

End Point of Exploration (Trial and Error)

$$tf := EP$$

Iteration for life time of bubble

Solve

$$\mathbf{D}(\mathbf{x}, \mathbf{y}) := \begin{bmatrix} y_1 \\ \left[\frac{1}{\mathbf{DI}} \cdot \left[\frac{-\mathbf{Pb}}{y_0} + \mathbf{Pa} \cdot \frac{(\sin(\mathbf{f} \cdot \mathbf{x}))}{y_0} + 2 \cdot \mathbf{Ps} \cdot \frac{\mathbf{R2}^{(3 \cdot \mathbf{Alpha})}}{(y_0)^{[(3 \cdot \mathbf{Alpha}) + 1]}} - 2 \cdot \frac{\mathbf{sigma}}{(y_0)^2} \right] - 1.5 \cdot \frac{(y_1)^2}{y_0} \right] \end{bmatrix}$$

$$\mathbf{Q}(\mathbf{tf}) := \text{rkfixed} \left[\begin{pmatrix} \mathbf{R2} \\ \mathbf{dRdt} \end{pmatrix}, \mathbf{EP1}, \mathbf{tf}, 200, \mathbf{D} \right] \quad \mathbf{n} := 0, 1..200$$

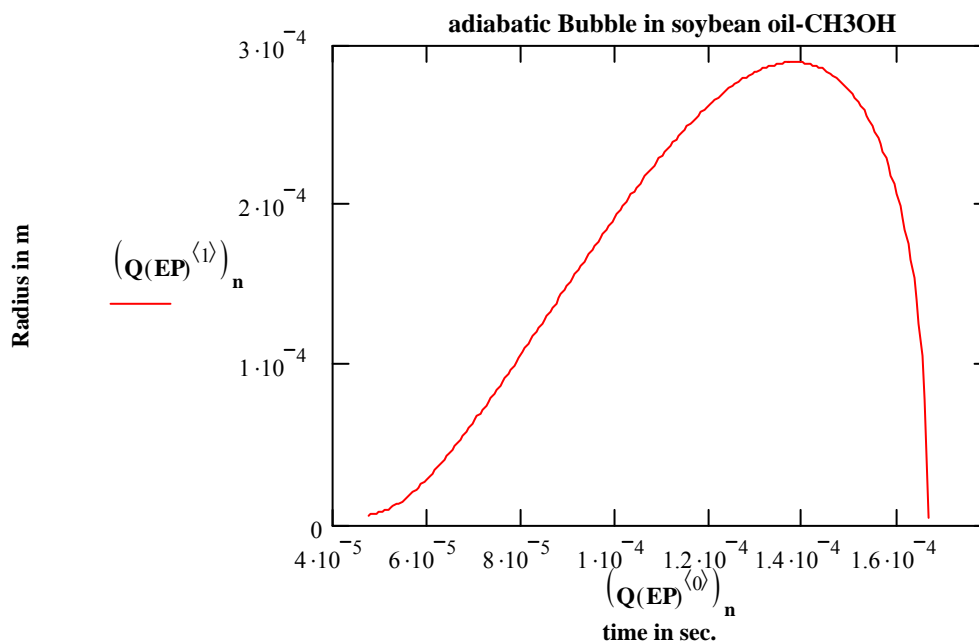
$$\mathbf{Diff2}(\mathbf{tf}) := \left[\text{Speed} - \left| \left(\mathbf{Q}(\mathbf{tf})^{(2)} \right)_{200} \right| \right] \quad \text{Optimization function}$$

$$\mathbf{Diff2}(\mathbf{EP}) = -0.093254348652636$$

$$\left(\mathbf{Q}(\mathbf{EP})^{(1)} \right)_{200} = 0.000003997927703 \quad \text{meters, bubble radius at collapse}$$

$$\left(\mathbf{Q}(\mathbf{EP})^{(2)} \right)_{200} = -1460.09325434865 \quad \text{Speed of the wall bubble at collapse in m/s}$$

Checking the solution for adiabatic collapse of the bubble



$$Rf(EP) := (Q(EP)^{\langle 1 \rangle})_{200}$$

$$Rf(EP) = 0.000003997927703$$

$$TEMPf := Temp \left(\frac{R2}{Rf(EP)} \right)^{3 \cdot (GAMMA - 1)}$$

$$TEMPf = 426.570972900065$$

Temperature at collapse in Kelvin

$$PRESSf := \left(\left(\frac{R2}{Rf(EP)} \right) \right)^{3 \cdot GAMMA} \cdot (2 \cdot Ps)$$

PRESSf = 40899.2355624648

Pressure at collapse in Pascal

RMAX := $\max(Q(EP)^{\langle 1 \rangle})$

RMAX = 0.000409734992994 **meters**

Maximum Radius of the bubble

D. Final Solution for isothermal growing and adiabatic collapse of the bubble

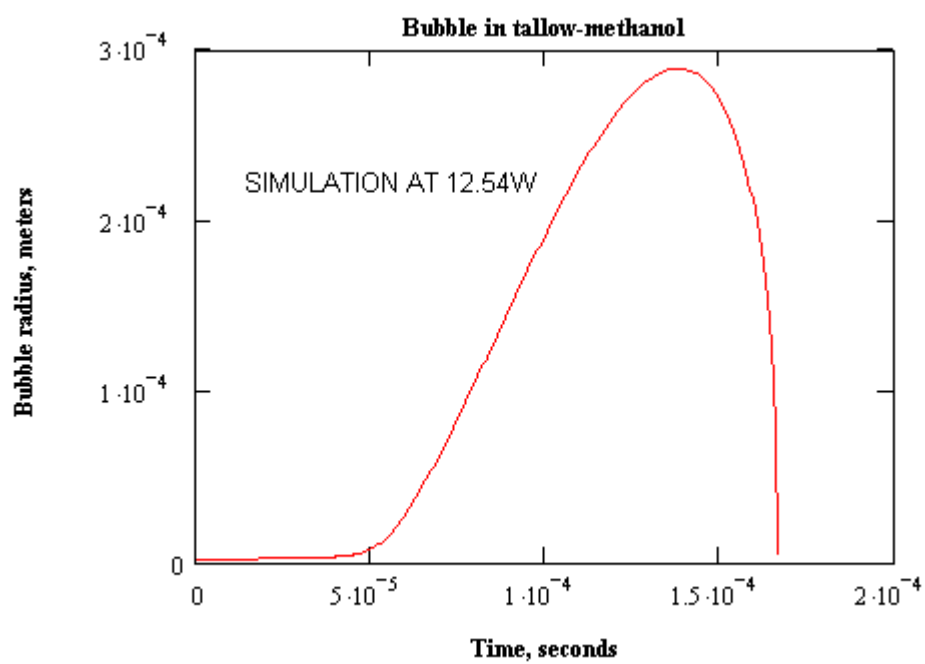
m := 0, 1 .. 401

HH := $\text{stack}[(P(EP1)^{\langle 0 \rangle}), (Q(EP)^{\langle 0 \rangle})]$

HHH := $\text{stack}[(P(EP1)^{\langle 1 \rangle}), (Q(EP)^{\langle 1 \rangle})]$

HHHH(m) := $[(m \leq 200) \cdot \mathbf{HH}_m + (m > 200) \cdot \mathbf{HH}_{m+1}]$ Axis X

HHHHH(m) := $[(m \leq 200) \cdot \mathbf{HHH}_m + (m > 200) \cdot \mathbf{HHH}_{m+1}]$ Axis Y



APPENDIX 5: Mass transfer diffusion into a sphere

SOLUTION CODE FOR MASS TRANSFER DIFFUSION INTO A SPHERE ASSUMING ZERO EXTERNAL RESISTENCE

$\Phi := 0.5$ Module of Thiele

$$\text{Solve } y'' = \begin{cases} y^2 \cdot \frac{\Phi^2}{3} & \text{for } x < 0.1 \\ y^2 \cdot \Phi^2 - 2 \cdot \frac{y'}{x} & \text{for } x \geq 0.1 \end{cases} \quad \text{where } y(1)=1 \text{ and } y'(0)=0$$

$$D(x,y) := \begin{bmatrix} y_1 \\ (x < 0.1) \cdot \left[(y_0)^2 \cdot \frac{(\Phi)^2}{3} \right] + (x \geq 0.1) \cdot \left[(y_0)^2 \cdot \Phi^2 - 2 \cdot \frac{y_1}{x} \right] \end{bmatrix} \quad \text{xf} := 0.1 \quad \text{point of discontinuity}$$

$v1_0 := 0.6$

guess value for $y(0)$

Valores validos para Φ entre 0.5 y 3

$v2_0 := 0.88$

guess value for $y'(1)$

$$\text{load1}(x1, v1) := \begin{pmatrix} v1_0 \\ 0 \end{pmatrix}$$

guess value for $y(0)$

value for $y'(0)$

$$\text{load2}(x2, v2) := \begin{pmatrix} 1 \\ v2_0 \end{pmatrix}$$

$y(1)$

guess value for $y'(1)$

$\text{score}(xf, y) := y$

tells mathcad to match the two halves of the solution at $x=xf$

$S := \text{bvalfit}(v1, v2, 0, 1, 0.1, D, \text{load1}, \text{load2}, \text{score})_*$

$S = (0.9606 \ 0.0807)$

contains $(y(0) \ y'(1))$

PROFILES OF DIMENSIONLESS CONCENTRATION

I. First Equation using L'Hopital Theorem for $0 < t < 0.1$

$$y_0 = y$$

$$\frac{d}{dt}y_0 = y_1$$

$$3 \cdot \frac{d}{dt}y_1 = \phi^2 \cdot y_0^2$$

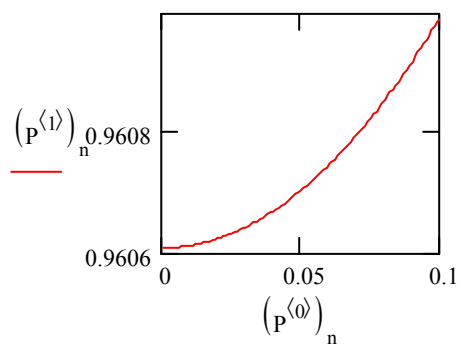
$$\text{Ini1} := S_{0,0}$$

value of y_0 obtained from the use of Bvalfit function

$$D(t, Y) := \begin{bmatrix} Y_1 \\ \left[(Y_0)^2 \cdot \frac{\Phi^2}{3} \right] \end{bmatrix}$$

$$P := \text{Bulstoer} \left[\begin{pmatrix} \text{Ini1} \\ 0 \end{pmatrix}, 0, 0.1, 100, D \right]$$

$$n := 0, 1.. 100$$



$$\left(P^{(1)} \right)_{100} = 0.961$$

$$\left(P^{(2)} \right)_{100} = 7.6918 \times 10^{-3}$$

II. The second equation is solved using the same method for 0.1 L.E. t and t L.E. 1
(results of part I are used as initial values for the numerical solution)

$$z_0 = z$$

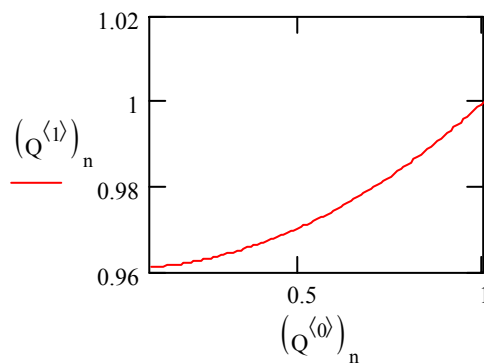
$$\frac{d}{dt} z_0 = z_1$$

$$\left(\frac{d}{dt} z_1 \right) = \Phi^2 \cdot z_0^2 - 2 \cdot \frac{z_1}{t}$$

$$\text{Ini2} := (P^{(1)})_{100} \quad \text{Ini3} := (P^{(2)})_{100}$$

$$D(t, Z) := \begin{bmatrix} Z_1 \\ \left[(Z_0)^2 \cdot \Phi^2 - 2 \cdot \frac{Z_1}{t} \right] \end{bmatrix}$$

$$Q := \text{Bulstoer} \left[\begin{bmatrix} \text{Ini2} \\ \text{Ini3} \end{bmatrix}, 0.1, 1, 100, D \right]$$



$$(Q^{(1)})_{100} = 1$$

$$(Q^{(2)})_{100} = 0.0807$$

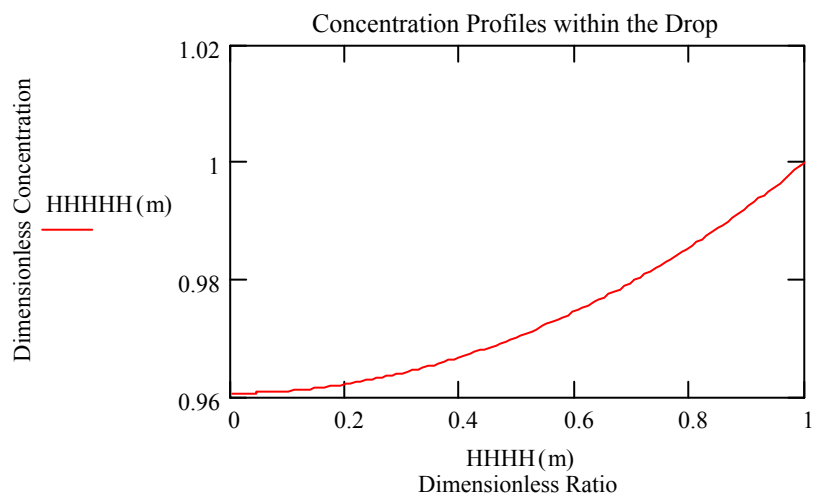
III. Final Solution of profiles and Calculus of Effective diffusivity

 $m := 0, 1..201$

$$HH := \text{stack}\left[\left(P^{(\phi)}\right), \left(Q^{(\phi)}\right)\right] \quad HHH := \text{stack}\left[\left(P^{(1)}\right), \left(Q^{(1)}\right)\right]$$

$$HHHH(m) := \left[(m \leq 100) \cdot HH_m + (m > 100) \cdot HH_{m+1} \right] \quad \text{Axis X}$$

$$HHHHH(m) := \left[(m \leq 100) \cdot HHH_m + (m > 100) \cdot HHH_{m+1} \right] \quad \text{Axis Y}$$



$$\text{DERIVOFCONCin1} = S_{0,1}$$

$$\text{EFFECT} := 3 \cdot \frac{\text{DERIVOFCONCin1}}{\phi^2}$$

$$\text{EFFECT} = 0.9685$$

Effectiveness